

Figure S1. Popularity of different DR methods as measured by their use in existing scRNAseq cell clustering tools or lineage inference tools. We counted the number of DR methods that are used in each of the 32 scRNAseq cell clustering methods (**A**) or in each of the 46 scRNAseq lineage inference methods (**B**). We used *geom_treemap* functions in R package to draw both panels, where the font size of each DR method represents its popularity, which is measured by the frequency of DR method used in these scRNAseq tools.

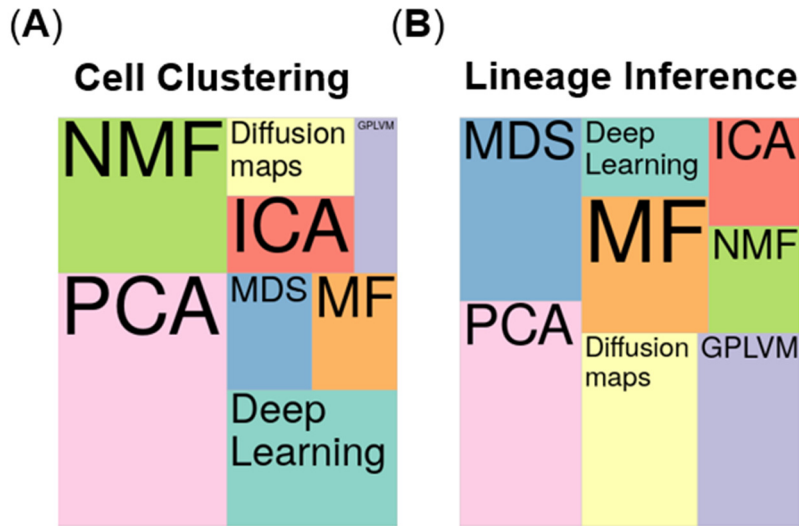


Figure S2. DR method performance evaluated by Jaccard index on cell clustering data sets with 10 neighborhood cells. We compared 18 DR methods (columns), including factor analysis (FA), principal component analysis (PCA), independent component analysis (ICA), Diffusion Map, nonnegative matrix factorization (NMF), Poisson NMF, zero-inflated factor analysis (ZIFA), zero-inflated negative binomial based wanted variation extraction (ZINB-WaVE), probabilistic count matrix factorization (pCMF), deep count autoencoder network (DCA), scScope, generalized linear model principal component analysis (GLMPCA), multidimensional scaling (MDS), locally linear embedding (LLE), local tangent space alignment (LTSA), Isomap, uniform manifold approximation and projection (UMAP), and t-distributed stochastic neighbor embedding (tSNE). We evaluated their performance on 14 real scRNASeq data sets (UMI-based data are colored as blue while non-UMI based data are colored as purple) and 2 simulated data sets (rows). The simulated data based on Kumar data is labeled with #. We used log2 count transformation for the subset of DR methods that use normalized data. For each data set, we compared the four different number of low-dimensional data. The four numbers we used equal to 0.5%, 1%, 2%, and 3% of the total number of cells in big data and equal to 2, 6, 14, and 20 in small data (which are labeled with *). No results for ICA are shown in the Pancreatic data (grey fills) because ICA cannot handle the large number of features in the data. Note that, for tSNE, we only extracted two low-dimensional components due to the limitation of the tSNE software.

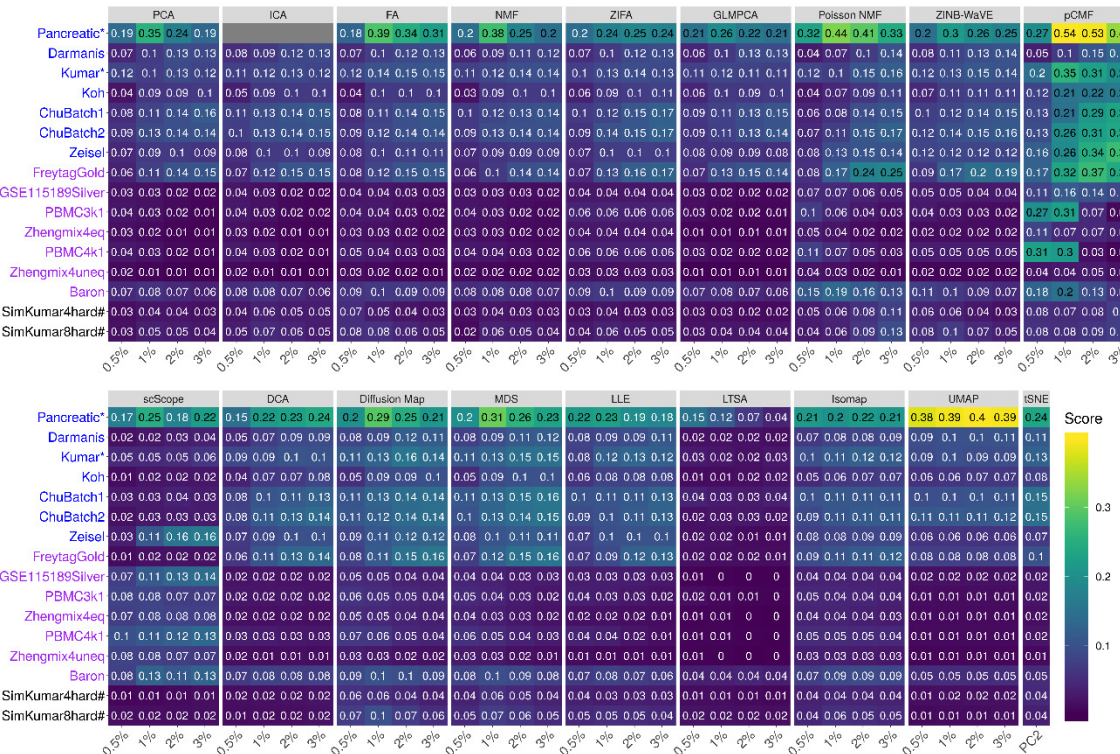


Figure S3. Bar plots show the average Jaccard index of different DR methods with 10 neighborhood cells based on cell clustering data. The performance is measured by average Jaccard index across 16 data sets. We compared 18 DR methods, including factor analysis (FA; light green), principal component analysis (PCA; light blue), independent component analysis (ICA; blue), Diffusion Map (pink), nonnegative matrix factorization (NMF; green), Poisson NMF (light orange), zero-inflated factor analysis (ZIFA; light pink), zero-inflated negative binomial based wanted variation extraction (ZINB-WaVE; orange), probabilistic count matrix factorization (pCMF; light purple), deep count autoencoder network (DCA; yellow), scScope (purple), generalized linear model principal component analysis (GLMPCA; red), multidimensional scaling (MDS; cyan), locally linear embedding (LLE; blue green), local tangent space alignment (LTSA; teal blue), Isomap (grey), uniform manifold approximation and projection (UMAP; brown), and t-distributed stochastic neighbor embedding (tSNE; dark red). We used log2 count transformation for the subset of DR methods that use normalized data. For each data set, we compared the four different number of low-dimensional data. The four numbers we used equal to 0.5%, 1%, 2%, and 3% of the total number of cells in big data and equal to 2, 6, 14, and 20 in small data. For convenience, we only listed 0.5%, 1%, 2%, and 3% on x-axis. Note that, for tSNE, we only extracted two low-dimensional components due to the limitation of the tSNE software.

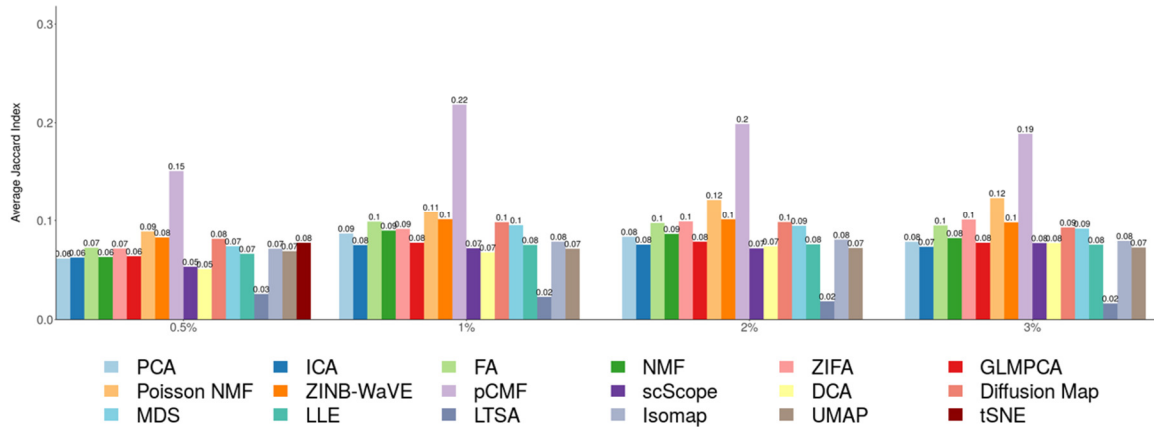


Figure S4. DR method performance evaluated by Jaccard index on cell clustering data sets with 20 neighborhood cells. We compared 18 DR methods (columns), including factor analysis (FA), principal component analysis (PCA), independent component analysis (ICA), Diffusion Map, nonnegative matrix factorization (NMF), Poisson NMF, zero-inflated factor analysis (ZIFA), zero-inflated negative binomial based wanted variation extraction (ZINB-WaVE), probabilistic count matrix factorization (pCMF), deep count autoencoder network (DCA), scScope, generalized linear model principal component analysis (GLMPCA), multidimensional scaling (MDS), locally linear embedding (LLE), local tangent space alignment (LTSA), Isomap, uniform manifold approximation and projection (UMAP), and t-distributed stochastic neighbor embedding (tSNE). We evaluated their performance on 14 real scRNAseq data sets (UMI-based data are colored as blue while non-UMI based data are colored as purple) and 2 simulated data sets (rows). The simulated data based on Kumar data is labeled with #. We used log2 count transformation for the subset of DR methods that use normalized data. For each data set, we compared the four different number of low-dimensional data. The four numbers we used equal to 0.5%, 1%, 2%, and 3% of the total number of cells in big data and equal to 2, 6, 14, and 20 in small data (which are labeled with *). No results for ICA are shown in the Pancreatic data (grey fills) because ICA cannot handle the large number of features in the data. Note that, for tSNE, we only extracted two low-dimensional components due to the limitation of the tSNE software.

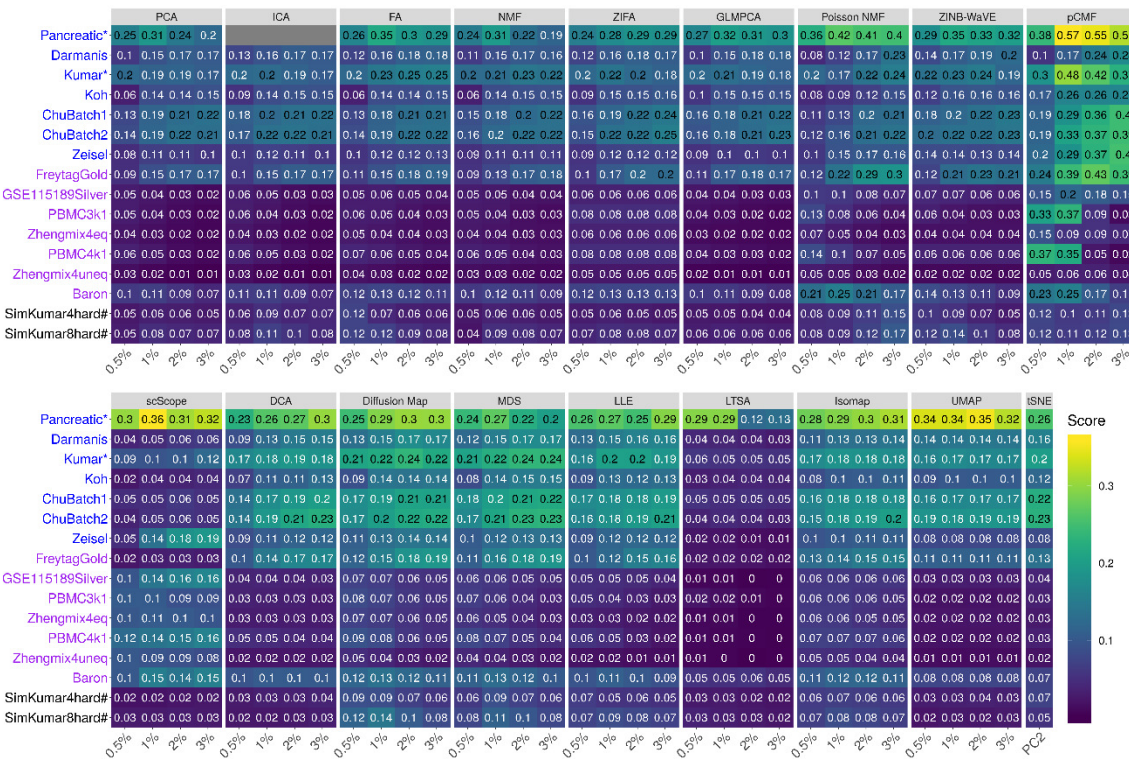


Figure S5. Bar plots show the average Jaccard index of different DR methods with 20 neighborhood cells based on cell clustering data. The performance is measured by average Jaccard index across 16 data sets. We compared 18 DR methods, including factor analysis (FA; light green), principal component analysis (PCA; light blue), independent component analysis (ICA; blue), Diffusion Map (pink), nonnegative matrix factorization (NMF; green), Poisson NMF (light orange), zero-inflated factor analysis (ZIFA; light pink), zero-inflated negative binomial based wanted variation extraction (ZINB-WaVE; orange), probabilistic count matrix factorization (pCMF; light purple), deep count autoencoder network (DCA; yellow), scScope (purple), generalized linear model principal component analysis (GLMPCA; red), multidimensional scaling (MDS; cyan), locally linear embedding (LLE; blue green), local tangent space alignment (LTSA; teal blue), Isomap (grey), uniform manifold approximation and projection (UMAP; brown), and t-distributed stochastic neighbor embedding (tSNE; dark red). We used log2 count transformation for the subset of DR methods that use normalized data. For each data set, we compared the four different number of low-dimensional data. The four numbers we used equal to 0.5%, 1%, 2%, and 3% of the total number of cells in big data and equal to 2, 6, 14, and 20 in small data. For convenience, we only listed 0.5%, 1%, 2%, and 3% on x-axis. Note that, for tSNE, we only extracted two low-dimensional components due to the limitation of the tSNE software.

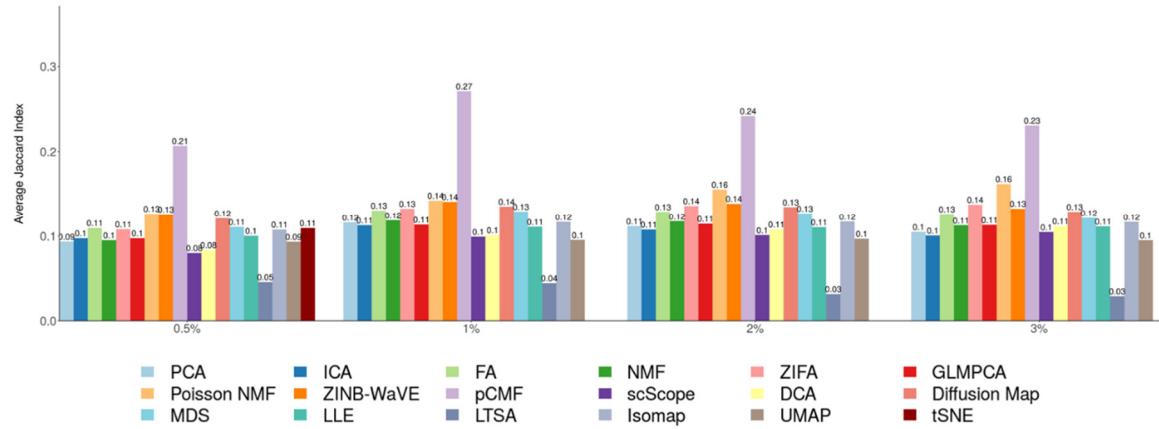


Figure S6. DR method performance evaluated by Jaccard index on cell clustering data sets with 30 neighborhood cells. We compared 18 DR methods (columns), including factor analysis (FA), principal component analysis (PCA), independent component analysis (ICA), Diffusion Map, nonnegative matrix factorization (NMF), Poisson NMF, zero-inflated factor analysis (ZIFA), zero-inflated negative binomial based wanted variation extraction (ZINB-WaVE), probabilistic count matrix factorization (pCMF), deep count autoencoder network (DCA), scScope, generalized linear model principal component analysis (GLMPCA), multidimensional scaling (MDS), locally linear embedding (LLE), local tangent space alignment (LTSA), Isomap, uniform manifold approximation and projection (UMAP), and t-distributed stochastic neighbor embedding (tSNE). We evaluated their performance on 14 real scRNAseq data sets (UMI-based data are colored as blue while non-UMI based data are colored as purple) and 2 simulated data sets (rows). The simulated data based on Kumar data is labeled with #. We used log2 count transformation for the subset of DR methods that use normalized data. For each data set, we compared the four different number of low-dimensional data. The four numbers we used equal to 0.5%, 1%, 2%, and 3% of the total number of cells in big data and equal to 2, 6, 14, and 20 in small data (which are labeled with *). No results for ICA are shown in the Pancreatic data (grey fills) because ICA cannot handle the large number of features in the data. Note that, for tSNE, we only extracted two low-dimensional components due to the limitation of the tSNE software.

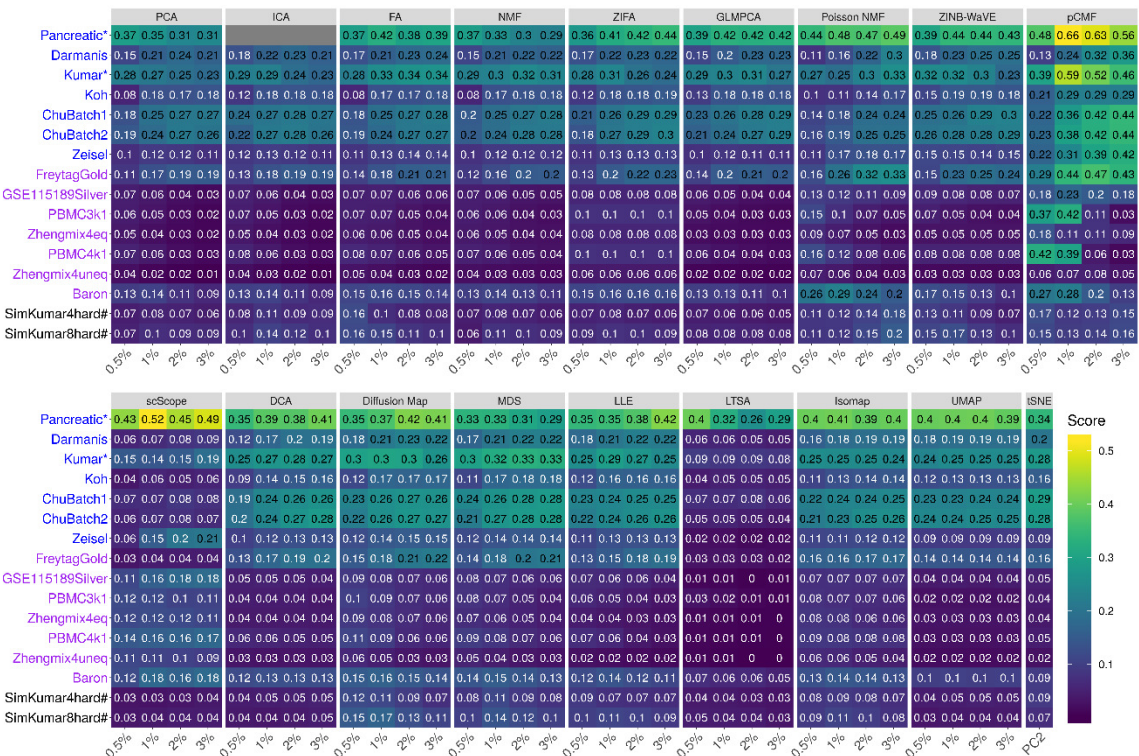


Figure S7. Bar plots show the average Jaccard index of different DR methods with 30 neighborhood cells based on cell clustering data. The performance is measured by average Jaccard index across 16 data sets. We compared 18 DR methods, including factor analysis (FA; light green), principal component analysis (PCA; light blue), independent component analysis (ICA; blue), Diffusion Map (pink), nonnegative matrix factorization (NMF; green), Poisson NMF (light orange), zero-inflated factor analysis (ZIFA; light pink), zero-inflated negative binomial based wanted variation extraction (ZINB-WaVE; orange), probabilistic count matrix factorization (pCMF; light purple), deep count autoencoder network (DCA; yellow), scScope (purple), generalized linear model principal component analysis (GLMPCA; red), multidimensional scaling (MDS; cyan), locally linear embedding (LLE; blue green), local tangent space alignment (LTSA; teal blue), Isomap (grey), uniform manifold approximation and projection (UMAP; brown), and t-distributed stochastic neighbor embedding (tSNE). We used log2 count transformation for the subset of DR methods that use normalized data. For each data set, we compared the four different number of low-dimensional data. The four numbers we used equal to 0.5%, 1%, 2%, and 3% of the total number of cells in big data and equal to 2, 6, 14, and 20 in small data. For convenience, we only listed 0.5%, 1%, 2%, and 3% on x-axis. Note that, for tSNE, we only extracted two low-dimensional components due to the limitation of the tSNE software.

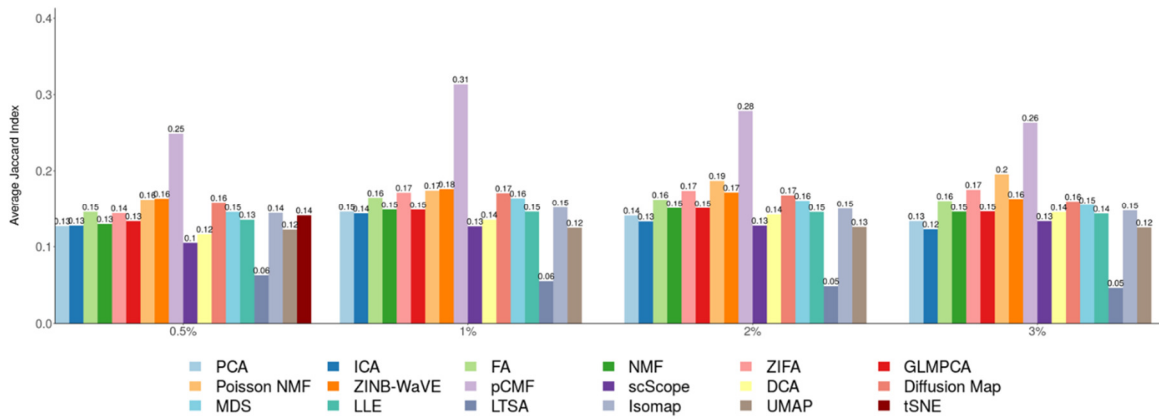


Figure S8. Bar plots show the average Jaccard index of different DR methods on UMI-based data and nonUMI-based data with 30 neighborhood cells. The performance is measured by average Jaccard index across UMI-based data (**A**; 7 data sets) or nonUMI-based data (**B**; 7 data sets). We compared 18 DR methods, including factor analysis (FA; light green), principal component analysis (PCA; light blue), independent component analysis (ICA; blue), Diffusion Map (pink), nonnegative matrix factorization (NMF; green), Poisson NMF (light orange), zero-inflated factor analysis (ZIFA; light pink), zero-inflated negative binomial based wanted variation extraction (ZINB-WaVE; orange), probabilistic count matrix factorization (pCMF; light purple), deep count autoencoder network (DCA; yellow), scScope (purple), generalized linear model principal component analysis (GLMPCA; red), multidimensional scaling (MDS; cyan), locally linear embedding (LLE; blue green), local tangent space alignment (LTSA; teal blue), Isomap (grey), uniform manifold approximation and projection (UMAP; brown), and t-distributed stochastic neighbor embedding (tSNE; dark red). We used log2 count transformation for the subset of DR methods that use normalized data. For each data set, we compared the four different number of low-dimensional data. The four numbers we used equal to 0.5%, 1%, 2%, and 3% of the total number of cells in big data and equal to 2, 6, 14, and 20 in small data. For convenience, we only listed 0.5%, 1%, 2%, and 3% on x-axis. Note that, for tSNE, we only extracted two low-dimensional components due to the limitation of the tSNE software.

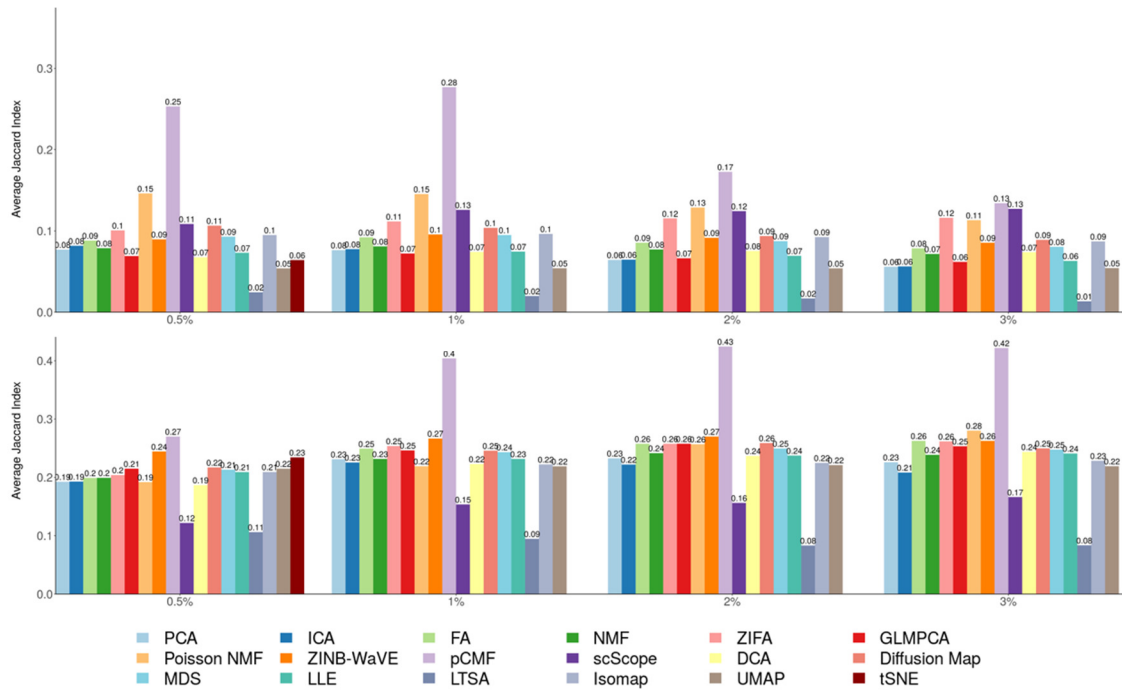


Figure S9. DR method performance evaluated by Jaccard index on trajectory inference data sets with 10 neighborhood cells. We compared 18 DR methods (columns), including factor analysis (FA), principal component analysis (PCA), independent component analysis (ICA), Diffusion Map, nonnegative matrix factorization (NMF), Poisson NMF, zero-inflated factor analysis (ZIFA), zero-inflated negative binomial based wanted variation extraction (ZINB-WaVE), probabilistic count matrix factorization (pCMF), deep count autoencoder network (DCA), scScope, generalized linear model principal component analysis (GLMPCA), multidimensional scaling (MDS), locally linear embedding (LLE), local tangent space alignment (LTSA), Isomap, and uniform manifold approximation and projection (UMAP), and t-distributed stochastic neighbor embedding (tSNE). We evaluated their performance on 14 real scRNAseq data sets (rows) in terms of lineage inference accuracy. The simulated data based on Kumar data is labeled with #. We used log2 count transformation for the subset of DR methods that use normalized data. For each data set, we compared the four different number of low-dimensional data. The four numbers we used equal to 2, 6, 14, and 20. Note that, for tSNE, we only extracted two low-dimensional components due to the limitation of the tSNE software.

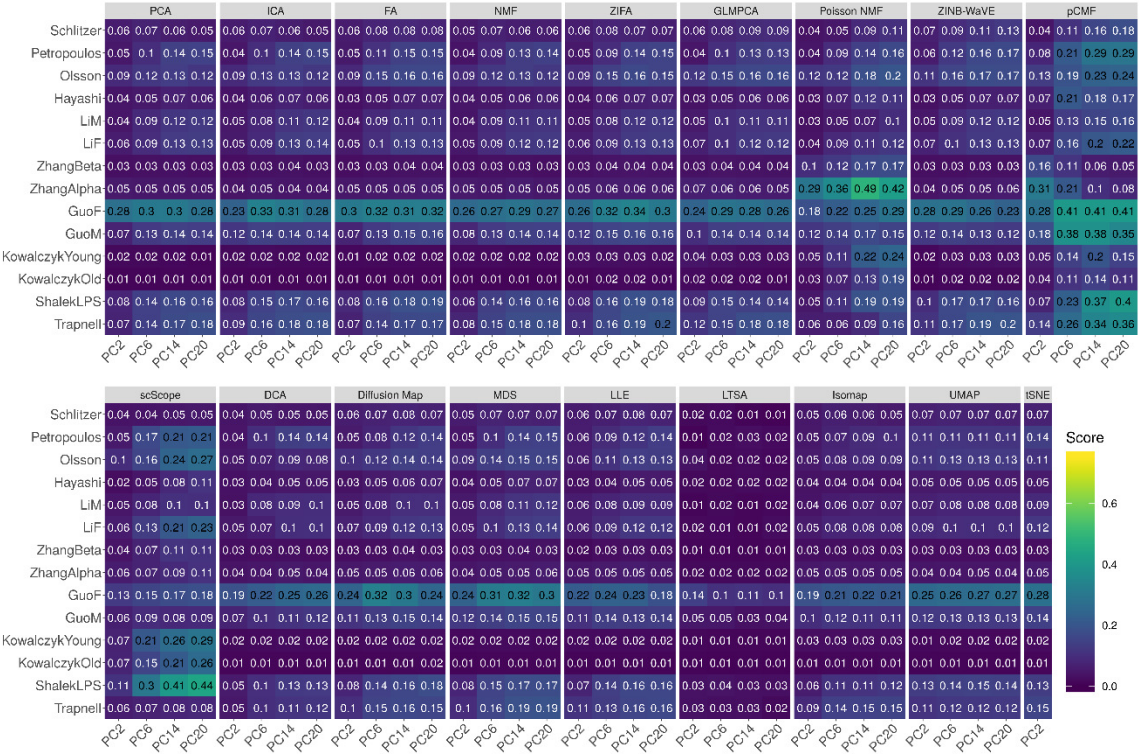


Figure S10. Bar plots show the average Jaccard index of different DR methods with 10 neighborhood cells based on trajectory inference data.

The performance is measured by average Jaccard index across 16 data sets. We compared 18 DR methods, including factor analysis (FA; light green), principal component analysis (PCA; light blue), independent component analysis (ICA; blue), Diffusion Map (pink), nonnegative matrix factorization (NMF; green), Poisson NMF (light orange), zero-inflated factor analysis (ZIFA; light pink), zero-inflated negative binomial based wanted variation extraction (ZINB-WaVE; orange), probabilistic count matrix factorization (pCMF; light purple), deep count autoencoder network (DCA; yellow), scScope (purple), generalized linear model principal component analysis (GLMPCA; red), multidimensional scaling (MDS; cyan), locally linear embedding (LLE; blue green), local tangent space alignment (LTSA; teal blue), Isomap (grey), uniform manifold approximation and projection (UMAP; brown), and t-distributed stochastic neighbor embedding (tSNE; dark red). We used log2 count transformation for the subset of DR methods that use normalized data. For each data set, we compared the four different number of low-dimensional data. The four numbers we used equal to 2, 6, 14, and 20 on x-axis. Note that, for tSNE, we only extracted two low-dimensional components due to the limitation of the tSNE software.

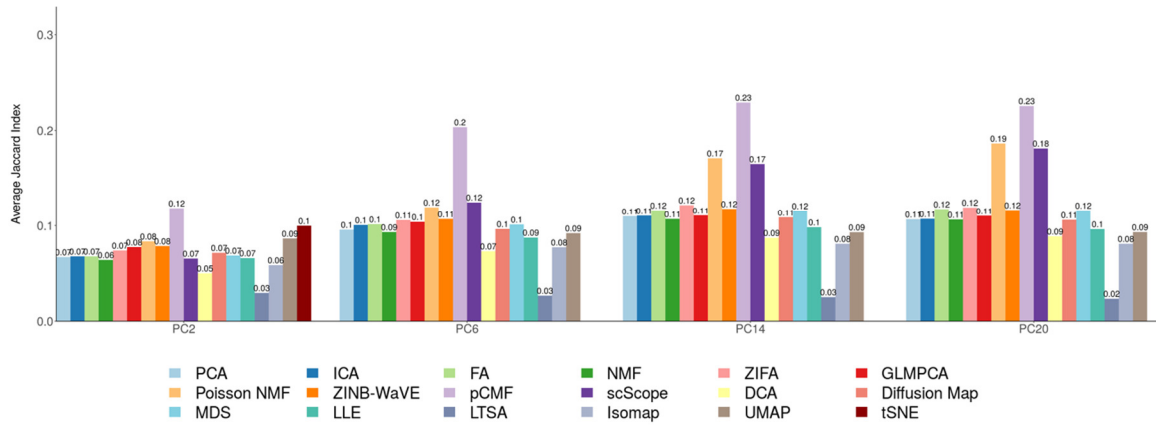


Figure S11. DR method performance evaluated by Jaccard index on trajectory inference data sets with 20 neighborhood cells. We compared 18 DR methods (columns), including factor analysis (FA), principal component analysis (PCA), independent component analysis (ICA), Diffusion Map, nonnegative matrix factorization (NMF), Poisson NMF, zero-inflated factor analysis (ZIFA), zero-inflated negative binomial based wanted variation extraction (ZINB-WaVE), probabilistic count matrix factorization (pCMF), deep count autoencoder network (DCA), scScope, generalized linear model principal component analysis (GLMPCA), multidimensional scaling (MDS), locally linear embedding (LLE), local tangent space alignment (LTSA), Isomap, uniform manifold approximation and projection (UMAP), and t-distributed stochastic neighbor embedding (tSNE). We evaluated their performance on 14 real scRNAseq data sets (rows) in terms of lineage inference accuracy. The simulated data based on Kumar data is labeled with #. We used log2 count transformation for the subset of DR methods that use normalized data. For each data set, we compared the four different number of low-dimensional data. The four numbers we used equal to 2, 6, 14, and 20. Note that, for tSNE, we only extracted two low-dimensional components due to the limitation of the tSNE software.

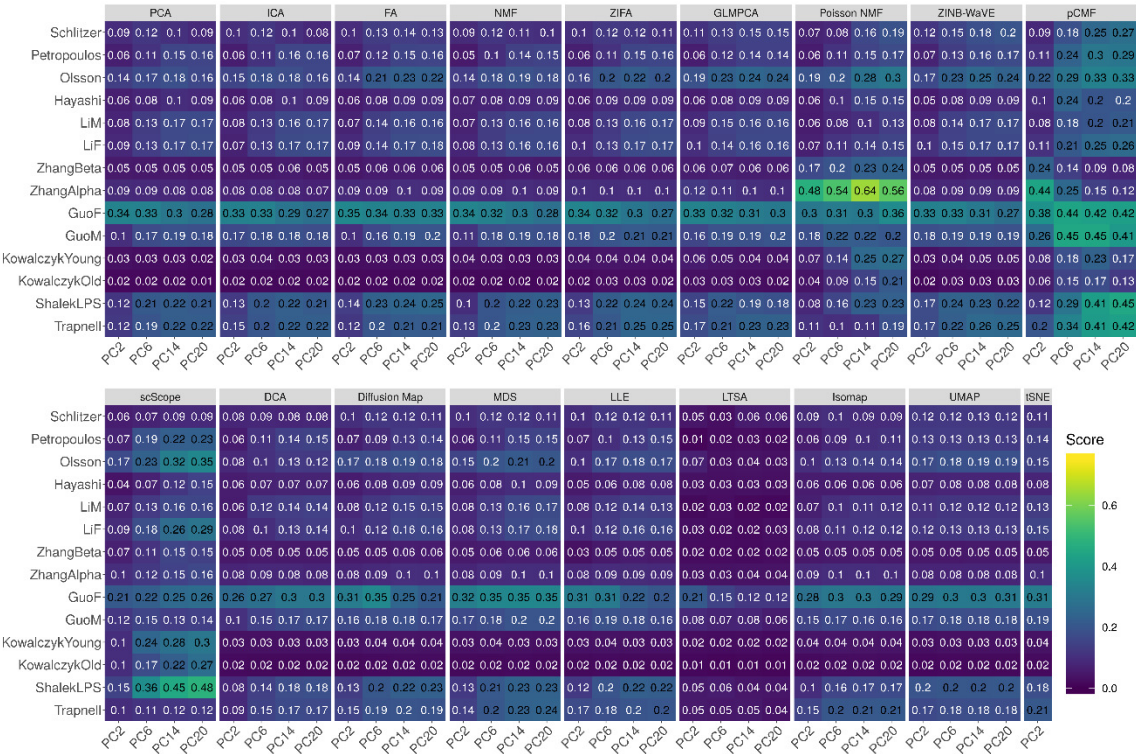


Figure S12. Bar plots show the average Jaccard index of different DR methods with 20 neighborhood cells based on trajectory inference data.

The performance is measured by average Jaccard index across 16 data sets. We compared 18 DR methods, including factor analysis (FA; light green), principal component analysis (PCA; light blue), independent component analysis (ICA; blue), Diffusion Map (pink), nonnegative matrix factorization (NMF; green), Poisson NMF (light orange), zero-inflated factor analysis (ZIFA; light pink), zero-inflated negative binomial based wanted variation extraction (ZINB-WaVE; orange), probabilistic count matrix factorization (pCMF; light purple), deep count autoencoder network (DCA; yellow), scScope (purple), generalized linear model principal component analysis (GLMPCA; red), multidimensional scaling (MDS; cyan), locally linear embedding (LLE; blue green), locally tangent space alignment (LTSA; teal blue), Isomap (grey), uniform manifold approximation and projection (UMAP; brown), and t-distributed stochastic neighbor embedding (tSNE; dark red). We used log2 count transformation for the subset of DR methods that use normalized data. For each data set, we compared the four different number of low-dimensional data. The four numbers we used equal to 2, 6, 14, and 20 on x-axis. Note that, for tSNE, we only extracted two low-dimensional components due to the limitation of the tSNE software.

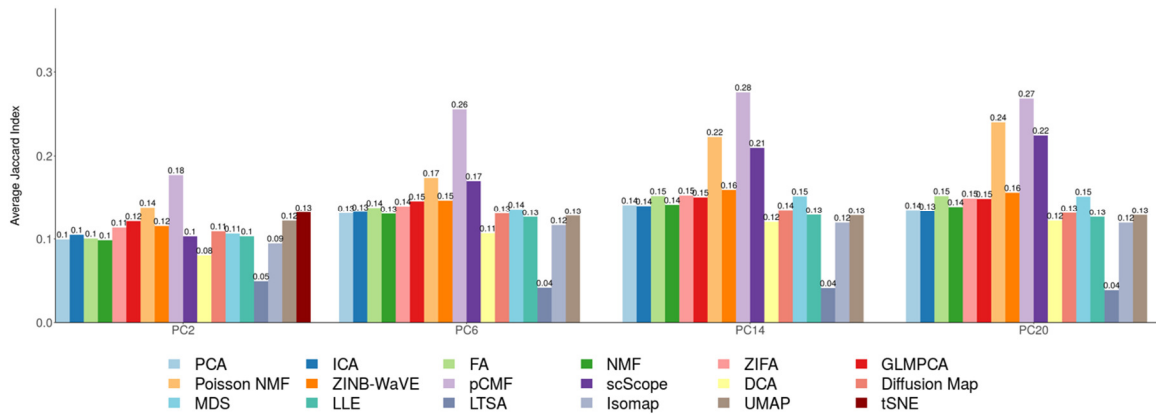


Figure S13. DR method performance evaluated by Jaccard index on trajectory inference data sets with 30 neighborhood cells. We compared 18 DR methods (columns), including factor analysis (FA), principal component analysis (PCA), independent component analysis (ICA), Diffusion Map, nonnegative matrix factorization (NMF), Poisson NMF, zero-inflated factor analysis (ZIFA), zero-inflated negative binomial based wanted variation extraction (ZINB-WaVE), probabilistic count matrix factorization (pCMF), deep count autoencoder network (DCA), scScope, generalized linear model principal component analysis (GLMPCA), multidimensional scaling (MDS), locally linear embedding (LLE), local tangent space alignment (LTSA), Isomap, uniform manifold approximation and projection (UMAP), and t-distributed stochastic neighbor embedding (tSNE). We evaluated their performance on 14 real scRNAseq data sets (rows) in terms of lineage inference accuracy. The simulated data based on Kumar data is labeled with #. We used log2 count transformation for the subset of DR methods that use normalized data. For each data set, we compared the four different number of low-dimensional data. The four numbers we used equal to 2, 6, 14, and 20. Note that, for tSNE, we only extracted two low-dimensional components due to the limitation of the tSNE software.

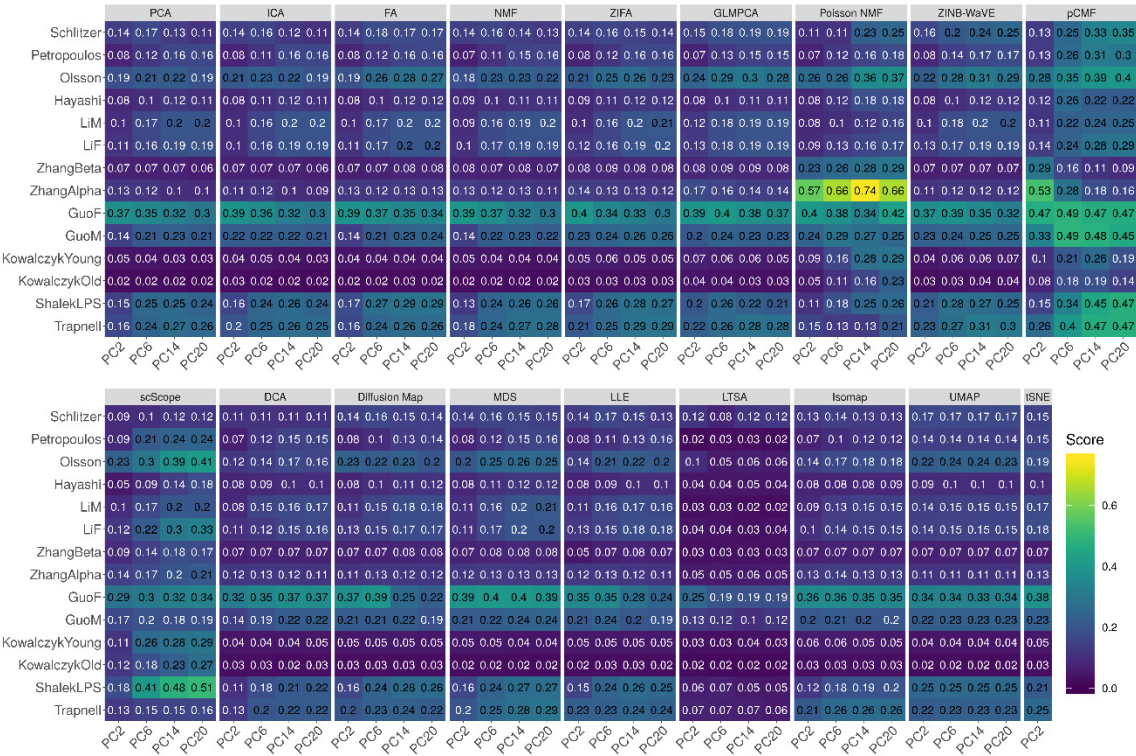


Figure S14. Bar plots show the average Jaccard index of different DR methods with 30 neighborhood cells based on trajectory inference data.

The performance is measured by average Jaccard index across 16 data sets. We compared 18 DR methods, including factor analysis (FA; light green), principal component analysis (PCA; light blue), independent component analysis (ICA; blue), Diffusion Map (pink), nonnegative matrix factorization (NMF; green), Poisson NMF (light orange), zero-inflated factor analysis (ZIFA; light pink), zero-inflated negative binomial based wanted variation extraction (ZINB-WaVE; orange), probabilistic count matrix factorization (pCMF; light purple), deep count autoencoder network (DCA; yellow), scScope (purple), generalized linear model principal component analysis (GLMPCA; red), multidimensional scaling (MDS; cyan), locally linear embedding (LLE; blue green), local tangent space alignment (LTSA; teal blue), Isomap (grey), uniform manifold approximation and projection (UMAP; brown), and t-distributed stochastic neighbor embedding (tSNE; dark red). We used log2 count transformation for the subset of DR methods that use normalized data. For each data set, we compared the four different number of low-dimensional data. The four numbers we used equal to 2, 6, 14, and 20 on x-axis. Note that, for tSNE, we only extracted two low-dimensional components due to the limitation of the tSNE software.

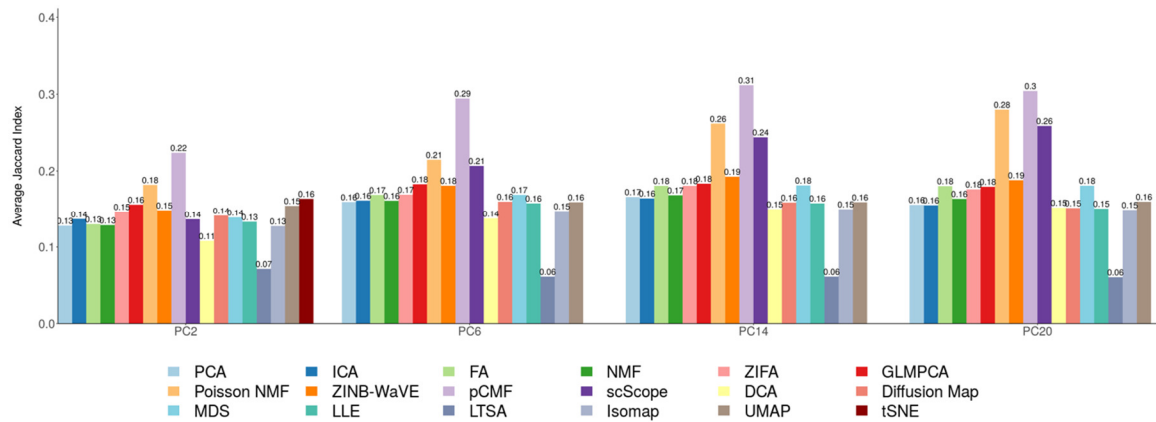


Figure S15. DR method performance evaluated by ARI in the downstream cell clustering analysis with k-means. We compared 18 DR methods (columns), including factor analysis (FA), principal component analysis (PCA), independent component analysis (ICA), Diffusion Map, nonnegative matrix factorization (NMF), Poisson NMF, zero-inflated factor analysis (ZIFA), zero-inflated negative binomial based wanted variation extraction (ZINB-WaVE), probabilistic count matrix factorization (pCMF), deep count autoencoder network (DCA), scScope, generalized linear model principal component analysis (GLMPCA), multidimensional scaling (MDS), locally linear embedding (LLE), local tangent space alignment (LTSA), Isomap, uniform manifold approximation and projection (UMAP), and t-distributed stochastic neighbor embedding (tSNE). We evaluated their performance on 14 real scRNASeq data sets (UMI-based data are labeled as purple; nonUMI-based data are labeled as blue) and 2 simulated data sets (rows). The simulated data based on Kumar data is labeled with #. The performance of each DR method is measured by normalized mutual information (NMI). For each data set, we compared the four different number of low-dimensional components. The four numbers equal to 0.5%, 1%, 2%, and 3% of the total number of cells in big data and equal to 2, 6, 14, and 20 in small data (which are labeled with *). For convenience, we only listed 0.5%, 1%, 2%, and 3% on x-axis. No results for ICA and LTSA are shown in the table (grey fills) because ICA cannot handle the large number of features in that data or estimated zero low-dimensional components. Note that, for tSNE, we only extracted two low-dimensional components due to the limitation of the tSNE software.

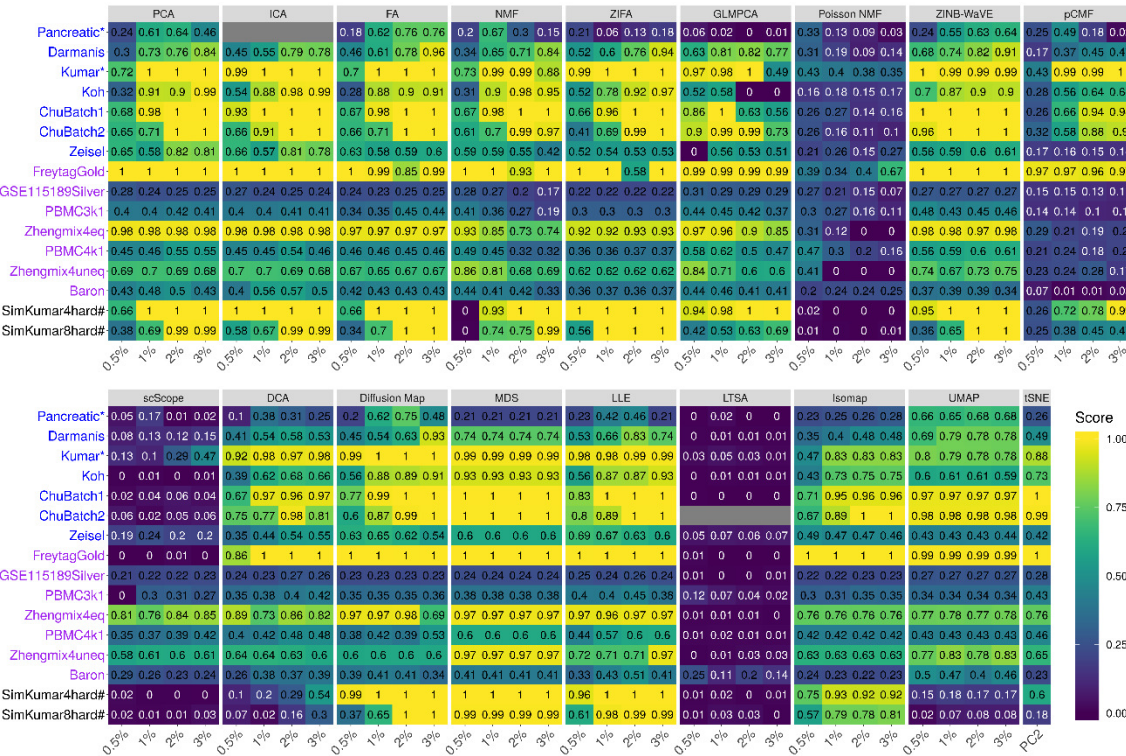


Figure S16. Bar plots show the average performance of different DR methods based on *k*-means clustering. The performance is measured by average normalized mutual information (NMI; **A**) or average adjusted rand index (ARI; **B**), both averaged across 16 data sets. We compared 18 DR methods, including factor analysis (FA; light green), principal component analysis (PCA; light blue), independent component analysis (ICA; blue), Diffusion Map (pink), nonnegative matrix factorization (NMF; green), Poisson NMF (light orange), zero-inflated factor analysis (ZIFA; light pink), zero-inflated negative binomial based wanted variation extraction (ZINB-WaVE; orange), probabilistic count matrix factorization (pCMF; light purple), deep count autoencoder network (DCA; yellow), scScope (purple), generalized linear model principal component analysis (GLMPCA; red), multidimensional scaling (MDS; cyan), locally linear embedding (LLE; blue green), local tangent space alignment (LTSA; teal blue), Isomap (grey), uniform manifold approximation and projection (UMAP; brown), and t-distributed stochastic neighbor embedding (tSNE; dark red). We used log2 Count transformation for the subset of DR methods that use normalized data. For each data set, we compared the four different number of low-dimensional data. The four numbers we used equal to 0.5%, 1%, 2%, and 3% of the total number of cells in big data and equal to 2, 6, 14, and 20 in small data. For convenience, we only listed 0.5%, 1%, 2%, and 3% on x-axis. Note that, for tSNE, we only extracted two low-dimensional components due to the limitation of the tSNE software.

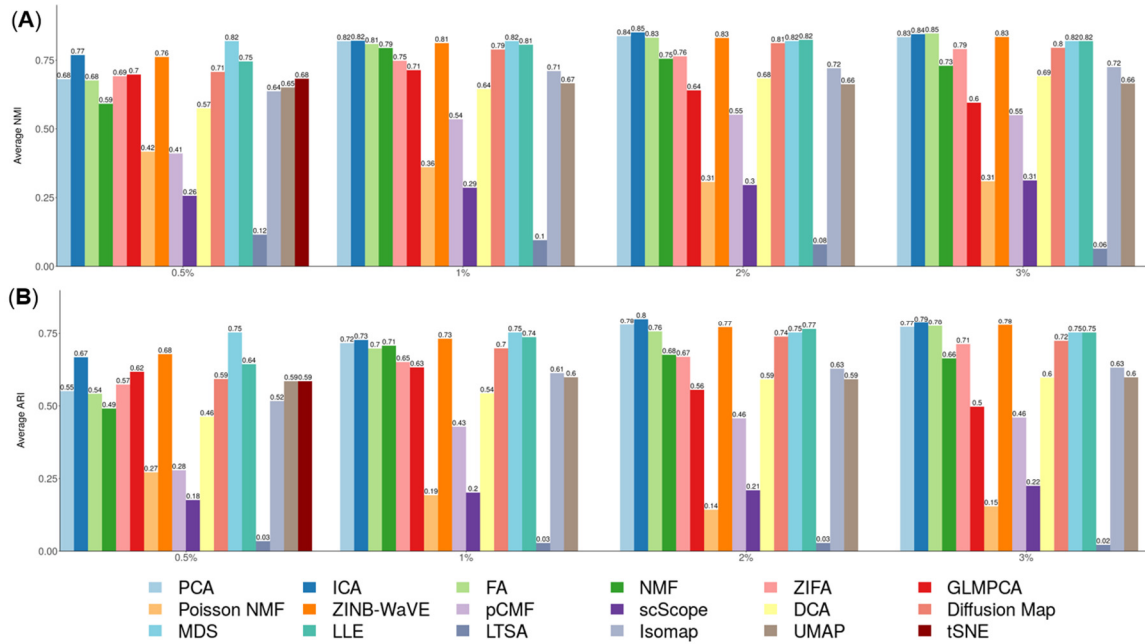


Figure S17. DR method performance evaluated by NMI in the downstream cell clustering analysis with hierarchical clustering. We compared 17 DR methods (columns), including factor analysis (FA), principal component analysis (PCA), independent component analysis (ICA), Diffusion Map, nonnegative matrix factorization (NMF), Poisson NMF, zero-inflated factor analysis (ZIFA), zero-inflated negative binomial based wanted variation extraction (ZINB-WaVE), probabilistic count matrix factorization (pCMF), deep count autoencoder network (DCA), generalized linear model principal component analysis (GLMPCA), multidimensional scaling (MDS), locally linear embedding (LLE), local tangent space alignment (LTSA), Isomap, uniform manifold approximation and projection (UMAP), and t-distributed stochastic neighbor embedding (tSNE). We evaluated their performance on 14 real scRNASeq data sets and 2 simulated data sets (rows). The simulated data based on Kumar data is labeled with #. We used log2 Count transformation for the subset of DR methods that use normalized data. For each data set, we compared the four different number of low-dimensional data. The four numbers we used equal to 0.5%, 1%, 2%, and 3% of the total number of cells in big data and equal to 2, 6, 14, and 20 in small data (which were labeled with *). For convenience, we only listed 0.5%, 1%, 2%, and 3% on x-axis. No results for ICA, tSNE or GLMPCA are shown in the table (grey fills) because ICA cannot handle the large number of features; tSNE and GLMPCA have error when clustering cells. Note that, for tSNE, we only extracted two low-dimensional components due to the limitation of the tSNE software.



Figure S18. DR method performance evaluated by ARI in the downstream cell clustering analysis with hierarchical clustering. We compared 17 DR methods (columns), including factor analysis (FA), principal component analysis (PCA), independent component analysis (ICA), Diffusion Map, nonnegative matrix factorization (NMF), Poisson NMF, zero-inflated factor analysis (ZIFA), zero-inflated negative binomial based wanted variation extraction (ZINB-WaVE), probabilistic count matrix factorization (pCMF), deep count autoencoder network (DCA), generalized linear model principal component analysis (GLMPCA), multidimensional scaling (MDS), locally linear embedding (LLE), local tangent space alignment (LTSA), Isomap, uniform manifold approximation and projection (UMAP), and t-distributed stochastic neighbor embedding (tSNE). We evaluated their performance on 14 real scRNASeq data sets and 2 simulated data sets (rows). The simulated data based on Kumar data is labeled with #. We used log2 Count transformation for the subset of DR methods that use normalized data. For each data set, we compared the four different number of low-dimensional data. The four numbers we used equal to 0.5%, 1%, 2%, and 3% of the total number of cells in big data and equal to 2, 6, 14, and 20 in small data (which were labeled with *). For convenience, we only listed 0.5%, 1%, 2%, and 3% on x-axis. No results for ICA or GLMPCA are shown in the table (grey fills) because ICA cannot handle the large number of features; GLMPCA has error when clustering cells. Note that, for tSNE, we only extracted two low-dimensional components due to the limitation of the tSNE software.

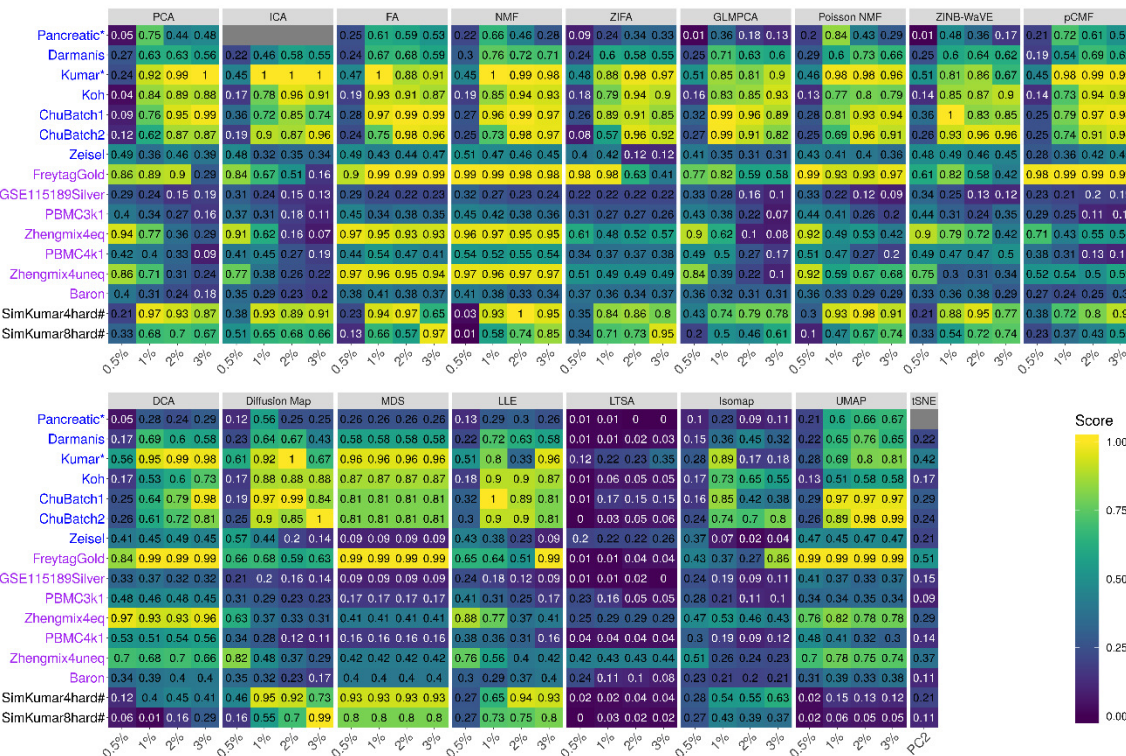


Figure S19. Bar plots show the average performance of different DR methods based on hierarchical clustering. The performance is measured by normalized mutual information (NMI; **A**) or adjusted rand index (ARI; **B**), both averaged across 16 data sets. We compared 17 DR methods, including factor analysis (FA; light green), principal component analysis (PCA; light blue), independent component analysis (ICA; blue), Diffusion Map (pink), nonnegative matrix factorization (NMF; green), Poisson NMF (light orange), zero-inflated factor analysis (ZIFA; light pink), zero-inflated negative binomial based wanted variation extraction (ZINB-WaVE; orange), probabilistic count matrix factorization (pCMF; light purple), deep count autoencoder network (DCA; yellow), generalized linear model principal component analysis (GLMPCA; red), multidimensional scaling (MDS; cyan), locally linear embedding (LLE; blue green), local tangent space alignment (LTSA; teal blue), Isomap (grey), uniform manifold approximation and projection (UMAP; brown), and t-distributed stochastic neighbor embedding (tSNE; dark red). We used log2 Count transformation for the subset of DR methods that use normalized data. For each data set, we compared the four different number of low-dimensional data. The four numbers we used equal to 0.5%, 1%, 2%, and 3% of the total number of cells in big data and equal to 2, 6, 14, and 20 in small data. For convenience, we only listed 0.5%, 1%, 2%, and 3% on x-axis. Note that, for tSNE, we only extracted two low-dimensional components due to the limitation of the tSNE software.

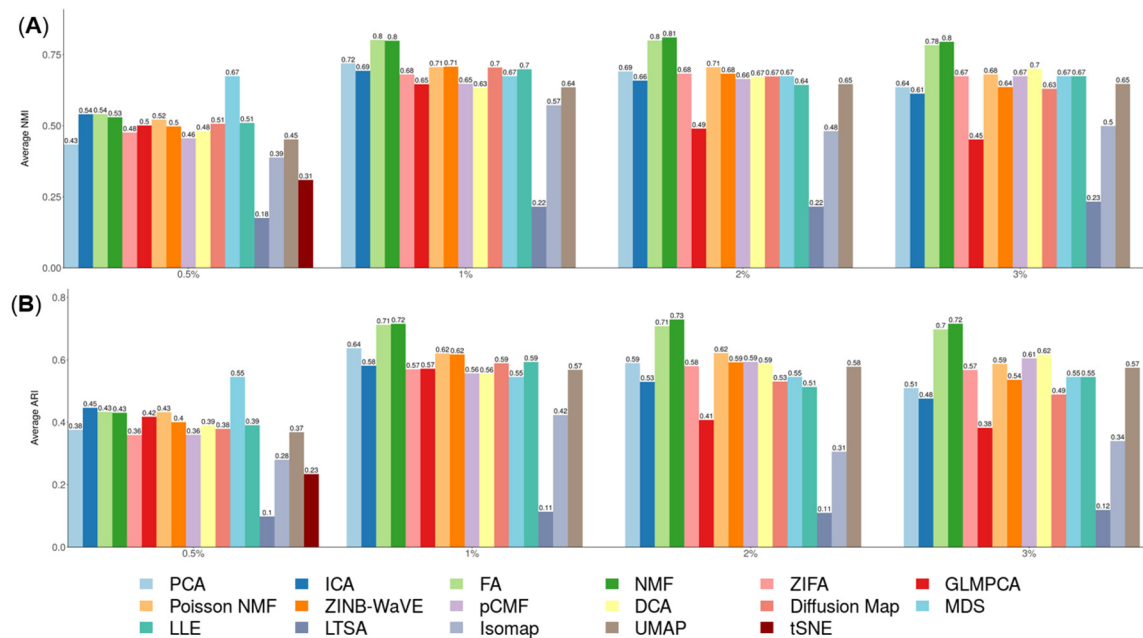


Figure S20. DR method performance evaluated by NMI in the downstream cell clustering analysis with Louvain clustering. We compared 18 DR methods (columns), including factor analysis (FA), principal component analysis (PCA), independent component analysis (ICA), Diffusion Map, nonnegative matrix factorization (NMF), Poisson NMF, zero-inflated factor analysis (ZIFA), zero-inflated negative binomial based wanted variation extraction (ZINB-WaVE), probabilistic count matrix factorization (pCMF), deep count autoencoder network (DCA), scScope, generalized linear model principal component analysis (GLMPCA), multidimensional scaling (MDS), locally linear embedding (LLE), local tangent space alignment (LTSA), Isomap, uniform manifold approximation and projection (UMAP), and t-distributed stochastic neighbor embedding (tSNE). We evaluated their performance on 14 real scRNASeq data sets and 2 simulated data sets (rows). The simulated data based on Kumar data is labeled with #. We used log2 Count transformation for the subset of DR methods that use normalized data. For each data set, we compared the four different number of low-dimensional data. The four numbers we used equal to 0.5%, 1%, 2%, and 3% of the total number of cells in big data and equal to 2, 6, 14, and 20 in small data (which were labeled with *). For convenience, we only listed 0.5%, 1%, 2%, and 3% on x-axis. No results for ICA are shown in the table (grey fills) because ICA cannot handle the large number of features. Note that, for tSNE, we only extracted two low-dimensional components due to the limitation of the tSNE software.

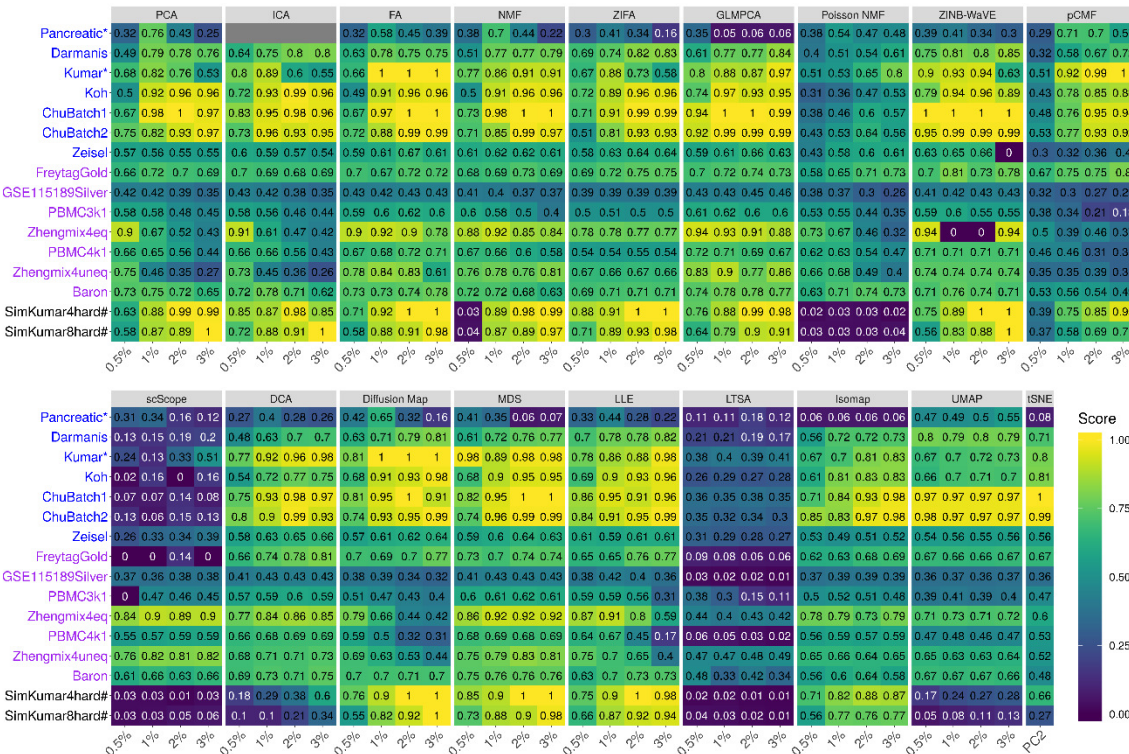


Figure S21. DR method performance evaluated by ARI in the downstream cell clustering analysis with Louvain clustering. We compared 18 DR methods (columns), including factor analysis (FA), principal component analysis (PCA), independent component analysis (ICA), Diffusion Map, nonnegative matrix factorization (NMF), Poisson NMF, zero-inflated factor analysis (ZIFA), zero-inflated negative binomial based wanted variation extraction (ZINB-WaVE), probabilistic count matrix factorization (pCMF), deep count autoencoder network (DCA), scScope, generalized linear model principal component analysis (GLMPCA), multidimensional scaling (MDS), locally linear embedding (LLE), local tangent space alignment (LTSA), Isomap, uniform manifold approximation and projection (UMAP), and t-distributed stochastic neighbor embedding (tSNE; dark red). We evaluated their performance on 14 real scRNASeq data sets and 2 simulated data sets (rows). The simulated data based on Kumar data is labeled with #. We used log2 Count transformation for the subset of DR methods that use normalized data. For each data set, we compared the four different number of low-dimensional data. The four numbers we used equal to 0.5%, 1%, 2%, and 3% of the total number of cells in big data and equal to 2, 6, 14, and 20 in small data (which were labeled with *). For convenience, we only listed 0.5%, 1%, 2%, and 3% on x-axis. No results for ICA are shown in the table (grey fills) because ICA cannot handle the large number of features. Note that, for tSNE, we only extracted two low-dimensional components due to the limitation of the tSNE software.

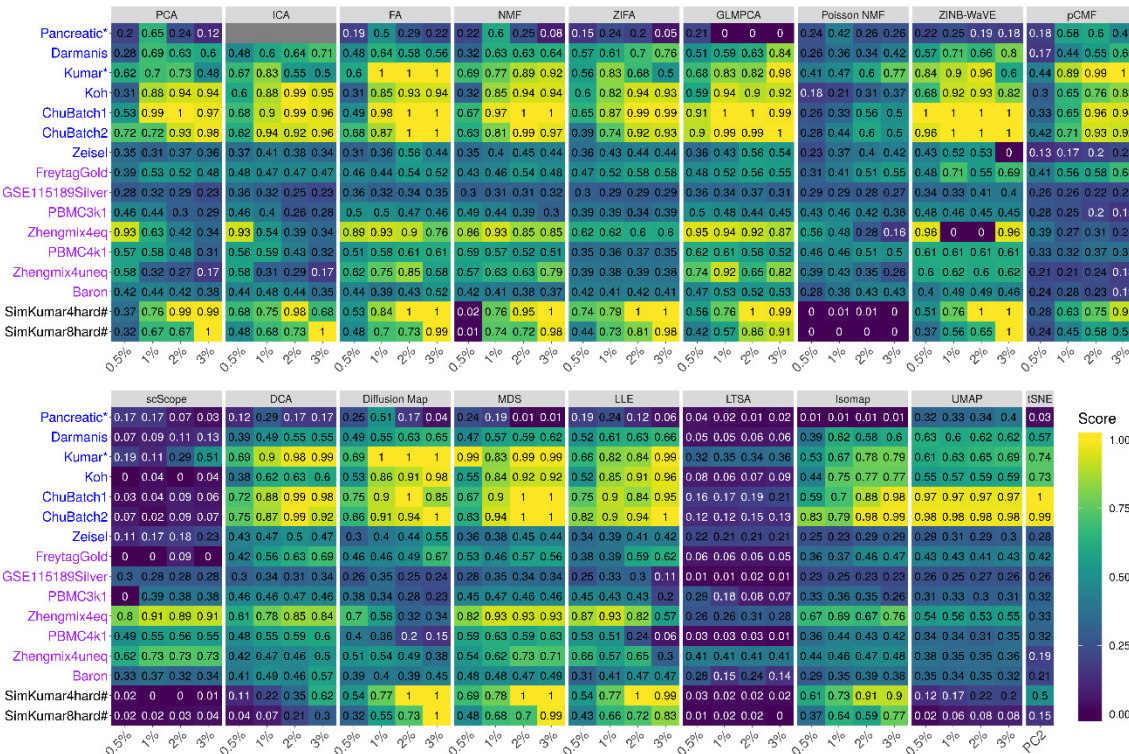


Figure S22. Bar plots show the average performance of different DR methods based on Louvain clustering. The performance is measured by normalized mutual information (NMI; **A**) or adjusted rand index (ARI; **B**), both averaged across 16 data sets. We compared 18 DR methods, including factor analysis (FA; light green), principal component analysis (PCA; light blue), independent component analysis (ICA; blue), Diffusion Map (pink), nonnegative matrix factorization (NMF; green), Poisson NMF (light orange), zero-inflated factor analysis (ZIFA; light pink), zero-inflated negative binomial based wanted variation extraction (ZINB-WaVE; orange), probabilistic count matrix factorization (pCMF; light purple), deep count autoencoder network (DCA; yellow), scScope, generalized linear model principal component analysis (GLMPCA; red), multidimensional scaling (MDS; cyan), locally linear embedding (LLE; blue green), local tangent space alignment (LTSA; teal blue), Isomap (grey), uniform manifold approximation and projection (UMAP; brown), and t-distributed stochastic neighbor embedding (tSNE; dark red). We used log2 Count transformation for the subset of DR methods that use normalized data. For each data set, we compared the four different number of low-dimensional data. The four numbers we used equal to 0.5%, 1%, 2%, and 3% of the total number of cells in big data and equal to 2, 6, 14, and 20 in small data. For convenience, we only listed 0.5%, 1%, 2%, and 3% on x-axis. Note that, for tSNE, we only extracted two low-dimensional components due to the limitation of the tSNE software.

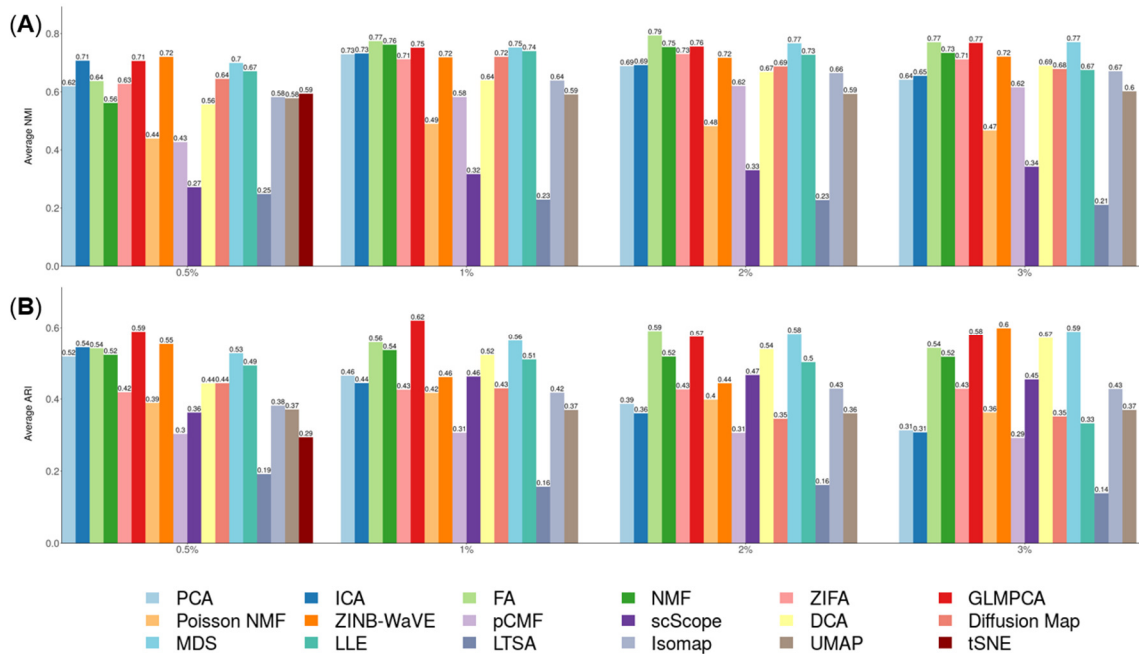


Figure S23. DR method performance with log-2 CPM transformed data evaluated based on downstream cell clustering analysis. Performance is evaluated by normalized mutual index (NMI) either based on k -means clustering. We compared 11 DR methods (columns), including factor analysis (FA), principal component analysis (PCA), independent component analysis (ICA), Diffusion Map, nonnegative matrix factorization (NMF), multidimensional scaling (MDS), locally linear embedding (LLE), local tangent space alignment (LTSA), Isomap, uniform manifold approximation and projection (UMAP), and t-distributed stochastic neighbor embedding (tSNE). We evaluated their performance on 14 real scRNASeq data sets and 2 simulated data sets (rows). The simulated data based on Kumar data is labeled with #. We used log2 CPM transformation for the subset of DR methods that use normalized data. For each data set, we compared the four different number of low-dimensional data. The four numbers we used equal to 0.5%, 1%, 2%, and 3% of the total number of cells in big data and equal to 2, 6, 14, and 20 in small data (labeled with *). No results for ICA are shown in the Pancreatic data (grey fills) because ICA cannot handle the large number of features in the data. Note that, for tSNE, we only extracted two low-dimensional components due to the limitation of the tSNE software.

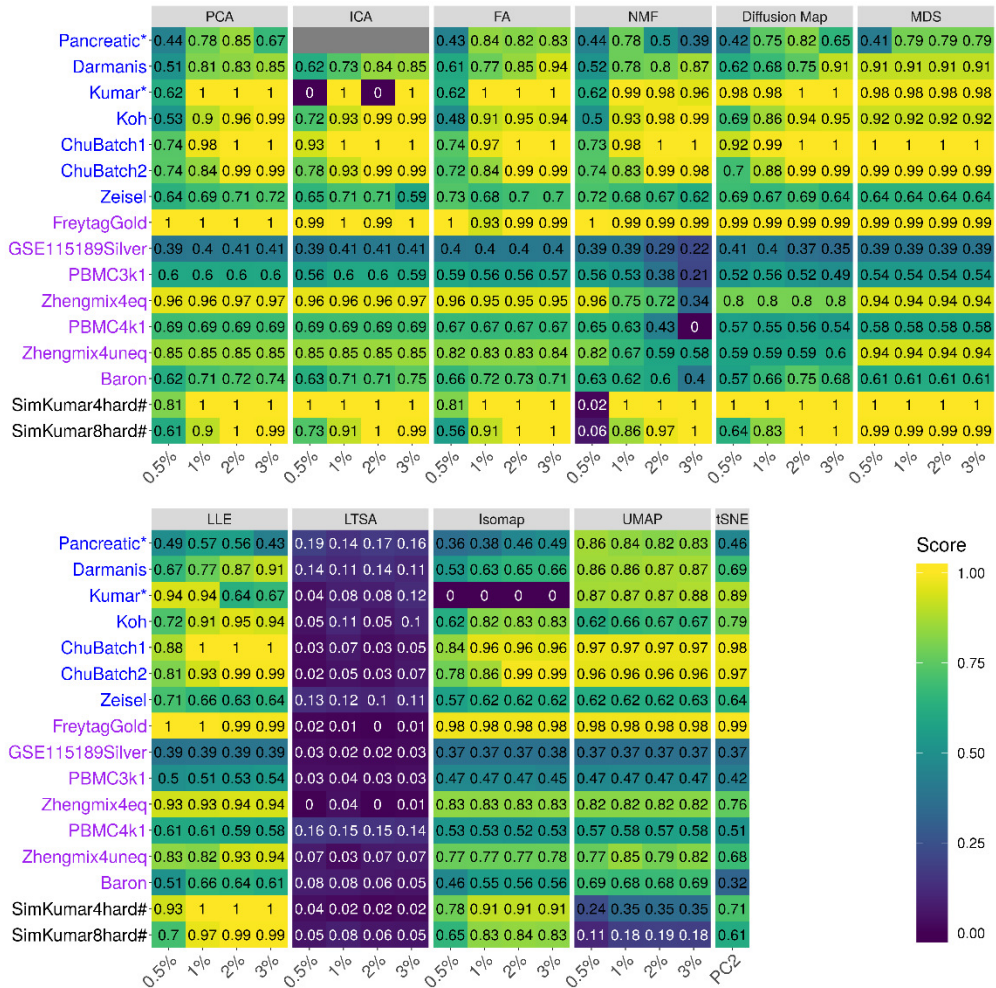


Figure S24. DR method performance with log-2 CPM transformed data evaluated based on downstream cell clustering analysis. Performance is evaluated by normalized mutual index (NMI) either based on hierarchical clustering. We compared 11 DR methods (columns), including factor analysis (FA), principal component analysis (PCA), independent component analysis (ICA), Diffusion Map, nonnegative matrix factorization (NMF), multidimensional scaling (MDS), locally linear embedding (LLE), local tangent space alignment (LTSA), Isomap, uniform manifold approximation and projection (UMAP), and t-distributed stochastic neighbor embedding (tSNE). We evaluated their performance on 14 real scRNASeq data sets and 2 simulated data sets (rows). The simulated data based on Kumar data is labeled with #. We used log2 CPM transformation for the subset of DR methods that use normalized data. For each data set, we compared the four different number of low-dimensional data. The four numbers we used equal to 0.5%, 1%, 2%, and 3% of the total number of cells in big data and equal to 2, 6, 14, and 20 in small data (labeled with *). No results for ICA are shown in the Pancreatic data (grey fills) because ICA cannot handle the large number of features in the data. Note that, for tSNE, we only extracted two low-dimensional components due to the limitation of the tSNE software.

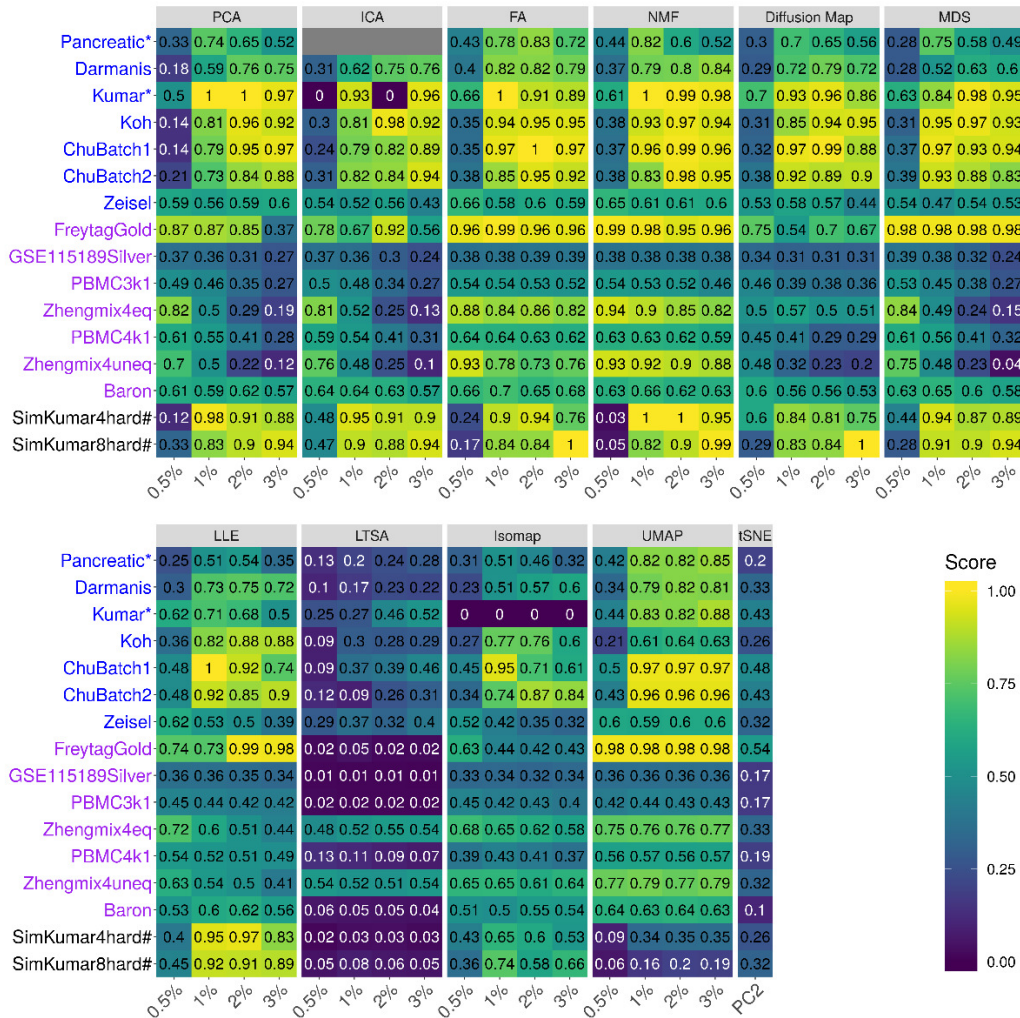


Figure S25. DR method performance with log-2 CPM transformed data evaluated based on downstream cell clustering analysis. Performance is evaluated by normalized mutual index (NMI) either based on Louvain method. We compared 11 DR methods (columns), including factor analysis (FA), principal component analysis (PCA), independent component analysis (ICA), Diffusion Map, nonnegative matrix factorization (NMF), multidimensional scaling (MDS), locally linear embedding (LLE), local tangent space alignment (LTSA), Isomap, uniform manifold approximation and projection (UMAP), and t-distributed stochastic neighbor embedding (tSNE). We evaluated their performance on 14 real scRNASeq data sets and 2 simulated data sets (rows). The simulated data based on Kumar data is labeled with #. We used log2 CPM transformation for the subset of DR methods that use normalized data. For each data set, we compared the four different number of low-dimensional data. The four numbers we used equal to 0.5%, 1%, 2%, and 3% of the total number of cells in big data and equal to 2, 6, 14, and 20 in small data (labeled with *). No results for ICA are shown in the Pancreatic data (zeros) because ICA cannot handle the large number of features in the data. Note that, for tSNE, we only extracted two low-dimensional components due to the limitation of the tSNE software.

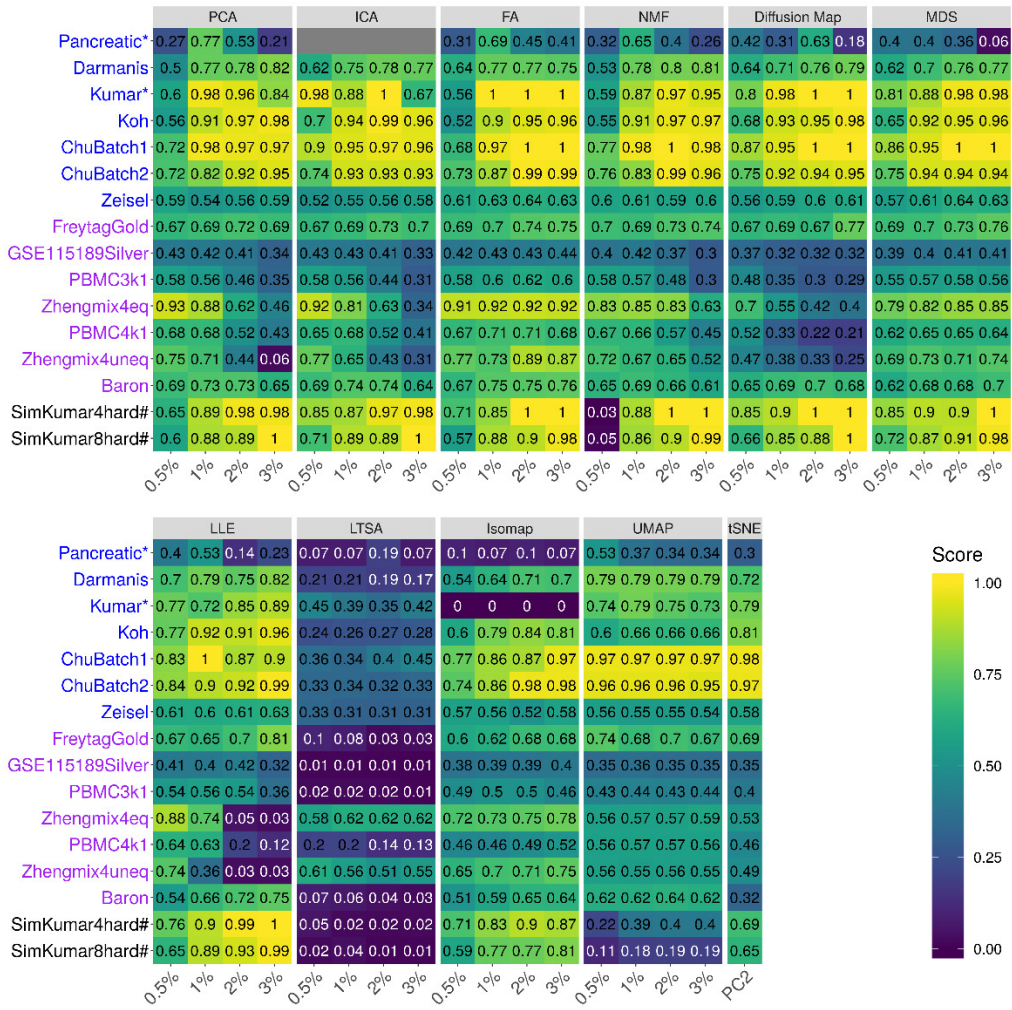


Figure S26. Bar plots show the average performance of a subset of DR methods that use log2 CPM normalized data. The performance of each DR method is measured by normalized mutual index (NMI) using either *k*-means clustering (**A**), hierarchical clustering (**B**) or Louvain method (**C**), the averaged across 16 date sets. We used log2 CPM transformation for the subset of DR methods that use normalized data. We compared 11 DR methods that use normalized data, including factor analysis (FA; light green), principal component analysis (PCA; light blue), independent component analysis (ICA; blue), Diffusion Map (pink), nonnegative matrix factorization (NMF; green), multidimensional scaling (MDS; cyan), locally linear embedding (LLE; blue green), local tangent space alignment (LTSA; teal blue), Isomap (grey), uniform manifold approximation and projection (UMAP; brown), and t-distributed stochastic neighbor embedding (tSNE; dark red). For each data set, we compared the four different number of low-dimensional data. The four numbers we used equal to 0.5%, 1%, 2%, and 3% of the total number of cells in big data and equal to 2, 6, 14, and 20 in small data. For convenience, we only listed 0.5%, 1%, 2%, and 3% on x-axis. Note that, for tSNE, we only extracted two low-dimensional components due to the limitation of the tSNE software.

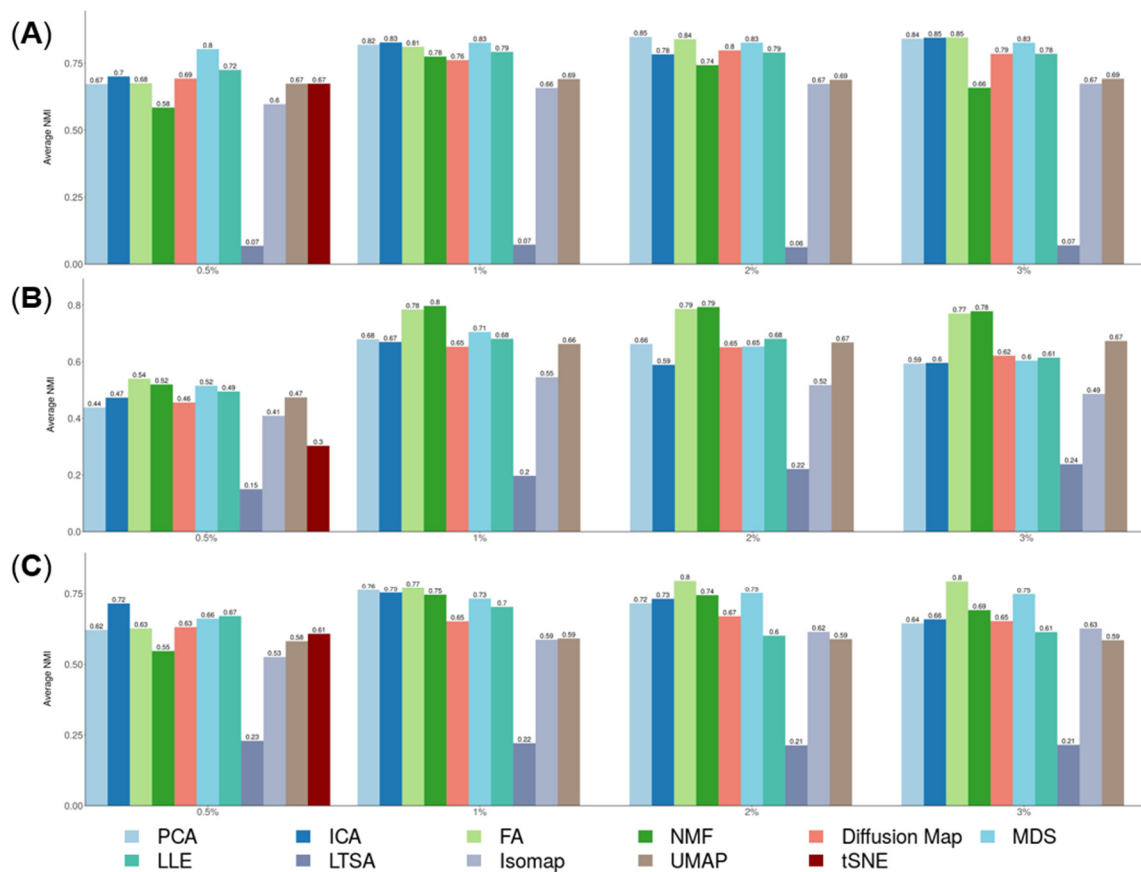


Figure S27. DR method performance with z-score transformed data in downstream cell clustering analysis. Performance is evaluated by normalized mutual index (NMI) either based on k -means clustering. We compared 10 DR methods (columns), including factor analysis (FA), principal component analysis (PCA), independent component analysis (ICA), Diffusion Map, multidimensional scaling (MDS), locally linear embedding (LLE), local tangent space alignment (LTSA), Isomap, uniform manifold approximation and projection (UMAP), and t-distributed stochastic neighbor embedding (tSNE). We evaluated their performance on 14 real scRNASeq data sets and 2 simulated data sets (rows). The simulated data based on Kumar data is labeled with #. We used z-score transformation for the subset of DR methods that use normalized data. For each data set, we compared the four different number of low-dimensional data. The four numbers we used equal to 0.5%, 1%, 2%, and 3% of the total number of cells in big data and equal to 2, 6, 14, and 20 in small data which were labeled with *. For convenience, we only listed 0.5%, 1%, 2%, and 3% on x-axis. No results for ICA are shown in the Pancreatic data (grey fills) because ICA cannot handle the large number of features in the data. No results for NMF are shown because z-score normalization have negative values. Note that, for tSNE, we only extracted two low-dimensional components due to the limitation of the tSNE software.

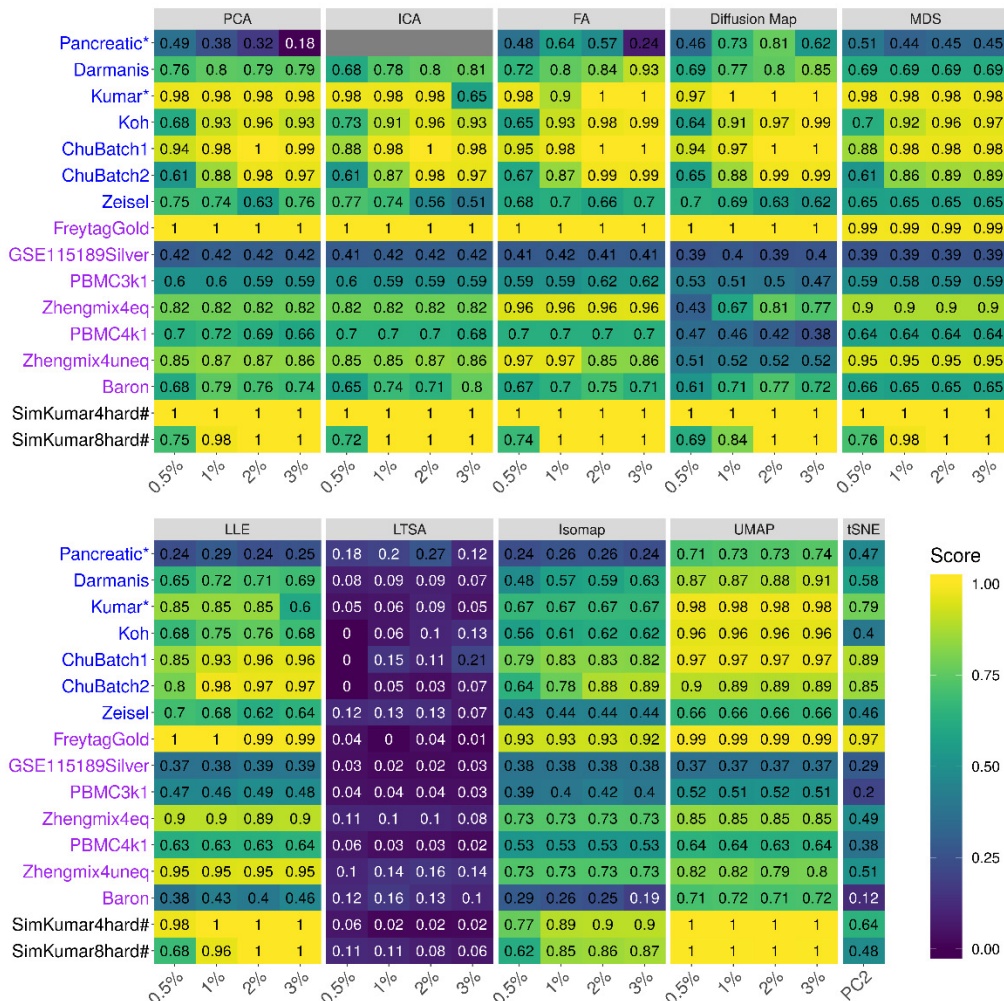


Figure S28. DR method performance with z-score transformed data in downstream cell clustering analysis. Performance is evaluated by normalized mutual index (NMI) either based on hierarchical clustering. We compared 10 DR methods (columns), including factor analysis (FA), principal component analysis (PCA), independent component analysis (ICA), Diffusion Map, multidimensional scaling (MDS), locally linear embedding (LLE), local tangent space alignment (LTSA), Isomap, uniform manifold approximation and projection (UMAP), and t-distributed stochastic neighbor embedding (tSNE). We evaluated their performance on 14 real scRNASeq data sets and 2 simulated data sets (rows). The simulated data based on Kumar data is labeled with #. We used z-score transformation for the subset of DR methods that use normalized data. For each data set, we compared the four different number of low-dimensional data. The four numbers we used equal to 0.5%, 1%, 2%, and 3% of the total number of cells in big data and equal to 2, 6, 14, and 20 in small data which were labeled with *. For convenience, we only listed 0.5%, 1%, 2%, and 3% on x-axis. No results for ICA are shown in the Pancreatic data (grey fills) because ICA cannot handle the large number of features in the data. No results for NMF are shown because z-score normalization have negative values. Note that, for tSNE, we only extracted two low-dimensional components due to the limitation of the tSNE software.

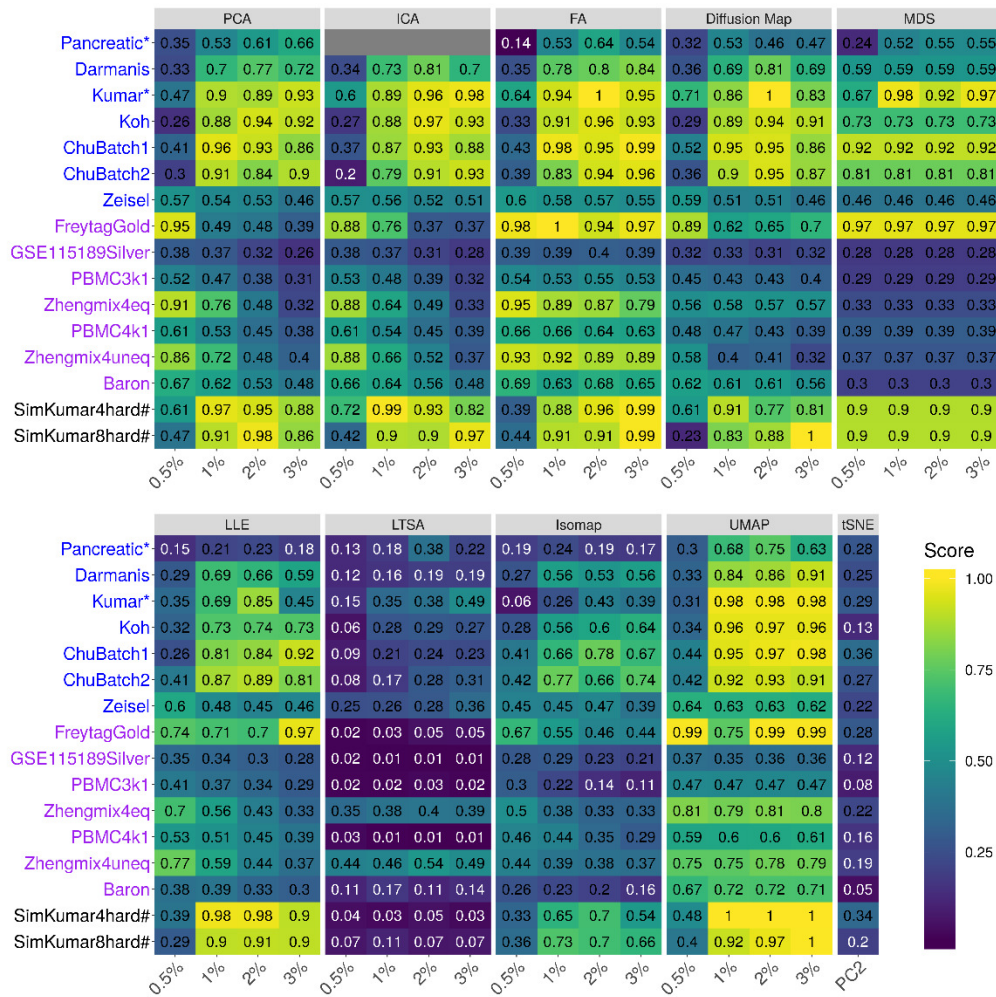


Figure S29. DR method performance with z-score transformed data in downstream cell clustering analysis. Performance is evaluated by normalized mutual index (NMI) either based on Louvain method. We compared 10 DR methods (columns), including factor analysis (FA), principal component analysis (PCA), independent component analysis (ICA), Diffusion Map, multidimensional scaling (MDS), locally linear embedding (LLE), local tangent space alignment (LTSA), Isomap, uniform manifold approximation and projection (UMAP), and t-distributed stochastic neighbor embedding (tSNE). We evaluated their performance on 14 real scRNASeq data sets and 2 simulated data sets (rows). The simulated data based on Kumar data is labeled with #. We used z-score transformation for the subset of DR methods that use normalized data. For each data set, we compared the four different number of low-dimensional data. The four numbers we used equal to 0.5%, 1%, 2%, and 3% of the total number of cells in big data and equal to 2, 6, 14, and 20 in small data which were labeled with *. For convenience, we only listed 0.5%, 1%, 2%, and 3% on x-axis. No results for ICA are shown in the Pancreatic data (grey fills) because ICA cannot handle the large number of features in the data. No results for NMF are shown because z-score normalization have negative values. Note that, for tSNE, we only extracted two low-dimensional components due to the limitation of the tSNE software.

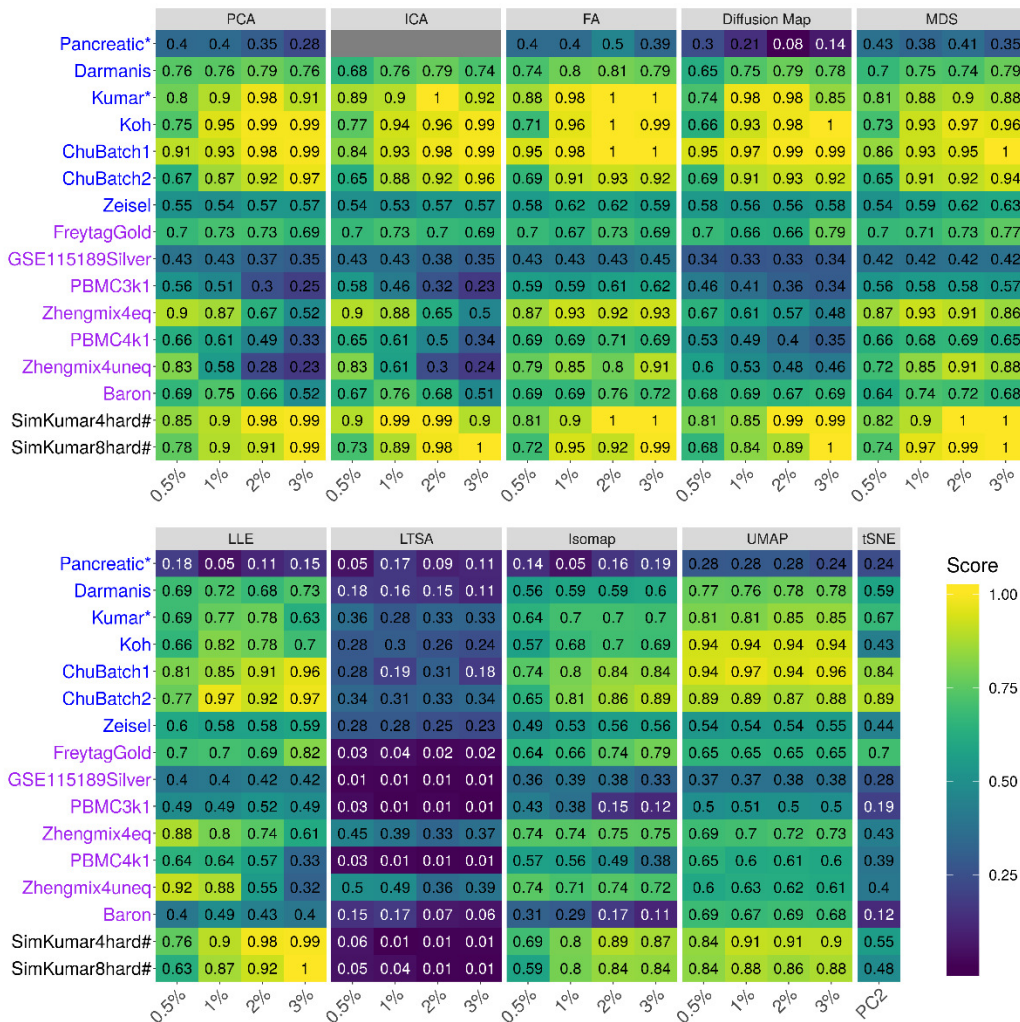


Figure S30. Bar plots show the average performance of a subset of DR methods that use z-score normalized data. The performance of each DR method is measured by normalized mutual index (NMI) using either k -means clustering (**A**), hierarchical clustering (**B**) or Louvain method (**C**), the averaged across 16 date sets. We used z-score transformation for the subset of DR methods that use normalized data. We compared 10 DR methods that use normalized data, including factor analysis (FA; light green), principal component analysis (PCA; light blue), independent component analysis (ICA; blue), Diffusion Map (pink), multidimensional scaling (MDS; cyan), locally linear embedding (LLE; blue green), local tangent space alignment (LTSA; teal blue), Isomap (grey), uniform manifold approximation and projection (UMAP; brown), and t-distributed stochastic neighbor embedding (tSNE; dark red). For each data set, we compared the four different number of low-dimensional data. The four numbers we used equal to 0.5%, 1%, 2%, and 3% of the total number of cells in big data and equal to 2, 6, 14, and 20 in small data. For convenience, we only listed 0.5%, 1%, 2%, and 3% on x-axis. The four numbers we used equal to 0.5%, 1%, 2%, and 3% of the total number of cells in big data and equal to 2, 6, 14, and 20 in small data. For convenience, we only listed 0.5%, 1%, 2%, and 3% on x-axis. Note that, for tSNE, we only extracted two low-dimensional components due to the limitation of the tSNE software.

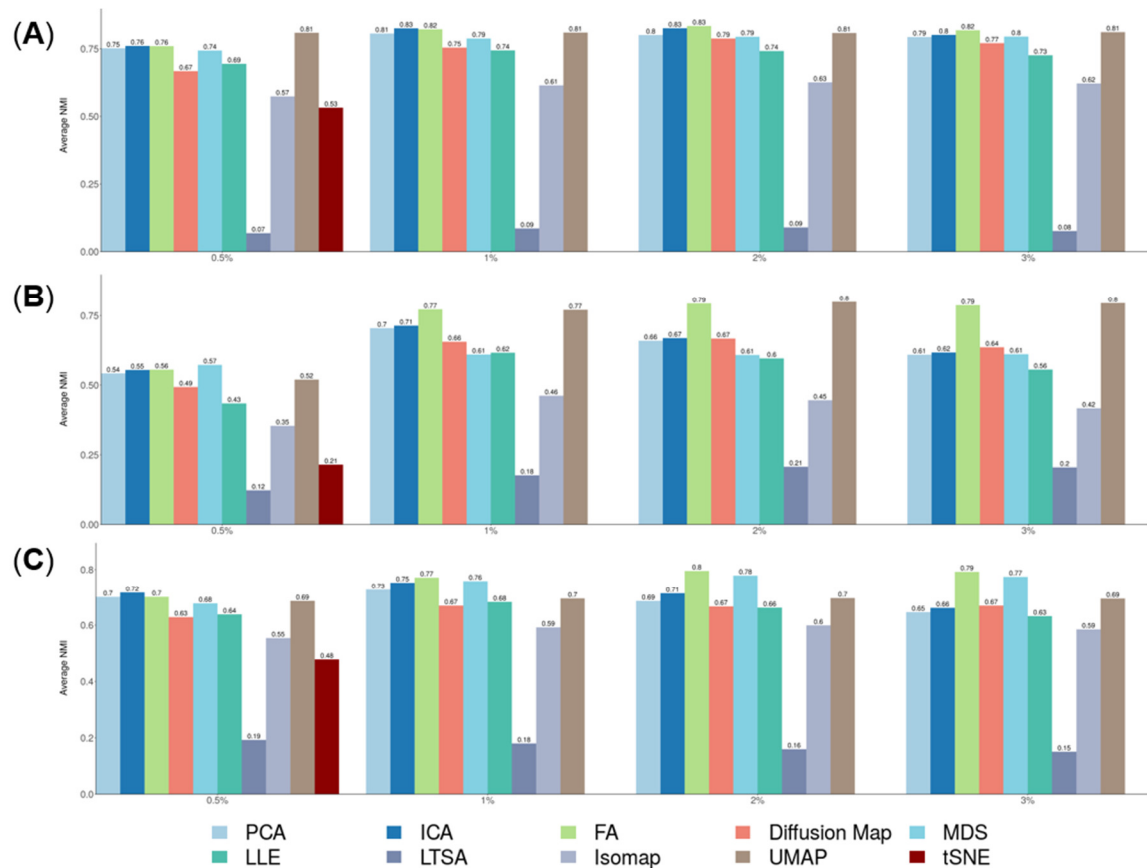


Figure S31. Bar plots show the average NMI of different DR methods on UMI-based data and nonUMI-based data. The performance is measured by average NMI across UMI-based data (**A**; 7 data sets) or nonUMI-based data (**B**; 7 data sets). We compared 18 DR methods, including factor analysis (FA; light green), principal component analysis (PCA; light blue), independent component analysis (ICA; blue), Diffusion Map (pink), nonnegative matrix factorization (NMF; green), Poisson NMF (light orange), zero-inflated factor analysis (ZIFA; light pink), zero-inflated negative binomial based wanted variation extraction (ZINB-WaVE; orange), probabilistic count matrix factorization (pCMF; light purple), deep count autoencoder network (DCA; yellow), scScope (purple), generalized linear model principal component analysis (GLMPCA; red), multidimensional scaling (MDS; cyan), locally linear embedding (LLE; blue green), local tangent space alignment (LTSA; teal blue), Isomap (grey), uniform manifold approximation and projection (UMAP; brown), and t-distributed stochastic neighbor embedding (tSNE; dark red). We used log2 count transformation for the subset of DR methods that use normalized data. For each data set, we compared the four different number of low-dimensional data. The four numbers we used equal to 0.5%, 1%, 2%, and 3% of the total number of cells in big data and equal to 2, 6, 14, and 20 in small data. For convenience, we only listed 0.5%, 1%, 2%, and 3% on x-axis. Note that, for tSNE, we only extracted two low-dimensional components due to the limitation of the tSNE software.

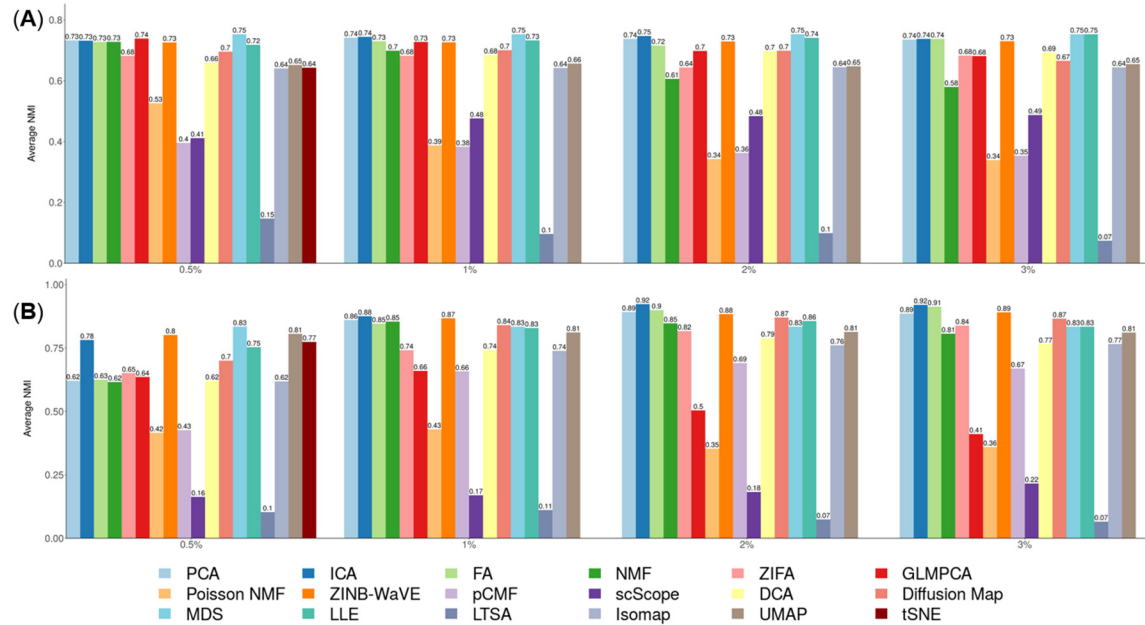


Figure S32. Scatter plots visualize the clusters of different DR methods on Kumar data set. We compared 17 DR methods (columns), including factor analysis (FA), principal component analysis (PCA), independent component analysis (ICA), Diffusion Map, nonnegative matrix factorization (NMF), Poisson NMF, zero-inflated factor analysis (ZIFA), zero-inflated negative binomial based wanted variation extraction (ZINB-WaVE), probabilistic count matrix factorization (pCMF), deep count autoencoder network (DCA), scScope, generalized linear model principal component analysis (GLMPCA), multidimensional scaling (MDS), locally linear embedding (LLE) , Isomap, uniform manifold approximation and projection (UMAP), and t-distributed stochastic neighbor embedding (tSNE). We used log2 count transformation for the subset of DR methods that use normalized data. For each data set, we first reduced the dimension to 20, then applied tSNE to visualize the clusters. Local tangent space alignment (LTSA) was excluded because of failing to extract low-dimensional components.

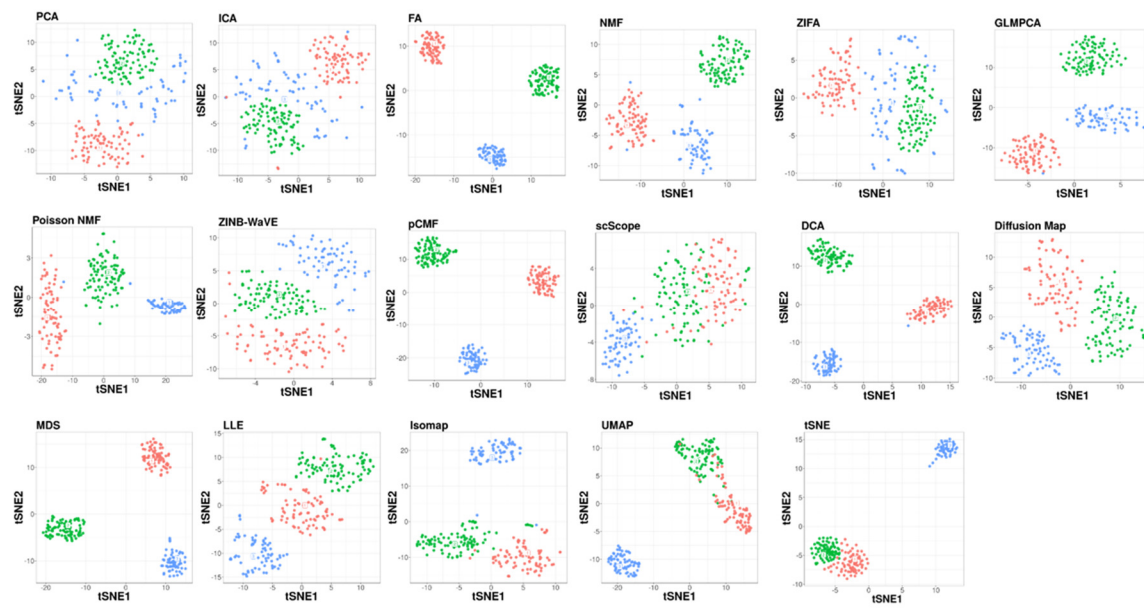


Figure S33. Scatter plots show the clusters of different DR methods on PBMC3k data set. We compared 18 DR methods (columns), including factor analysis (FA), principal component analysis (PCA), independent component analysis (ICA), Diffusion Map, nonnegative matrix factorization (NMF), Poisson NMF, zero-inflated factor analysis (ZIFA), zero-inflated negative binomial based wanted variation extraction (ZINB-WaVE), probabilistic count matrix factorization (pCMF), deep count autoencoder network (DCA), scScope, generalized linear model principal component analysis (GLMPCA), multidimensional scaling (MDS), locally linear embedding (LLE), local tangent space alignment (LTSA), Isomap, uniform manifold approximation and projection (UMAP), and t-distributed stochastic neighbor embedding (tSNE). We used log2 count transformation for the subset of DR methods that use normalized data. For each data set, we first reduced the dimension to 32, then applied tSNE to visualize the clusters.

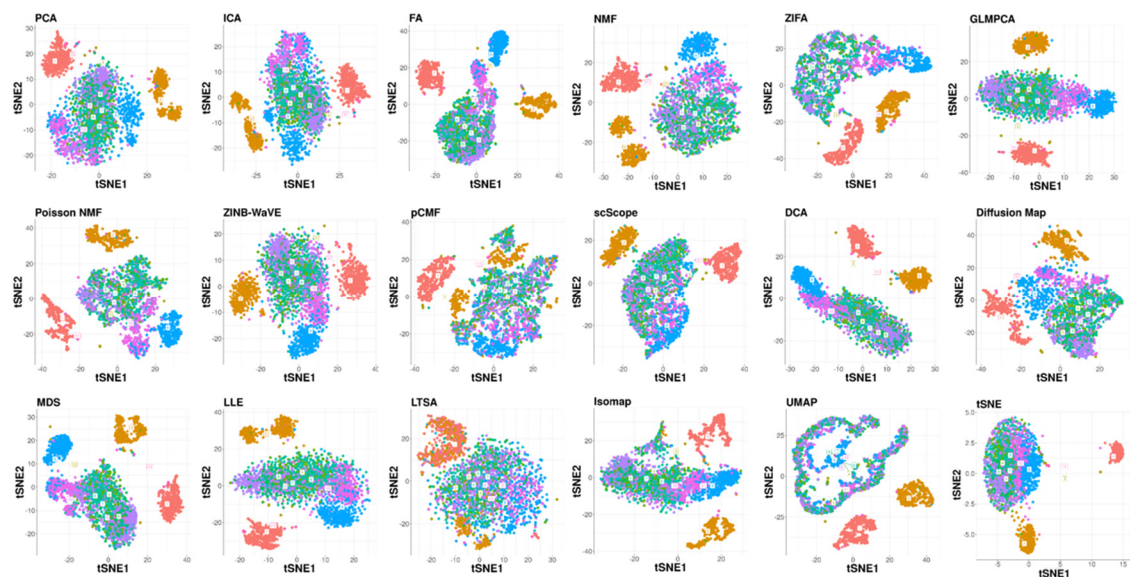


Figure S34. Bar plots show the F-measure of different DR methods on the rare data set PBMC3k1Rare1 (contains 4.0% CD34+ cells). The performance is measured by k -means clustering (**A**), hierarchical clustering (**B**) or Louvain method (**C**). We compared 18 DR methods, including factor analysis (FA; light green), principal component analysis (PCA; light blue), independent component analysis (ICA; blue), Diffusion Map (pink), nonnegative matrix factorization (NMF; green), Poisson NMF (light orange), zero-inflated factor analysis (ZIFA; light pink), zero-inflated negative binomial based wanted variation extraction (ZINB-WaVE; orange), probabilistic count matrix factorization (pCMF; light purple), deep count autoencoder network (DCA; yellow), scScope (purple), generalized linear model principal component analysis (GLMPCA; red), multidimensional scaling (MDS; cyan), locally linear embedding (LLE; blue green), local tangent space alignment (LTSA; teal blue), Isomap (grey), uniform manifold approximation and projection (UMAP; brown), and t-distributed stochastic neighbor embedding (tSNE; dark red). We used log2 count transformation for the subset of DR methods that use normalized data. For each data set, we compared the four different number of low-dimensional data. The four numbers we used equal to 0.5%, 1%, 2%, and 3% of the total number of cells. Note that, for tSNE, we only extracted two low-dimensional components due to the limitation of the tSNE software.

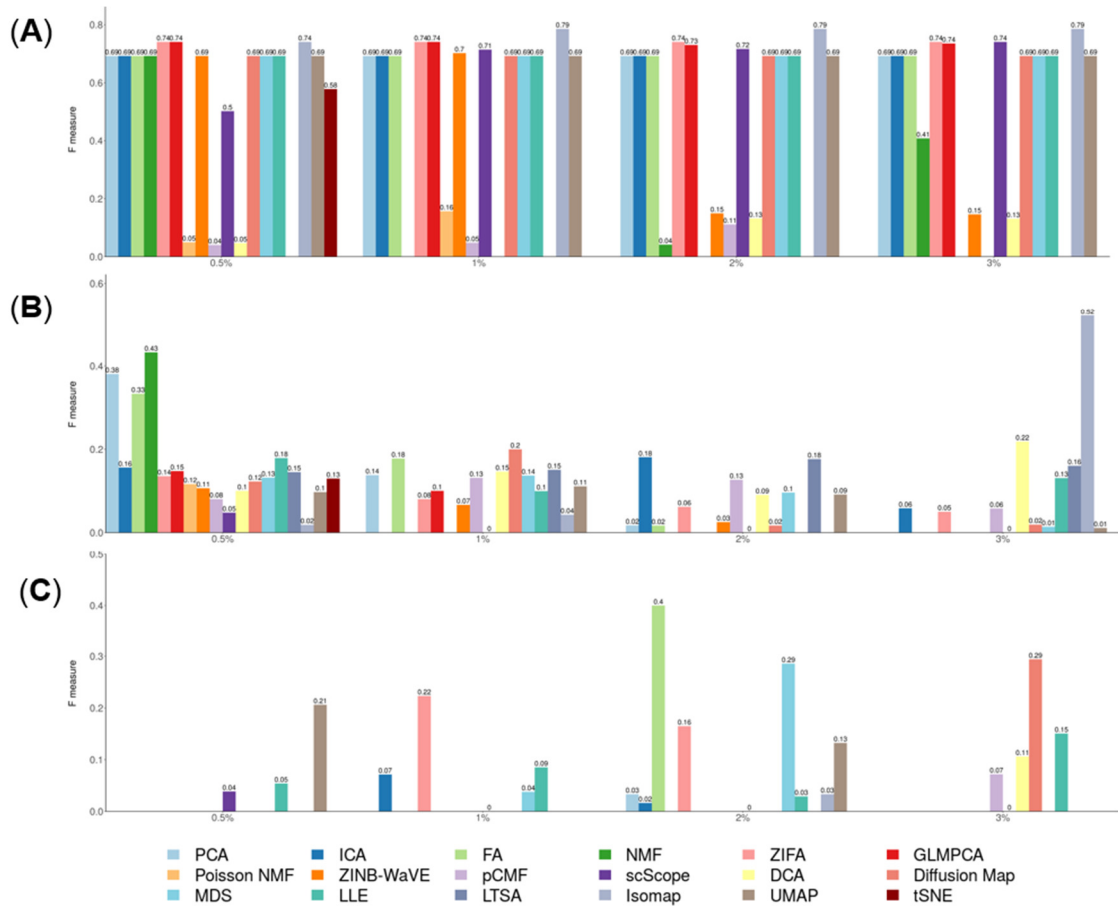


Figure S35. Bar plots show the F-measure of different DR methods on the rare data set PBMC3k1Rare2 (contains 7.9% CD34+ cells). The performance is measured by k-means clustering (**A**), hierarchical clustering (**B**) or Louvain method (**C**). We compared 18 DR methods, including factor analysis (FA; light green), principal component analysis (PCA; light blue), independent component analysis (ICA; blue), Diffusion Map (pink), nonnegative matrix factorization (NMF; green), Poisson NMF (light orange), zero-inflated factor analysis (ZIFA; light pink), zero-inflated negative binomial based wanted variation extraction (ZINB-WaVE; orange), probabilistic count matrix factorization (pCMF; light purple), deep count autoencoder network (DCA; yellow), scScope (purple), generalized linear model principal component analysis (GLMPCA; red), multidimensional scaling (MDS; cyan), locally linear embedding (LLE; blue green), locally linear embedding (LLE; blue green), local tangent space alignment (LTSA; teal blue), Isomap (grey), uniform manifold approximation and projection (UMAP; brown), and t-distributed stochastic neighbor embedding (tSNE; dark red). We used log2 count transformation for the subset of DR methods that use normalized data. For each data set, we compared the four different number of low-dimensional data. The four numbers we used equal to 0.5%, 1%, 2%, and 3% of the total number of cells. Note that, for tSNE, we only extracted two low-dimensional components due to the limitation of the tSNE software.

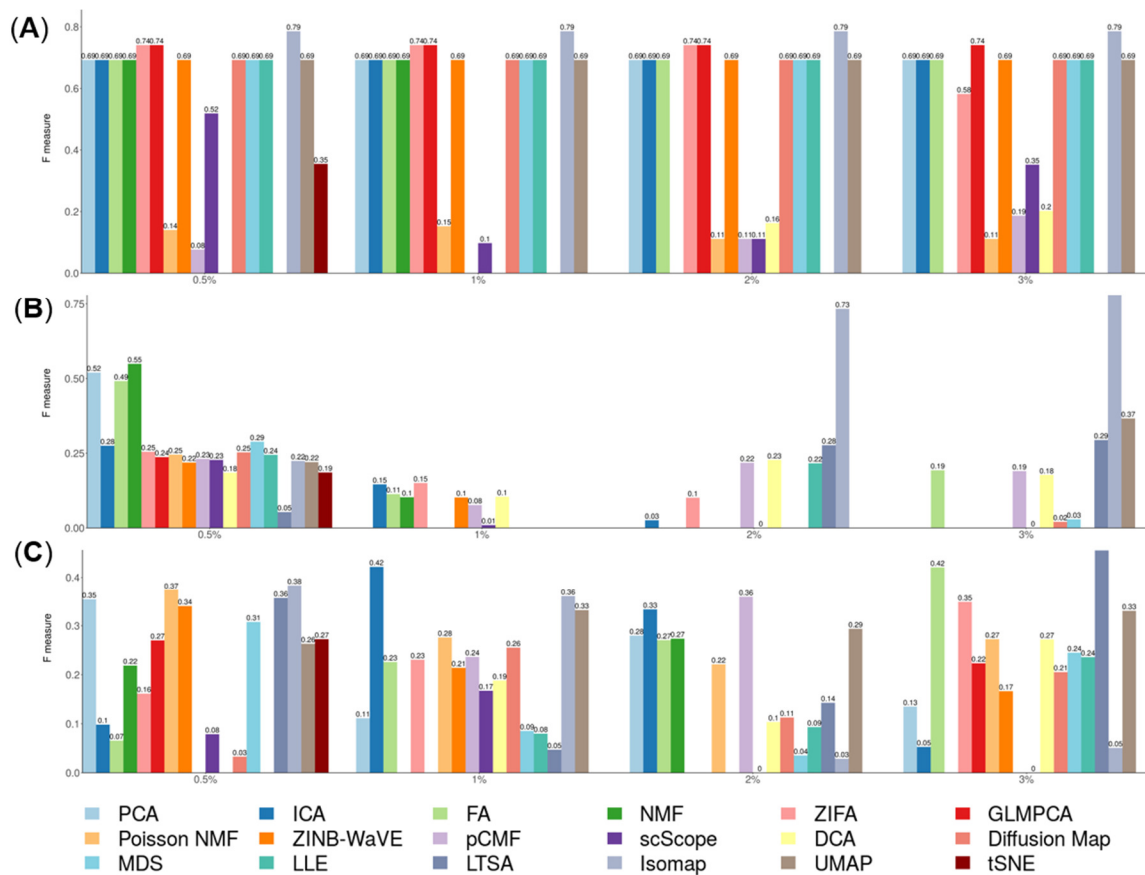


Figure S36. The stability and robustness of DR methods evaluated based on data split of the Kumar data. We compared 18 DR methods (columns), including factor analysis (FA), principal component analysis (PCA), independent component analysis (ICA), Diffusion Map, nonnegative matrix factorization (NMF), Poisson NMF, zero-inflated factor analysis (ZIFA), zero-inflated negative binomial based wanted variation extraction (ZINB-WaVE), probabilistic count matrix factorization (pCMF), deep count autoencoder network (DCA), scScope, generalized linear model principal component analysis (GLMPCA), multidimensional scaling (MDS), locally linear embedding (LLE), local tangent space alignment (LTSA), Isomap, uniform manifold approximation and projection (UMAP), and t-distributed stochastic neighbor embedding (tSNE). We split the Kumar data randomly into two subsets with equal number of cells in each cell type (one colored red; the other colored green). We applied each DR method to each subset separately to obtain clustering results. Performance is measured by normalized mutual index (NMI) after k -means clustering. We performed 10 replicates for each data and show the performance results across these replicates using boxplot. For each data set, we compared the four different number of low-dimensional data. The four numbers we used equal to 2, 6, 14, and 20 (x-axis). Note that, for tSNE, we only extracted two low-dimensional components due to the limitation of the tSNE software.

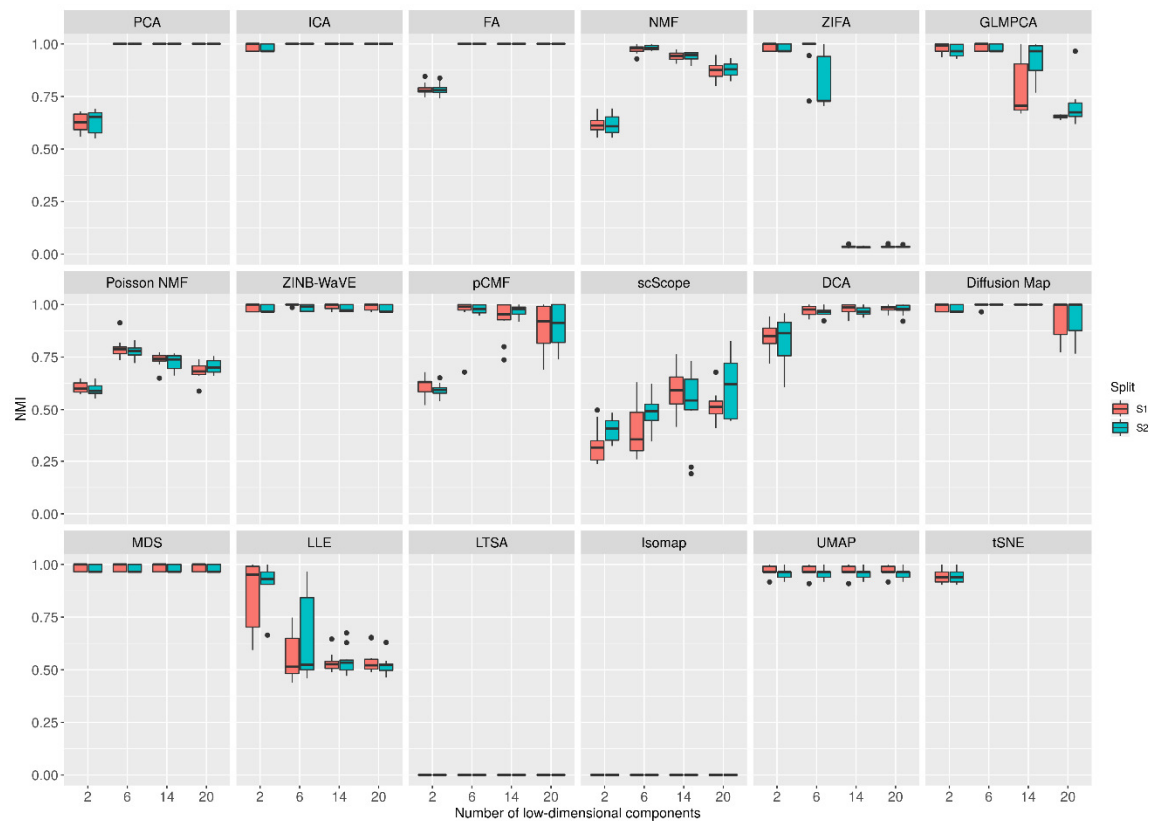


Figure S37. DR method performance evaluated by Kendal correlation for downstream trajectory inference analysis. For each method, we used *Slingshot* to perform trajectory inference with hierarchical clustering as the initial step. We compared 17 DR methods (columns), including factor analysis (FA), principal component analysis (PCA), independent component analysis (ICA), Diffusion Map, nonnegative matrix factorization (NMF), Poisson NMF, zero-inflated factor analysis (ZIFA), zero-inflated negative binomial based wanted variation extraction (ZINB-WaVE), probabilistic count matrix factorization (pCMF), deep count autoencoder network (DCA), generalized linear model principal component analysis (GLMPCA), multidimensional scaling (MDS), locally linear embedding (LLE), local tangent space alignment (LTSA), Isomap, uniform manifold approximation and projection (UMAP), and t-distributed stochastic neighbor embedding (tSNE). We evaluated their performance on 14 real scRNASeq data sets. We used log2 Count transformation for the subset of DR methods that use normalized data. For each data set, we compared the four different number of low-dimensional data. The four numbers we used equal to 2, 6, 14, and 20 (x-axis). Some results of LTSA are empty because it is not compatible with *Slingshot*. Note that, for tSNE, we only extracted two low-dimensional components due to the limitation of the tSNE software.

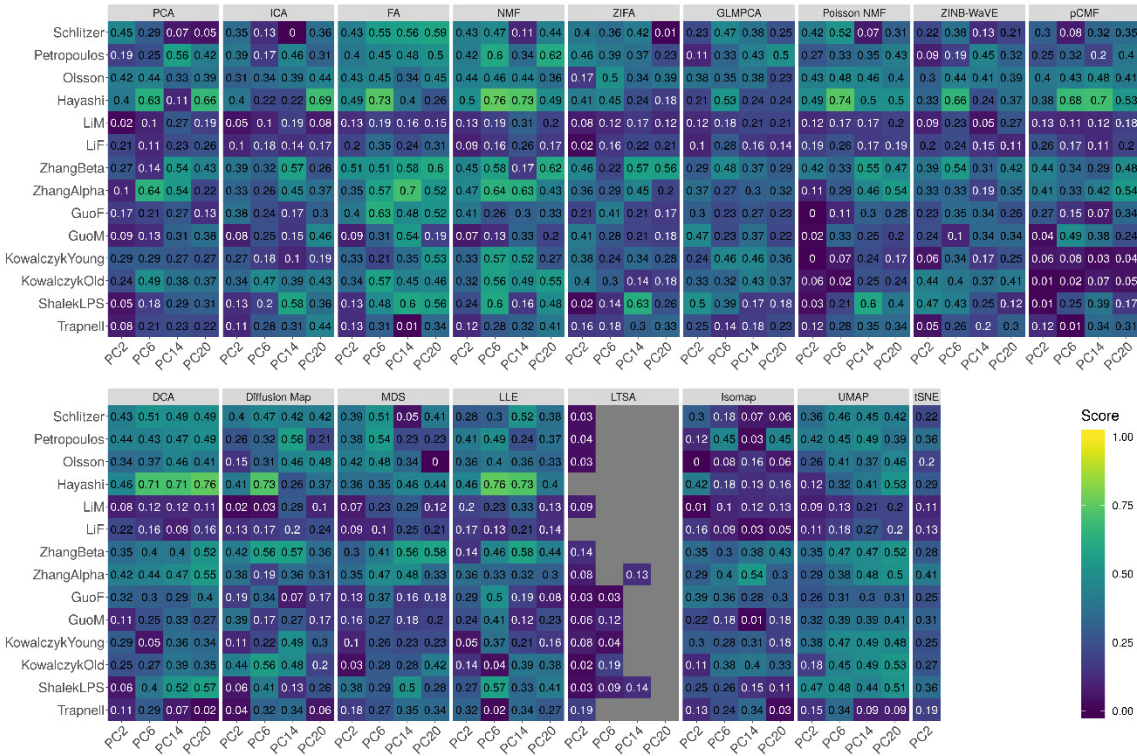


Figure S38. DR method performance evaluated by Kendal correlation for downstream trajectory inference analysis. For each method, we used *Slingshot* to perform trajectory inference with Louvain method as the initial step. We compared 17 DR methods (columns), including factor analysis (FA), principal component analysis (PCA), independent component analysis (ICA), Diffusion Map, nonnegative matrix factorization (NMF), Poisson NMF, zero-inflated factor analysis (ZIFA), zero-inflated negative binomial based wanted variation extraction (ZINB-WaVE), probabilistic count matrix factorization (pCMF), deep count autoencoder network (DCA), generalized linear model principal component analysis (GLMPCA), multidimensional scaling (MDS), locally linear embedding (LLE), local tangent space alignment (LTSA), Isomap, uniform manifold approximation and projection (UMAP), and t-distributed stochastic neighbor embedding (tSNE). We evaluated their performance on 14 real scRNASeq data sets. We used log2 Count transformation for the subset of DR methods that use normalized data. For each data set, we compared the four different number of low-dimensional data. The four numbers we used equal to 2, 6, 14, and 20 (x-axis). Some results of LTSA are empty because it is not compatible with *Slingshot*. Note that, for tSNE, we only extracted two low-dimensional components due to the limitation of the tSNE software.

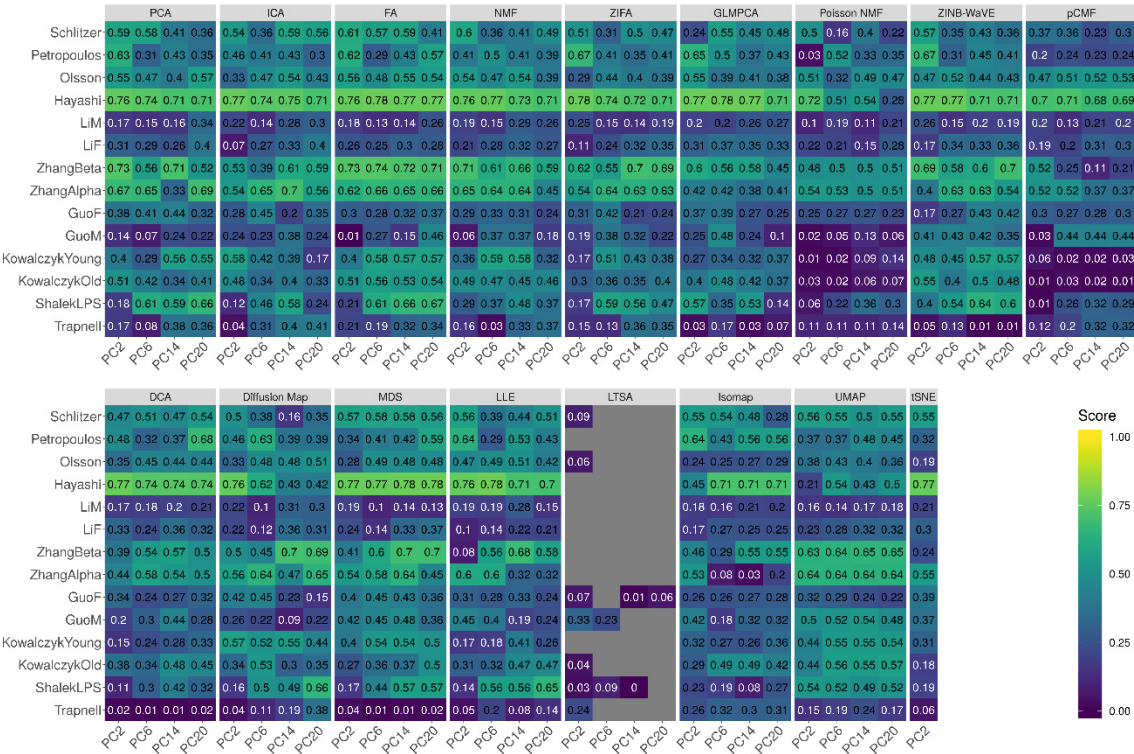


Figure S39. Bar plots show the average performance of different DR methods in downstream trajectory inference analysis. The performance is evaluated by Kendall correlation averaged across 14 data sets. For each method, we used *Slingshot* to perform trajectory inference with either *k*-means (**A**), hierarchical clustering (**B**) or Louvain method (**C**) as the initial step. We compared 17 DR methods, including factor analysis (FA; light green), principal component analysis (PCA; light blue), independent component analysis (ICA; blue), Diffusion Map (pink), nonnegative matrix factorization (NMF; green), Poisson NMF (light orange), zero-inflated factor analysis (ZIFA; light pink), zero-inflated negative binomial based wanted variation extraction (ZINB-WaVE; orange), probabilistic count matrix factorization (pCMF; light purple), deep count autoencoder network (DCA; yellow), generalized linear model principal component analysis (GLMPCA; red), multidimensional scaling (MDS; cyan), locally linear embedding (LLE; blue green), local tangent space alignment (LTSA; teal blue), Isomap (grey), uniform manifold approximation and projection (UMAP; brown), and t-distributed stochastic neighbor embedding (tSNE; dark red). We used log2 Count transformation for the subset of DR methods that use normalized data. For each data set, we compared the four different number of low-dimensional data. The four numbers we used equal to 2, 6, 14, and 20 (x-axis). Note that, for tSNE, we only extracted two low-dimensional components due to the limitation of the tSNE software.

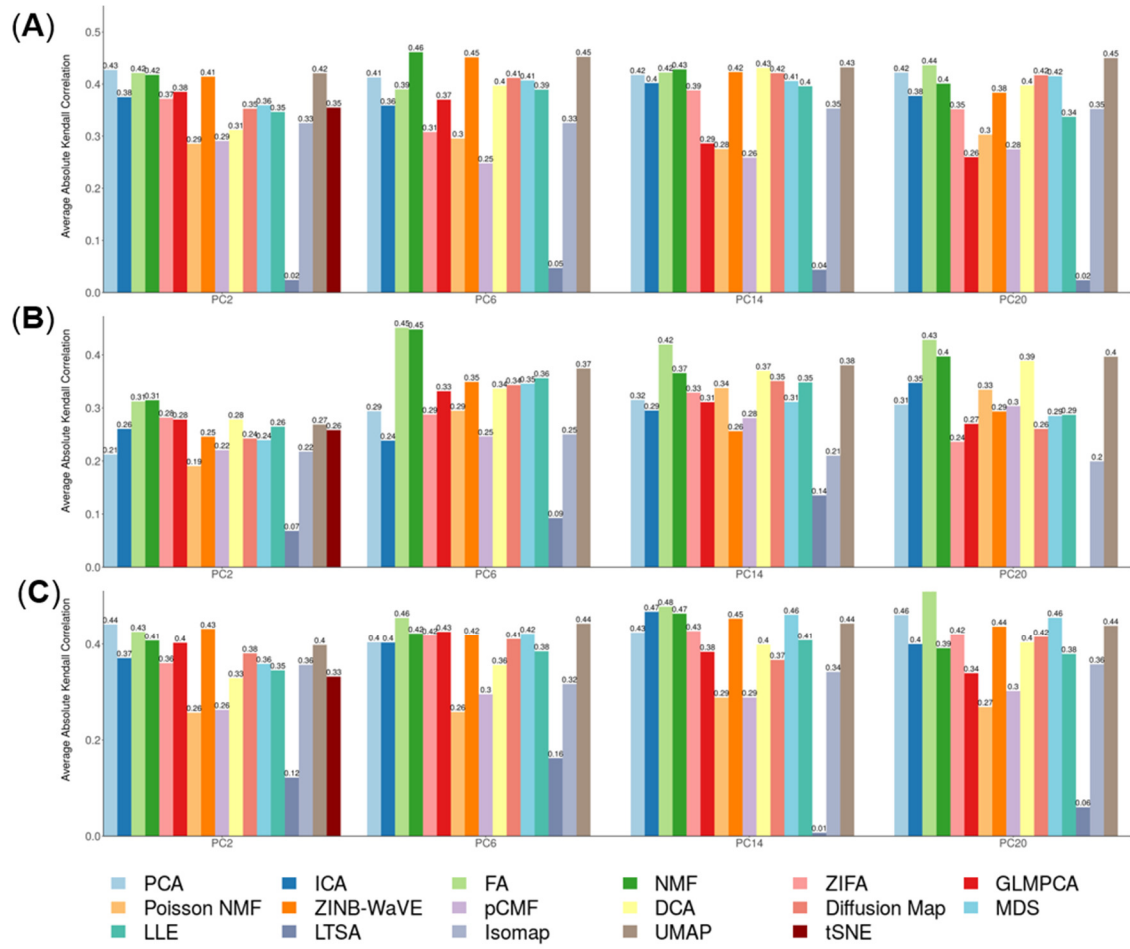


Figure S40. DR method performance evaluated by Kendal correlation for downstream trajectory inference analysis. For each method, we used *Monocle3* to perform trajectory inference. We compared 17 DR methods (columns), including factor analysis (FA), principal component analysis (PCA), independent component analysis (ICA), Diffusion Map, nonnegative matrix factorization (NMF), Poisson NMF, zero-inflated factor analysis (ZIFA), zero-inflated negative binomial based wanted variation extraction (ZINB-WaVE), probabilistic count matrix factorization (pCMF), deep count autoencoder network (DCA), generalized linear model principal component analysis (GLMPCA), multidimensional scaling (MDS), locally linear embedding (LLE), local tangent space alignment (LTSA), Isomap, uniform manifold approximation and projection (UMAP), and t-distributed stochastic neighbor embedding (tSNE). We evaluated their performance on 14 real scRNASeq data sets. We used log2 Count transformation for the subset of DR methods that use normalized data. For each data set, we compared the four different number of low-dimensional data. The four numbers we used equal to 2, 6, 14, and 20 (x-axis). Some results of LTSA are empty because it is not compatible with *Monocle3*. Note that, for tSNE, we only extracted two low-dimensional components due to the limitation of the tSNE software.

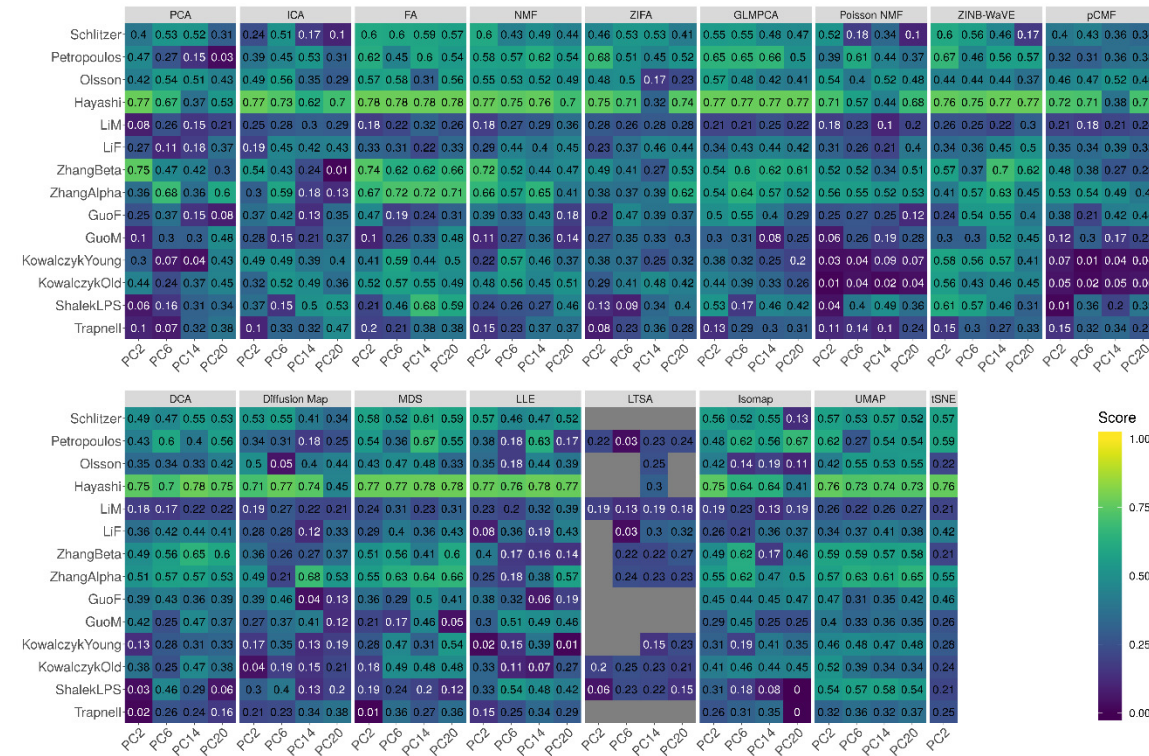


Figure S41. Bar plots show the average performance of different DR methods in downstream trajectory inference analysis. The performance is evaluated by Kendall correlation averaged across 14 data sets. For each method, we used *Monocle3* to perform trajectory inference. We compared 17 DR methods, including factor analysis (FA; light green), principal component analysis (PCA; light blue), independent component analysis (ICA; blue), Diffusion Map (pink), nonnegative matrix factorization (NMF; green), Poisson NMF(light orange), zero-inflated factor analysis (ZIFA; light pink), zero-inflated negative binomial based wanted variation extraction (ZINB-WaVE; orange), probabilistic count matrix factorization (pCMF; light purple), deep count autoencoder network (DCA; yellow), generalized linear model principal component analysis (GLMPCA; red), multidimensional scaling (MDS; cyan), locally linear embedding (LLE; blue green), local tangent space alignment (LTSA; teal blue), Isomap (grey), uniform manifold approximation and projection (UMAP; brown), and t-distributed stochastic neighbor embedding (tSNE; dark red). We used log2 Count transformation for the subset of DR methods that use normalized data. For each data set, we compared the four different number of low-dimensional data. The four numbers we used equal to 2, 6, 14, and 20 (x-axis). Note that, for tSNE, we only extracted two low-dimensional components due to the limitation of the tSNE software.

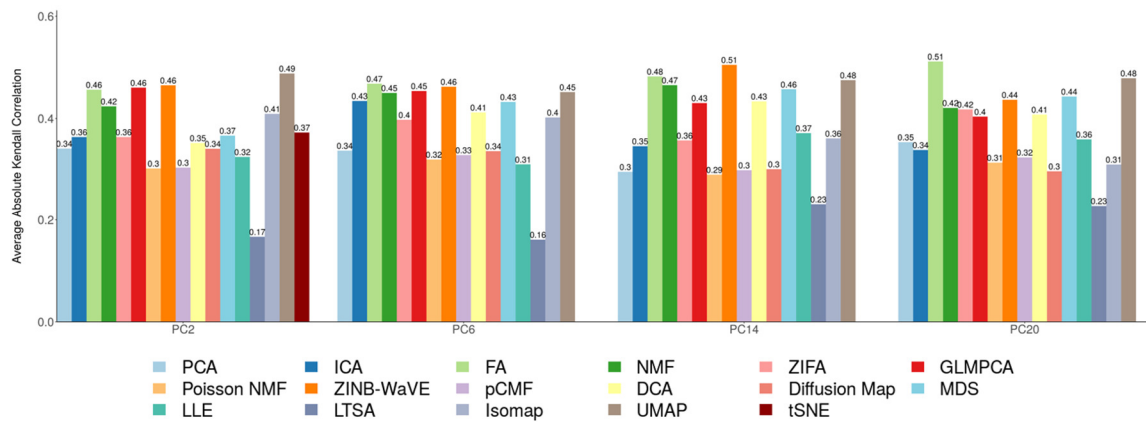


Figure S42. Trajectory visualization of different DR methods on ZhangBeta data set. We compared 17 DR methods (columns), including factor analysis (FA), principal component analysis (PCA), independent component analysis (ICA), Diffusion Map, nonnegative matrix factorization (NMF), Poisson NMF, zero-inflated factor analysis (ZIFA), zero-inflated negative binomial based wanted variation extraction (ZINB-WaVE), probabilistic count matrix factorization (pCMF), deep count autoencoder network (DCA), generalized linear model principal component analysis (GLMPCA), multidimensional scaling (MDS), locally linear embedding (LLE), local tangent space alignment (LTSA), Isomap, uniform manifold approximation and projection (UMAP), and t-distributed stochastic neighbor embedding (tSNE). We used log₂ Count transformation for the subset of DR methods that use normalized data. For each data set, we first reduced the dimension to 2, then applied UMAP to visualize the trajectory.

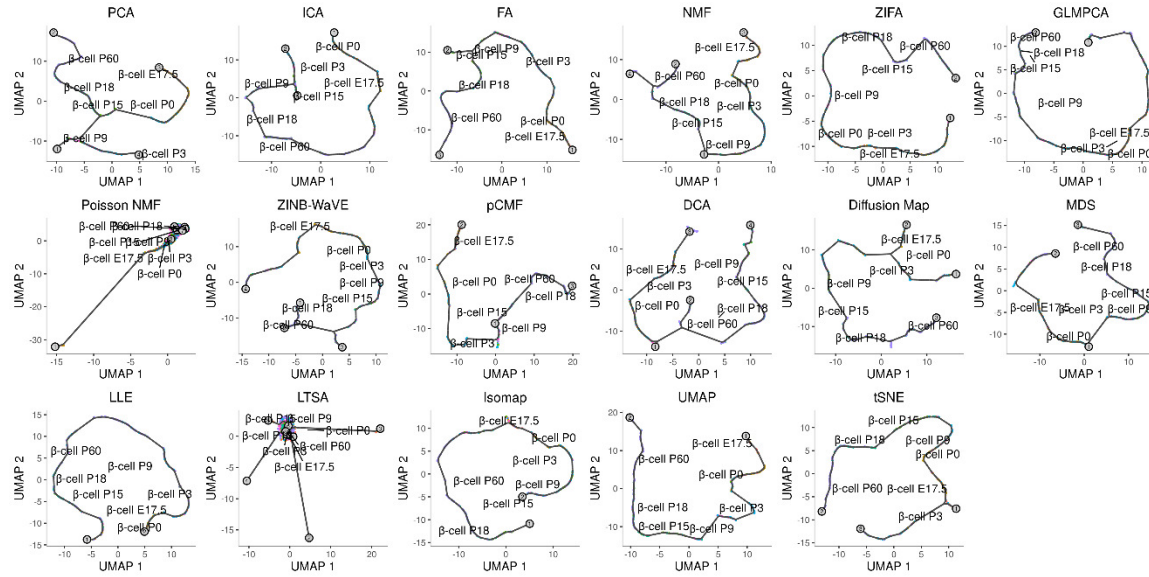


Figure S43. DR method performance with log-2 CPM transformed data for downstream trajectory inference analysis. Performance is evaluated by Kendal correlation coefficient. For each method, we used *Slingshot* to perform trajectory inference on log2 CPM transformed data with k -means as the initial step. We compared 11 DR methods (columns), including factor analysis (FA), principal component analysis (PCA), independent component analysis (ICA), nonnegative matrix factorization (NMF), Diffusion Map, multidimensional scaling (MDS), locally linear embedding (LLE), local tangent space alignment (LTSA), Isomap, uniform manifold approximation and projection (UMAP), and t-distributed stochastic neighbor embedding (tSNE). We evaluated their performance on 14 real scRNASeq data sets (rows). For each data set, we compared the four different number of low-dimensional data. The four numbers we used equal to 2, 6, 14, and 20 (x-axis). Some results for LTSA or NMF are not shown (grey fills) because error occurred when we applied *Slingshot* on LTSA or NMF extracted low-dimensional components there. Note that, for tSNE, we only extracted two low-dimensional components due to the limitation of the tSNE software.

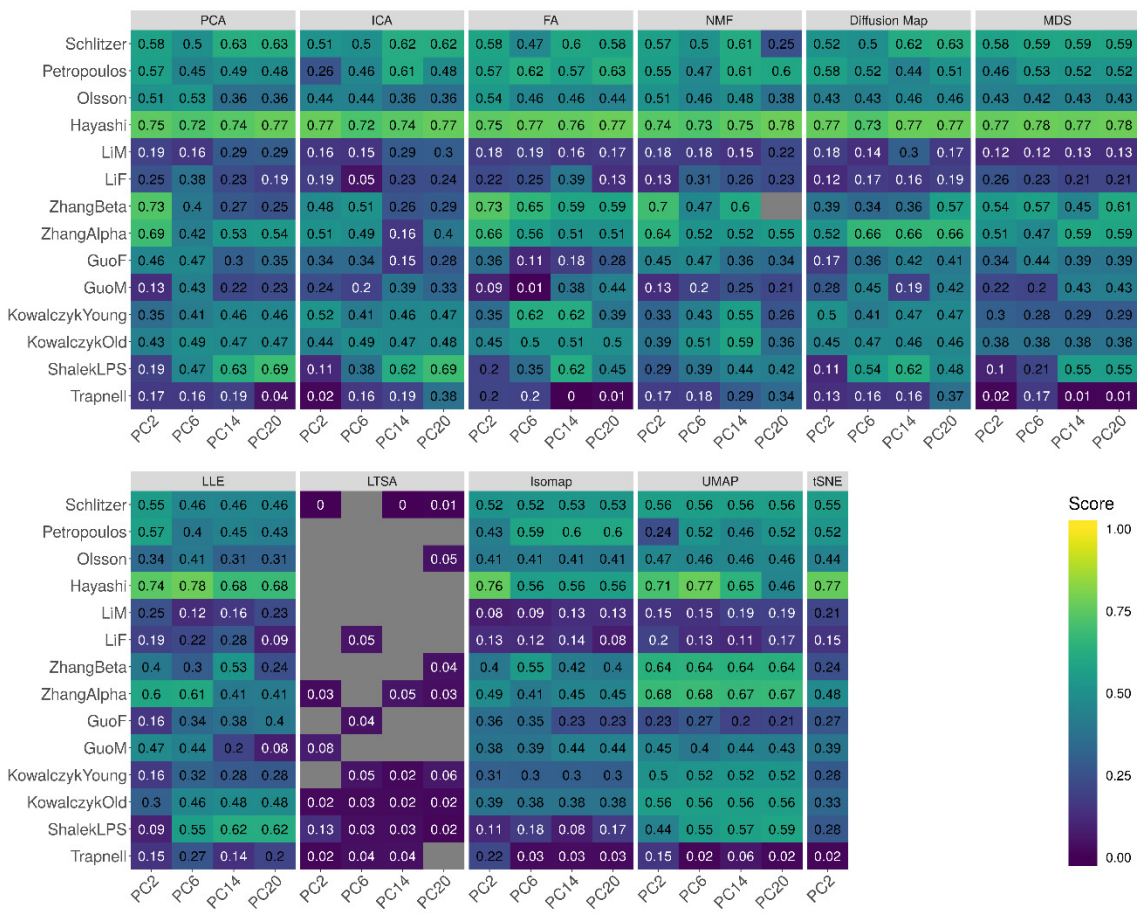


Figure S44. DR method performance with log-2 CPM transformed data for downstream trajectory inference analysis. Performance is evaluated by Kendal correlation coefficient. For each method, we used *Slingshot* to perform trajectory inference on log2 CPM transformed data with hierarchical clustering as the initial step. We compared 11 DR methods (columns), including factor analysis (FA), principal component analysis (PCA), independent component analysis (ICA), Diffusion Map, nonnegative matrix factorization (NMF), multidimensional scaling (MDS), locally linear embedding (LLE), local tangent space alignment (LTSA), Isomap, uniform manifold approximation and projection (UMAP), and t-distributed stochastic neighbor embedding (tSNE). We evaluated their performance on 14 real scRNASeq data sets (rows). For each data set, we compared the four different number of low-dimensional data. The four numbers we used equal to 2, 6, 14, and 20 (x-axis). Some results for LTSA are not shown (grey fills) because error occurred when we applied *Slingshot* on LTSA extracted low-dimensional components there. Note that, for tSNE, we only extracted two low-dimensional components due to the limitation of the tSNE software.

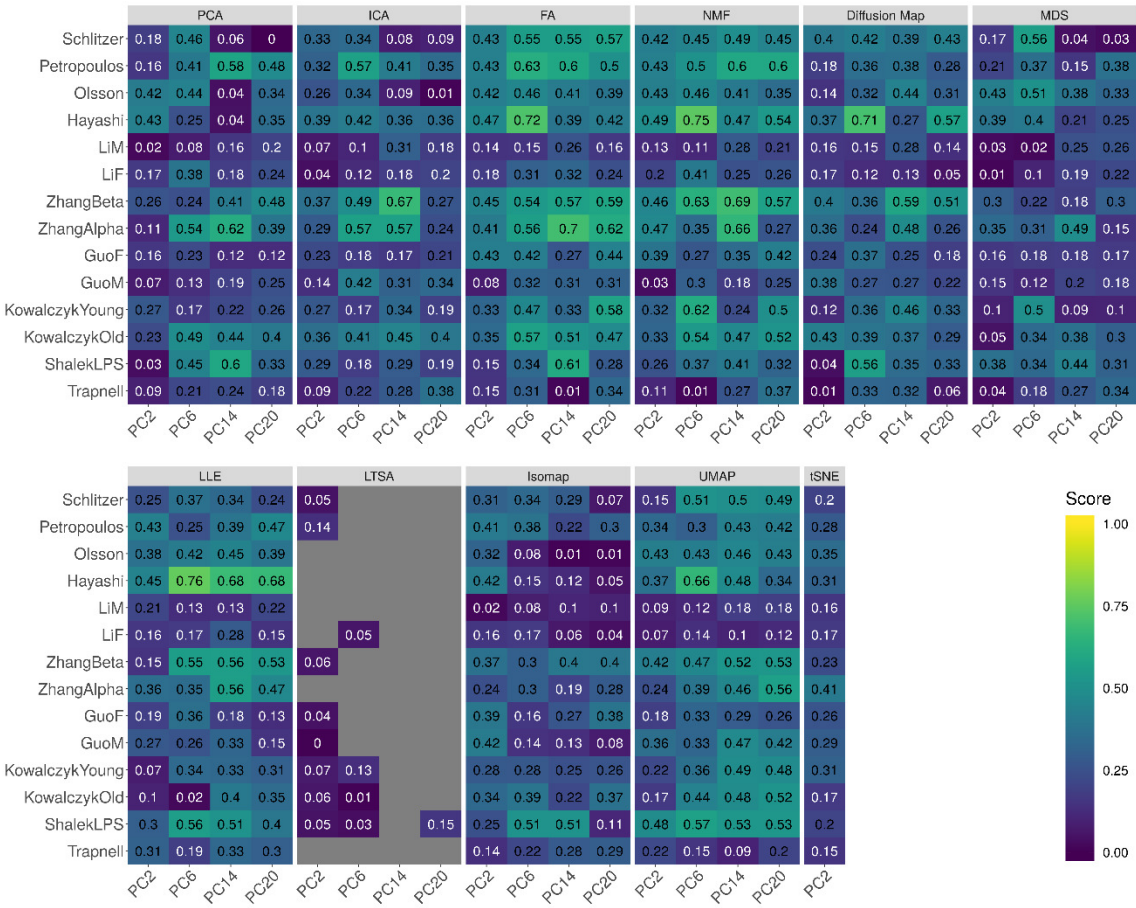


Figure S45. DR method performance with log-2 CPM transformed data for downstream trajectory inference analysis. Performance is evaluated by Kendal correlation coefficient. For each method, we used *Slingshot* to perform trajectory inference on log2 CPM transformed data with Louvain method as the initial step. We compared 11 DR methods (columns), including factor analysis (FA), principal component analysis (PCA), independent component analysis (ICA), Diffusion Map, nonnegative matrix factorization (NMF), multidimensional scaling (MDS), locally linear embedding (LLE), local tangent space alignment (LTSA), Isomap, uniform manifold approximation and projection (UMAP), and t-distributed stochastic neighbor embedding (tSNE). We evaluated their performance on 14 real scRNASeq data sets (rows). For each data set, we compared the four different number of low-dimensional data. The four numbers we used equal to 2, 6, 14, and 20 (x-axis). Some results for LTSA are not shown (grey fills) because error occurred when we applied *Slingshot* on LTSA extracted low-dimensional components there. Note that, for tSNE, we only extracted two low-dimensional components due to the limitation of the tSNE software.

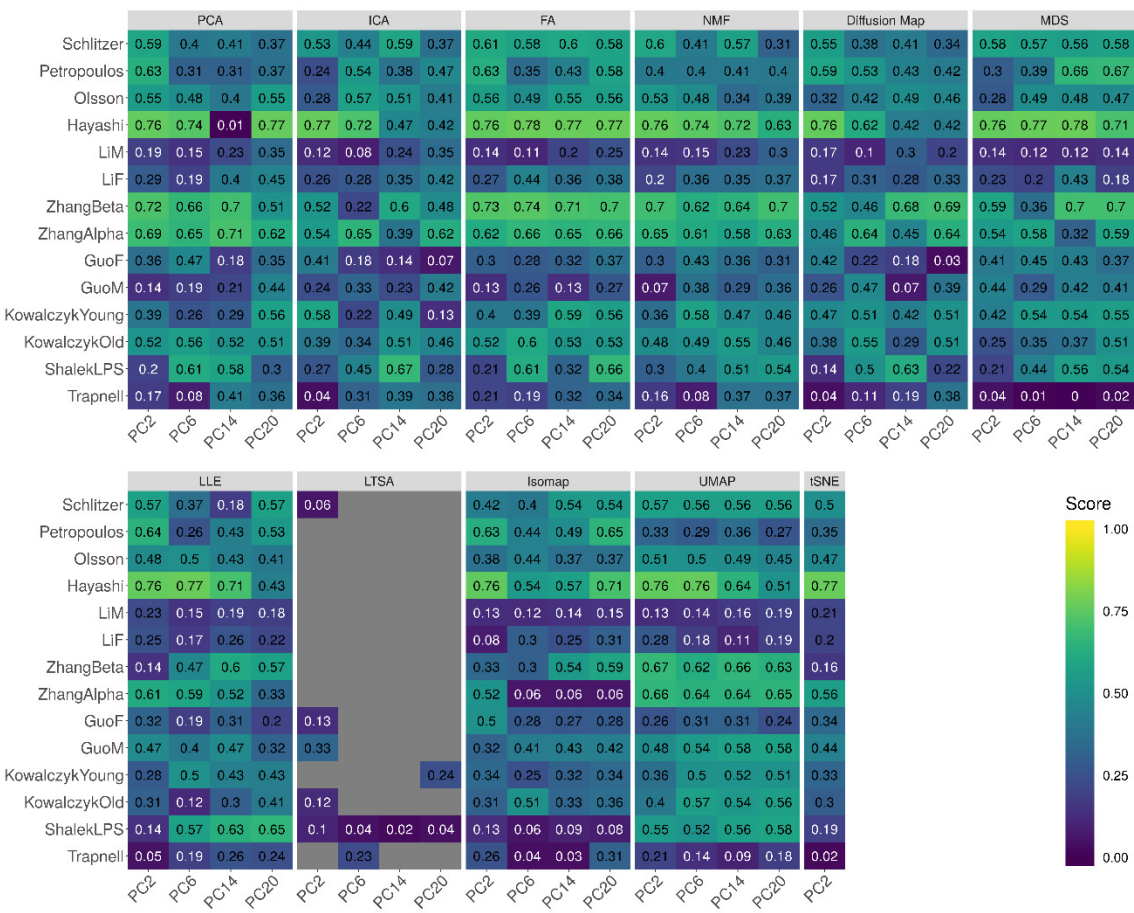


Figure S46. Bar plots show the average performance of a subset of DR methods that use log2 CPM transformed data in downstream trajectory inference analysis.

The performance is evaluated by Kendal correlation averaged across 14 data sets. For each method, we used *Slingshot* to perform trajectory inference with either *k*-means (**A**), hierarchical clustering (**B**) or Louvain method (**C**) as the initial step. We compared 11 DR methods, including factor analysis (FA; light green), principal component analysis (PCA; light blue), independent component analysis (ICA; blue), Diffusion Map (pink), nonnegative matrix factorization (NMF; green), multidimensional scaling (MDS; cyan), locally linear embedding (LLE; blue green), local tangent space alignment (LTSA; teal blue), Isomap (grey), uniform manifold approximation and projection (UMAP; brown), and t-distributed stochastic neighbor embedding (tSNE; dark red). For each data set, we compared the four different number of low-dimensional data. The four numbers we used equal to 2, 6, 14, and 20 (x-axis). Note that, for tSNE, we only extracted two low-dimensional components due to the limitation of the tSNE software.

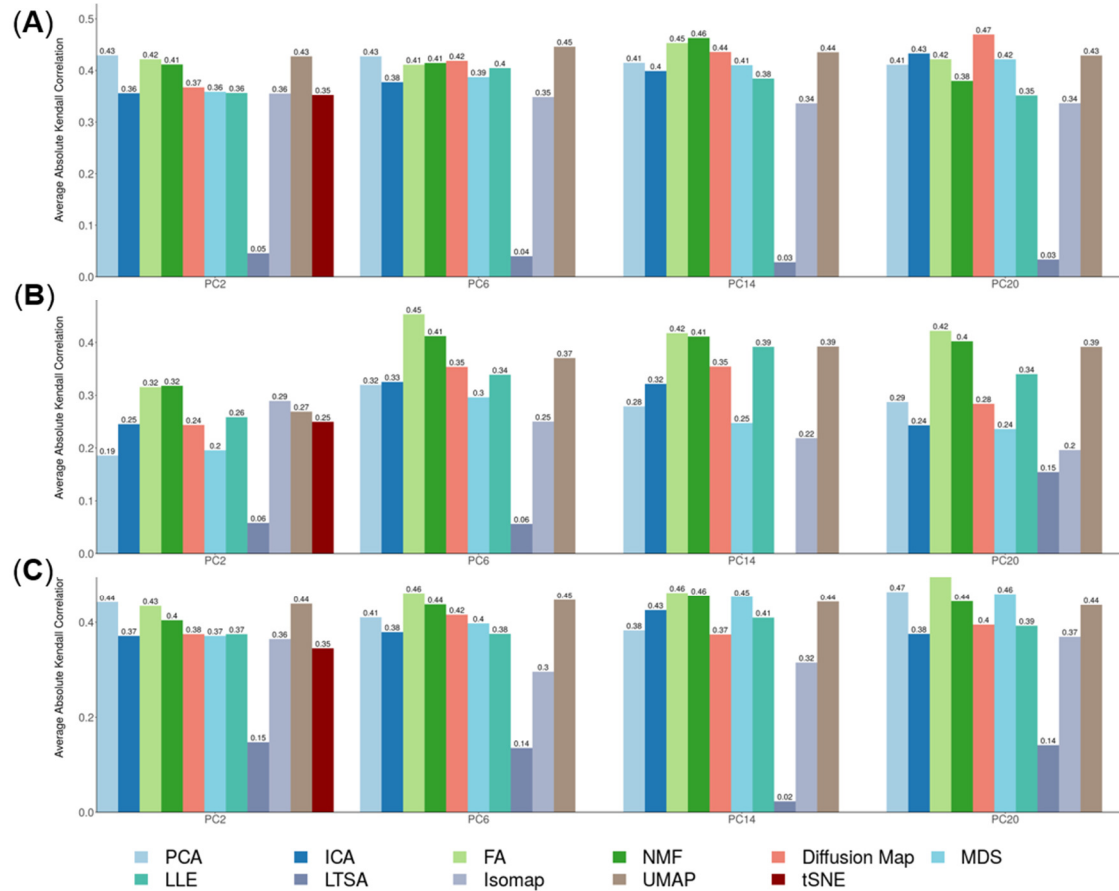


Figure S47. DR method performance with z-score transformed data for downstream trajectory inference analysis. Performance is evaluated by Kendal correlation coefficient. For each method, we used *Slingshot* to perform trajectory inference on z-score transformed data with k-means as the initial step. We compared 10 DR methods (columns), including factor analysis (FA), principal component analysis (PCA), independent component analysis (ICA), Diffusion Map, multidimensional scaling (MDS), locally linear embedding (LLE), local tangent space alignment (LTSA), Isomap, uniform manifold approximation and projection (UMAP), and t-distributed stochastic neighbor embedding (tSNE). We evaluated their performance on 14 real scRNASeq data sets (rows). For each data set, we compared the four different number of low-dimensional data. The four numbers we used equal to 2, 6, 14, and 20. No results for NMF are shown in Figure because z-score transformation yields negative values. Some results for LTSA or ICA are not shown (grey fills) because error occurred when we applied *Slingshot* on LTSA or ICA extracted low-dimensional components there. Note that, for tSNE, we only extracted two low-dimensional components due to the limitation of the tSNE software.

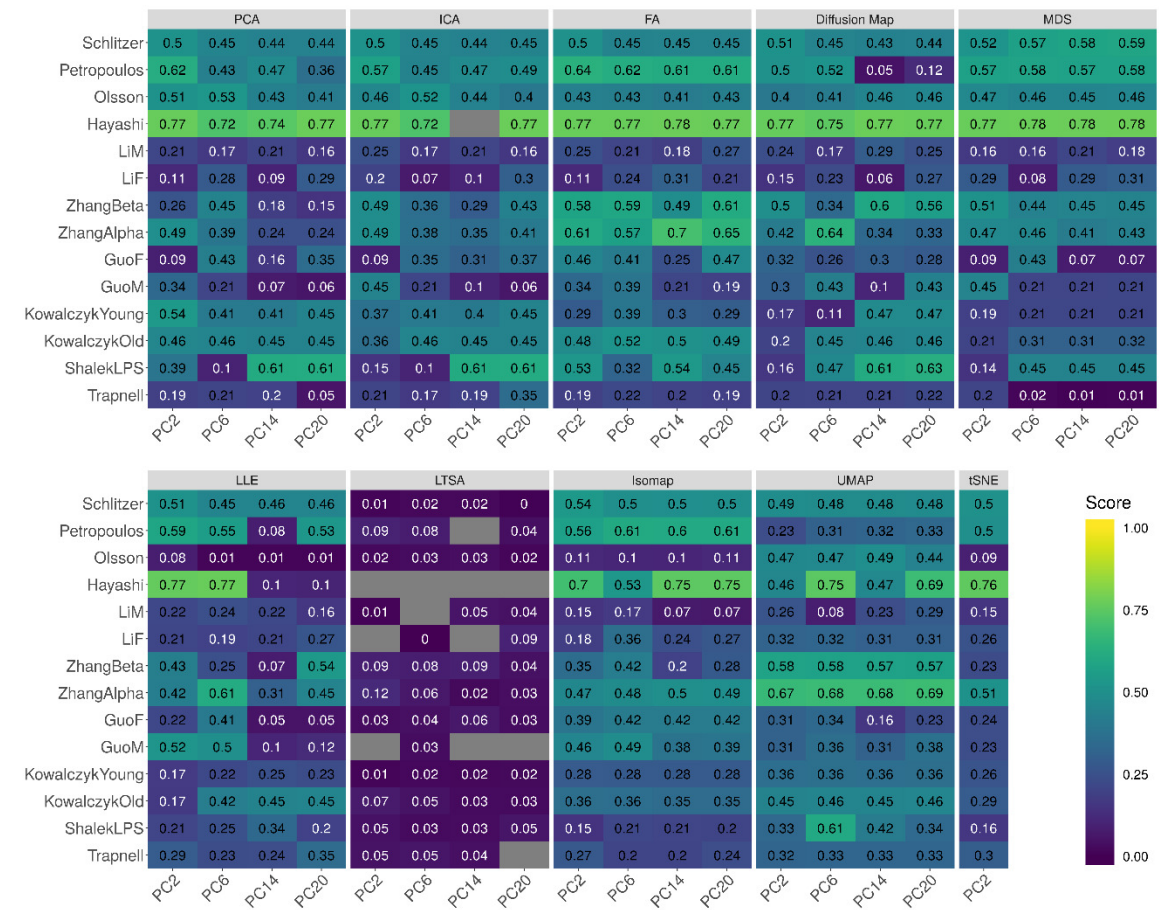


Figure S48. DR method performance with z-score transformed data for downstream trajectory inference analysis. Performance is evaluated by Kendal correlation coefficient. For each method, we used *Slingshot* to perform trajectory inference on z-score transformed data with hierarchical clustering as the initial step. We compared 10 DR methods (columns), including factor analysis (FA), principal component analysis (PCA), independent component analysis (ICA), Diffusion Map, multidimensional scaling (MDS), locally linear embedding (LLE), local tangent space alignment (LTSA), Isomap, uniform manifold approximation and projection (UMAP), and t-distributed stochastic neighbor embedding (tSNE). We evaluated their performance on 14 real scRNASeq data sets (rows). For each data set, we compared the four different number of low-dimensional data. The four numbers we used equal to 2, 6, 14, and 20. No results for NMF are shown in Figure because z-score transformation yields negative values. Some results for LTSA are not shown (grey fills) because error occurred when we applied *Slingshot* on LTSA extracted low-dimensional components there. Note that, for tSNE, we only extracted two low-dimensional components due to the limitation of the tSNE software.



Figure S49. DR method performance with z-score transformed data for downstream trajectory inference analysis. Performance is evaluated by Kendal correlation coefficient. For each method, we used *Slingshot* to perform trajectory inference on z-score transformed data with Louvain method as the initial step. We compared 10 DR methods (columns), including factor analysis (FA), principal component analysis (PCA), independent component analysis (ICA), Diffusion Map, multidimensional scaling (MDS), locally linear embedding (LLE), local tangent space alignment (LTSA), Isomap, uniform manifold approximation and projection (UMAP), and t-distributed stochastic neighbor embedding (tSNE). We evaluated their performance on 14 real scRNASeq data sets (rows). For each data set, we compared the four different number of low-dimensional data. The four numbers we used equal to 2, 6, 14, and 20. No results for NMF are shown in Figure because z-score transformation yields negative values. Some results for LTSA are not shown (grey fills) because error occurred when we applied *Slingshot* on LTSA extracted low-dimensional components there. Note that, for tSNE, we only extracted two low-dimensional components due to the limitation of the tSNE software.

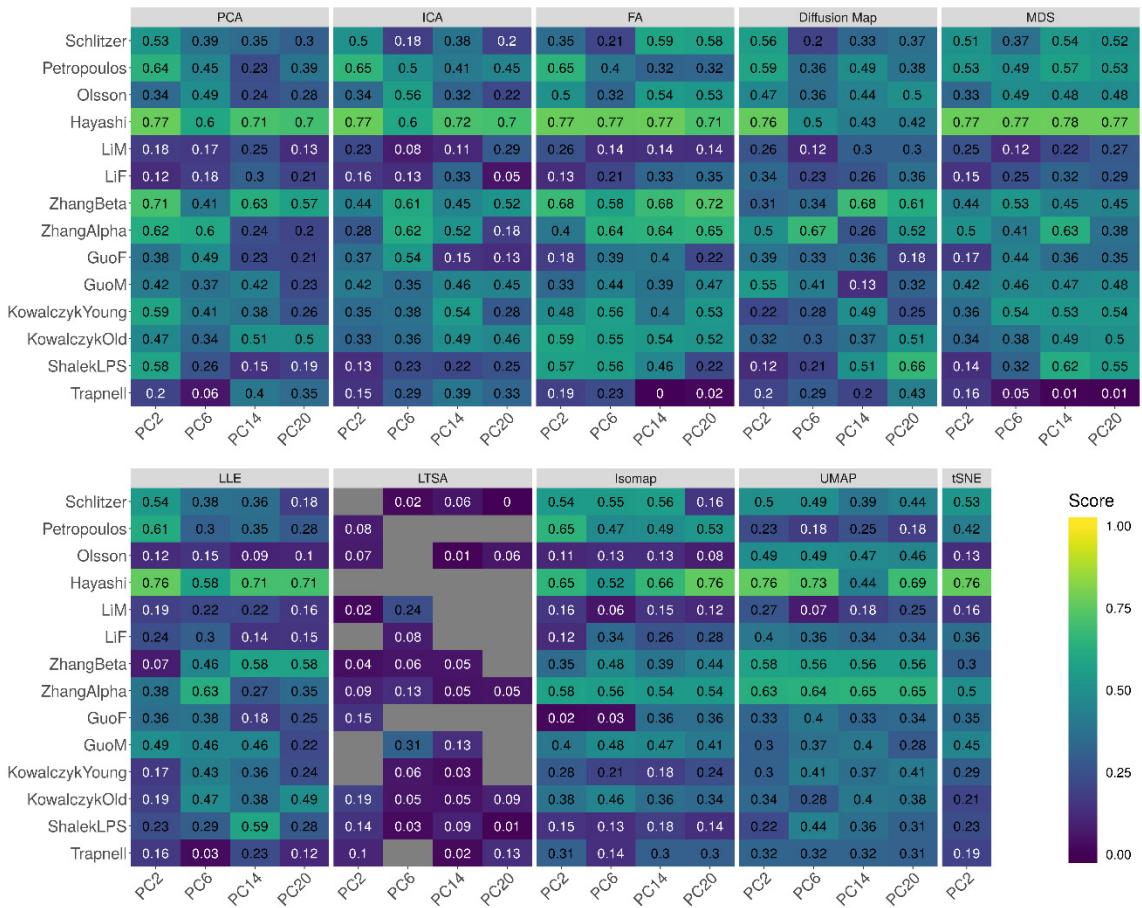


Figure S50. Bar plots show the average performance of a subset of DR methods that use z-score transformed data in downstream trajectory inference analysis.

The performance is evaluated by Kendal correlation averaged across 14 data sets. For each method, we used *Slingshot* to perform trajectory inference with either *k*-means (**A**), hierarchical clustering (**B**) or Louvain method (**C**) as the initial step. We compared 10 DR methods, including factor analysis (FA; light green), principal component analysis (PCA; light blue), independent component analysis (ICA; blue), Diffusion Map (pink), multidimensional scaling (MDS; cyan), locally linear embedding (LLE; blue green), local tangent space alignment (LTSA; teal blue), Isomap (grey), uniform manifold approximation and projection (UMAP; brown), and t-distributed stochastic neighbor embedding (tSNE; dark red). For each data set, we compared the four different number of low-dimensional data. The four numbers we used equal to 2, 6, 14, and 20 (x-axis). Note that, for tSNE, we only extracted two low-dimensional components due to the limitation of the tSNE software.

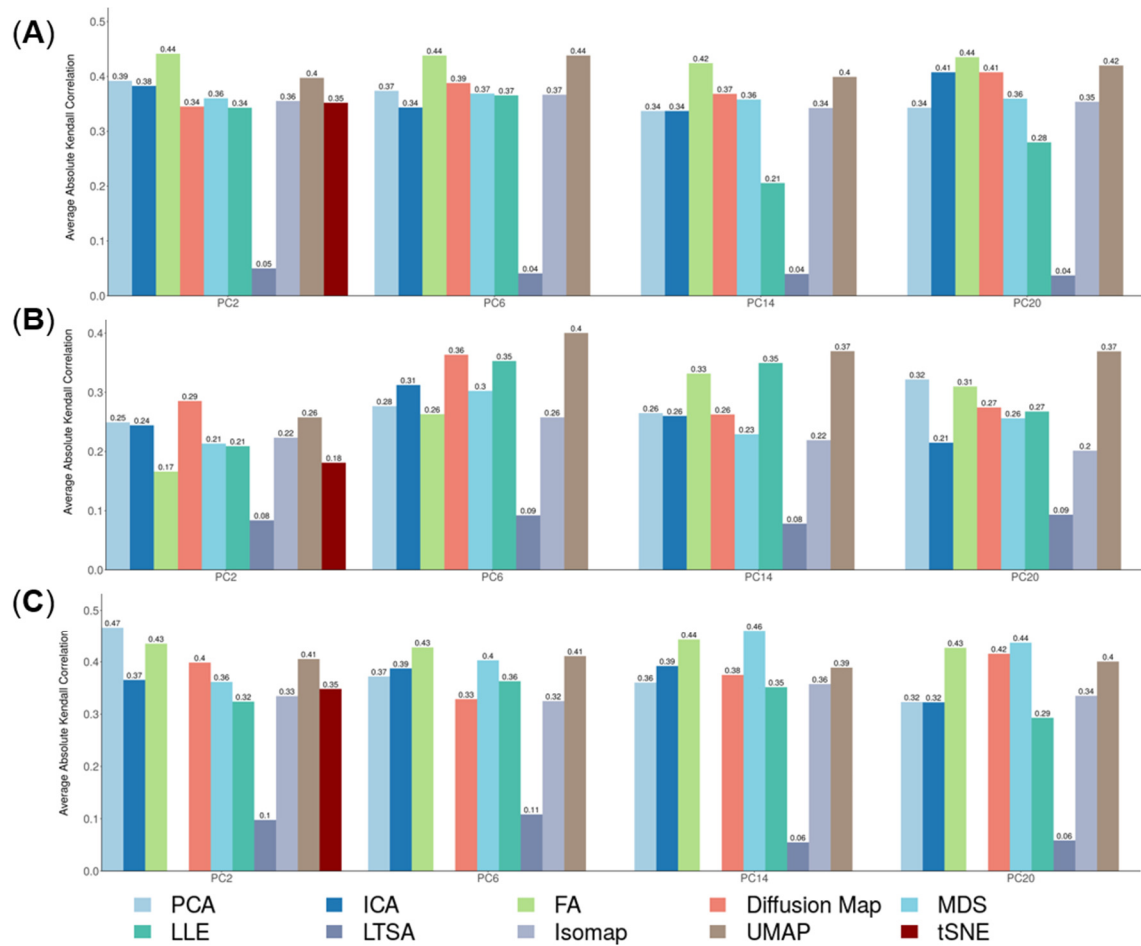


Figure S51. DR method performance with log-2 CPM transformed data for downstream trajectory inference analysis. Performance is evaluated by Kendal correlation coefficient. For each method, we used *Monocle3* to perform trajectory inference on log2 CPM transformed data. We compared 11 DR methods (columns), including factor analysis (FA), principal component analysis (PCA), independent component analysis (ICA), Diffusion Map, nonnegative matrix factorization (NMF), multidimensional scaling (MDS), locally linear embedding (LLE), local tangent space alignment (LTSA), Isomap, and uniform manifold approximation and projection (UMAP), and t-distributed stochastic neighbor embedding (tSNE). We evaluated their performance on 14 real scRNASeq data sets (rows). For each data set, we compared the four different number of low-dimensional data. The four numbers we used equal to 2, 6, 14, and 20 (x-axis). Some results for LTSA are not shown (grey fills) because error occurred when we applied *Slingshot* on LTSA extracted low-dimensional components there. Note that, for tSNE, we only extracted two low-dimensional components due to the limitation of the tSNE software.

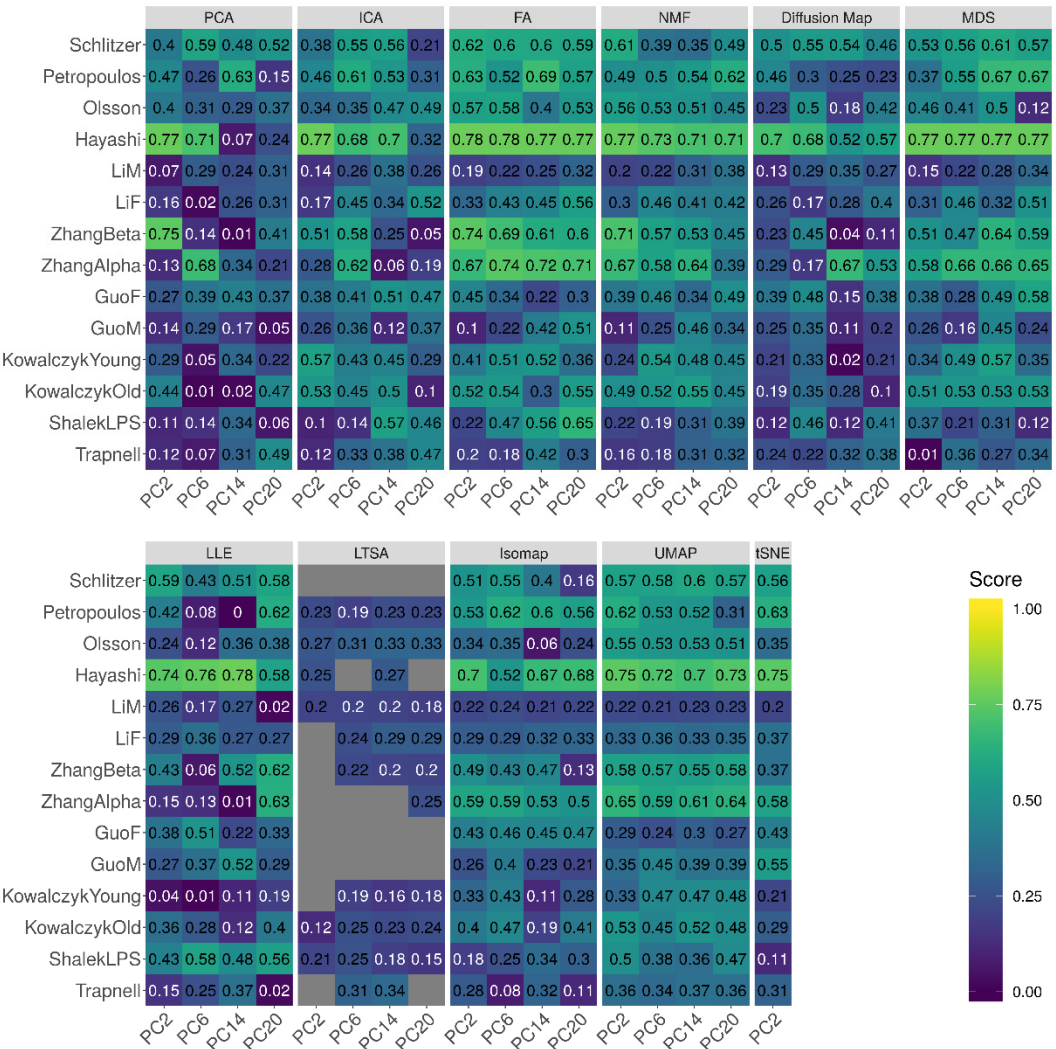


Figure S52. DR method performance with z-score transformed data for downstream trajectory inference analysis. Performance is evaluated by Kendal correlation coefficient. For each method, we used *Monocle3* to perform trajectory inference on z-score transformed data. We compared 10 DR methods (columns), including factor analysis (FA), principal component analysis (PCA), independent component analysis (ICA), Diffusion Map, multidimensional scaling (MDS), locally linear embedding (LLE), local tangent space alignment (LTSA), Isomap, and uniform manifold approximation and projection (UMAP), and t-distributed stochastic neighbor embedding (tSNE). We evaluated their performance on 14 real scRNASeq data sets (rows). For each data set, we compared the four different number of low-dimensional data. The four numbers we used equal to 2, 6, 14, and 20 (x-axis). No results for NMF are shown in Figure because z-score transformation yields negative values. Some results for LTSA are not shown (grey fills) because error occurred when we applied *Slingshot* on LTSA extracted low-dimensional components there. Note that, for tSNE, we only extracted two low-dimensional components due to the limitation of the tSNE software.

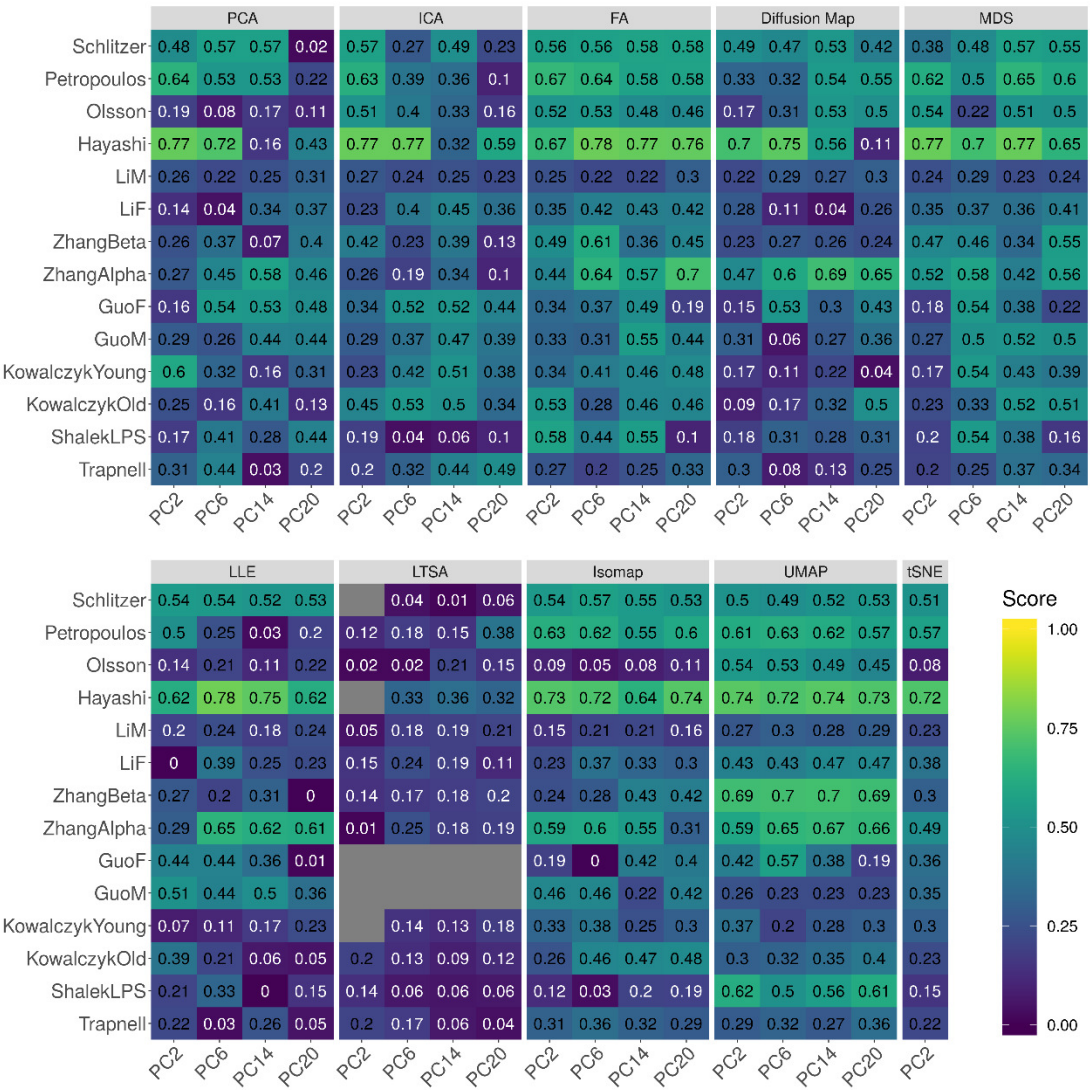


Figure S53. Bar plots show the average performance of a subset of DR methods in downstream trajectory inference analysis. The performance is evaluated by Kendal correlation averaged across 14 data sets. For each method, we used *Monocle3* to perform trajectory inference on either log-2 transformation (**A**) or z-score transformation (**B**) data. We compared 11 DR methods, including factor analysis (FA; light green), principal component analysis (PCA; light blue), independent component analysis (ICA; blue), Diffusion Map (pink), nonnegative matrix factorization (NMF; green), multidimensional scaling (MDS; cyan), locally linear embedding (LLE; blue green), local tangent space alignment (LTSA; teal blue), Isomap (grey), uniform manifold approximation and projection (UMAP; brown), and t-distributed stochastic neighbor embedding (tSNE; dark red). For each data set, we compared the four different number of low-dimensional data. The four numbers we used equal to 2, 6, 14, and 20 (x-axis). Note that, for tSNE, we only extracted two low-dimensional components due to the limitation of the tSNE software.

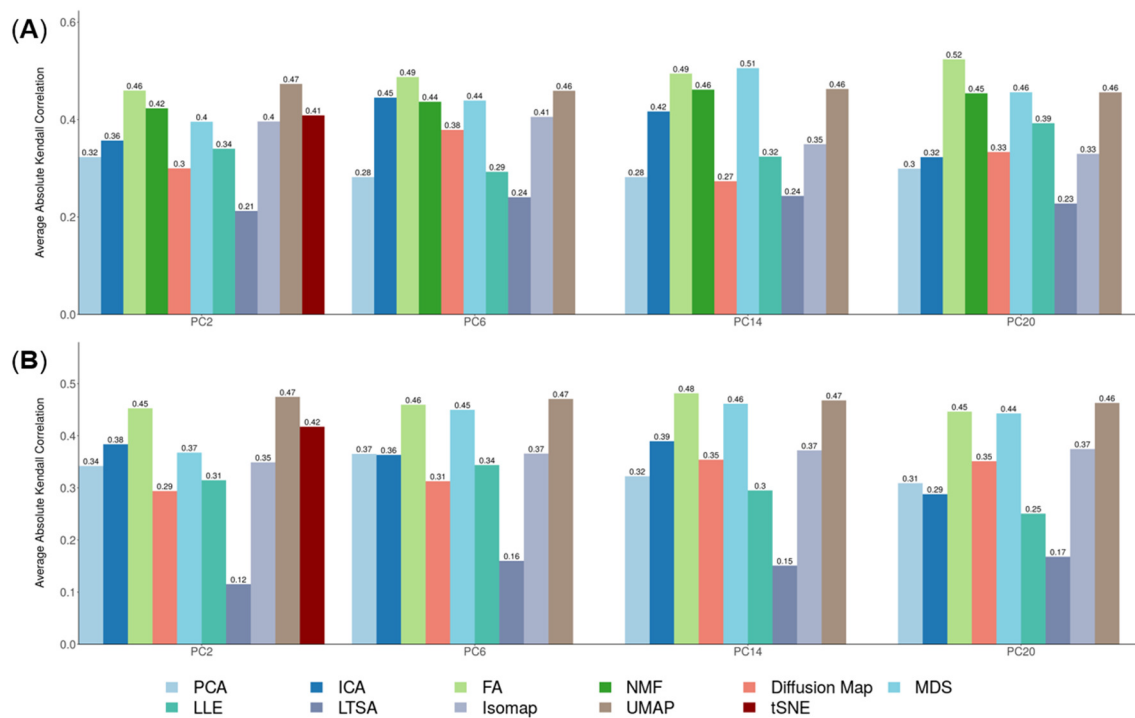


Figure S54. The stability and robustness of DR methods evaluated based on data split of the Hayashi data. We compared 17 DR methods (columns), including factor analysis (FA), principal component analysis (PCA), independent component analysis (ICA), Diffusion Map, nonnegative matrix factorization (NMF), Poisson NMF, zero-inflated factor analysis (ZIFA), zero-inflated negative binomial based wanted variation extraction (ZINB-WaVE), probabilistic count matrix factorization (pCMF), deep count autoencoder network (DCA), generalized linear model principal component analysis (GLMPCA), multidimensional scaling (MDS), locally linear embedding (LLE), local tangent space alignment (LTSA), Isomap, uniform manifold approximation and projection (UMAP), and t-distributed stochastic neighbor embedding (tSNE). We split the Hayashi data randomly into two subsets with equal number of cells in each cell type (one colored red; the other colored green). We applied each DR method to each subset separately to obtain lineage results. Performance is measured by Kendall correlation after *Slingshot*. We performed 10 replicates for each data and show the performance results across these replicates using boxplot. For each data set, we compared the four different number of low-dimensional data. The four numbers we used equal to 2, 6, 14, and 20 (x-axis). Note that, for tSNE, we only extracted two low-dimensional components due to the limitation of the tSNE software.

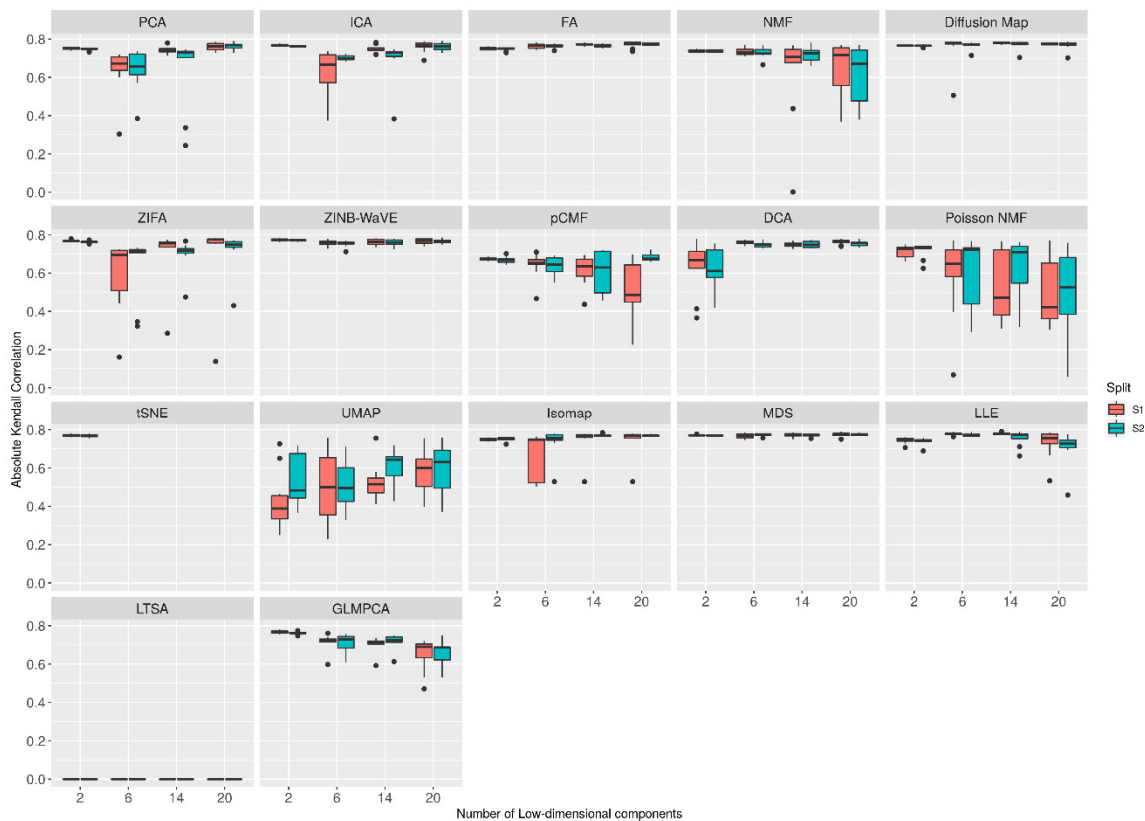


Figure S55. Bar plots show the performance of different DR methods with k-means clustering algorithm on raw Guo data set. The performance is measured by NMI (**A**) or ARI (**B**). We compared 18 DR methods, including factor analysis (FA; light green), principal component analysis (PCA; light blue), independent component analysis (ICA; blue), Diffusion Map (pink), nonnegative matrix factorization (NMF; green), Poisson NMF(light orange), zero-inflated factor analysis (ZIFA; light pink), zero-inflated negative binomial based wanted variation extraction (ZINB-WaVE; orange), probabilistic count matrix factorization (pCMF; light purple), deep count autoencoder network (DCA; yellow), scScope (purple), generalized linear model principal component analysis (GLMPCA; red), multidimensional scaling (MDS; cyan), locally linear embedding (LLE; blue green), local tangent space alignment (LTSA; teal blue), Isomap (grey), uniform manifold approximation and projection (UMAP; brown) , and t-distributed stochastic neighbor embedding (tSNE; dark red). We used log2 count transformation for the subset of DR methods that use normalized data. For each data set, we compared the four different number of low-dimensional data. The four numbers we used equal to 0.5%, 1%, 2%, and 3% of the total number of cells. Note that, for tSNE, we only extracted two low-dimensional components due to the limitation of the tSNE software.

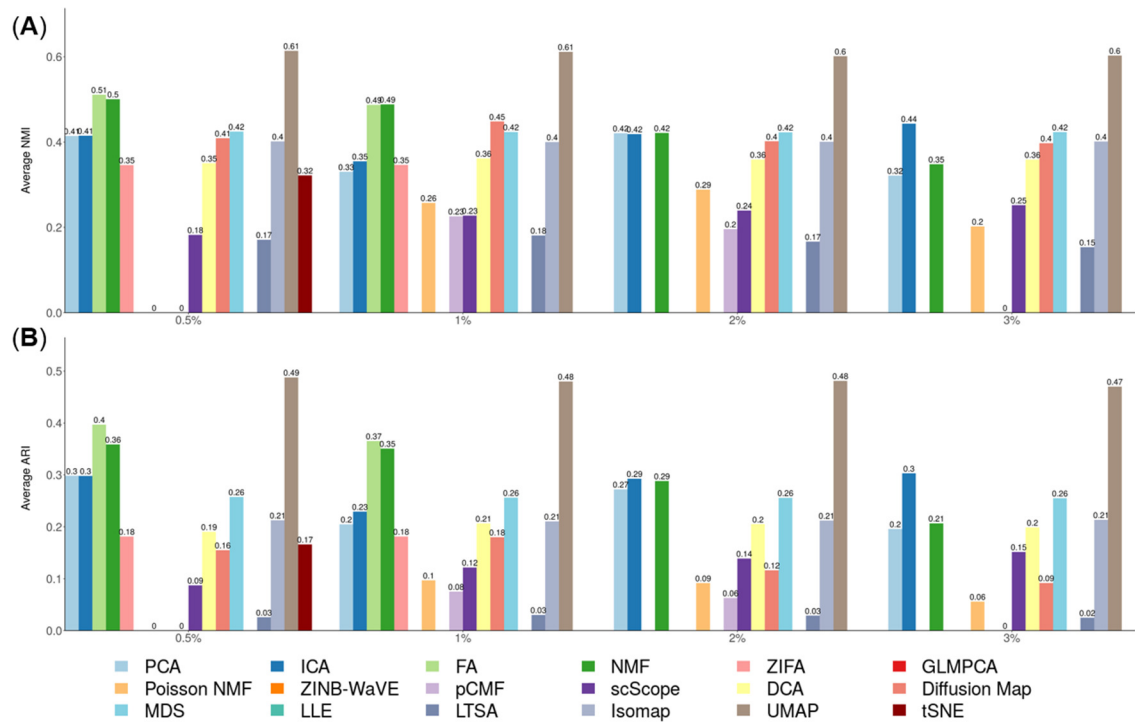


Figure S56. Bar plots show the performance of different DR methods with k-means clustering algorithm on Guo data set with subsampling procedure.

The performance is measured by NMI (**A**) or ARI (**B**). We compared 18 DR methods, including factor analysis (FA; light green), principal component analysis (PCA; light blue), independent component analysis (ICA; blue), Diffusion Map (pink), nonnegative matrix factorization (NMF; green), Poisson NMF(light orange), zero-inflated factor analysis (ZIFA; light pink), zero-inflated negative binomial based wanted variation extraction (ZINB-WaVE; orange), probabilistic count matrix factorization (pCMF; light purple), deep count autoencoder network (DCA; yellow), scScope (purple), generalized linear model principal component analysis (GLMPCA; red), multidimensional scaling (MDS; cyan), locally linear embedding (LLE; blue green), local tangent space alignment (LTSA; teal blue), Isomap (grey), uniform manifold approximation and projection (UMAP; brown) , and t-distributed stochastic neighbor embedding (tSNE). We used log2 count transformation for the subset of DR methods that use normalized data. For each data set, we compared the four different number of low-dimensional data. The four numbers we used equal to 0.5%, 1%, 2%, and 3% of the total number of cells. Note that, for tSNE, we only extracted two low-dimensional components due to the limitation of the tSNE software.

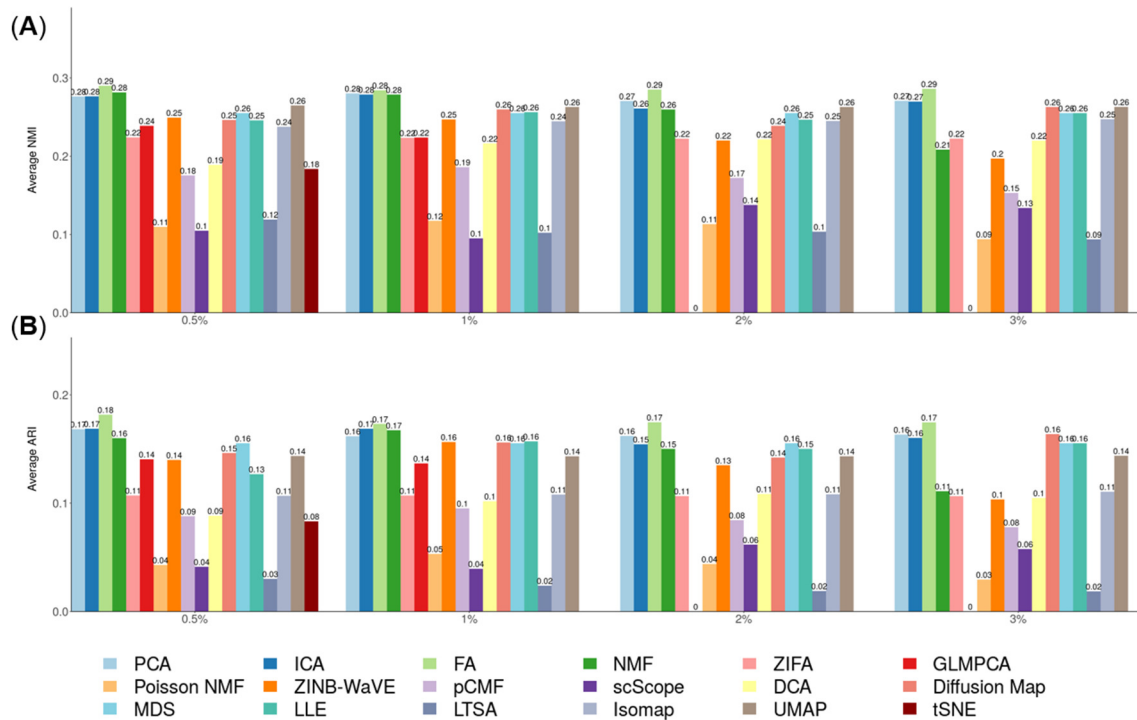


Figure S57. Bar plots show the performance of different DR methods with Slingshot on Cao data set with subsampling procedure. The performance is measured by NMI (A) or ARI (B). We compared 17 DR methods, including factor analysis (FA; light green), principal component analysis (PCA; light blue), independent component analysis (ICA; blue), Diffusion Map (pink), nonnegative matrix factorization (NMF; green), Poisson NMF(light orange), zero-inflated factor analysis (ZIFA; light pink), zero-inflated negative binomial based wanted variation extraction (ZINB-WaVE; orange), probabilistic count matrix factorization (pCMF; light purple), deep count autoencoder network (DCA; yellow), generalized linear model principal component analysis (GLMPCA; red), multidimensional scaling (MDS; cyan), locally linear embedding (LLE; blue green), local tangent space alignment (LTSA; teal blue), Isomap (grey), and uniform manifold approximation and projection (UMAP; brown), and t-distributed stochastic neighbor embedding (tSNE; dark red). We used log2 count transformation for the subset of DR methods that use normalized data. For each data set, we compared the four different number of low-dimensional data. The four numbers we used equal to 0.5%, 1%, 2%, and 3% of the total number of cells. Note that, for tSNE, we only extracted two low-dimensional components due to the limitation of the tSNE software.

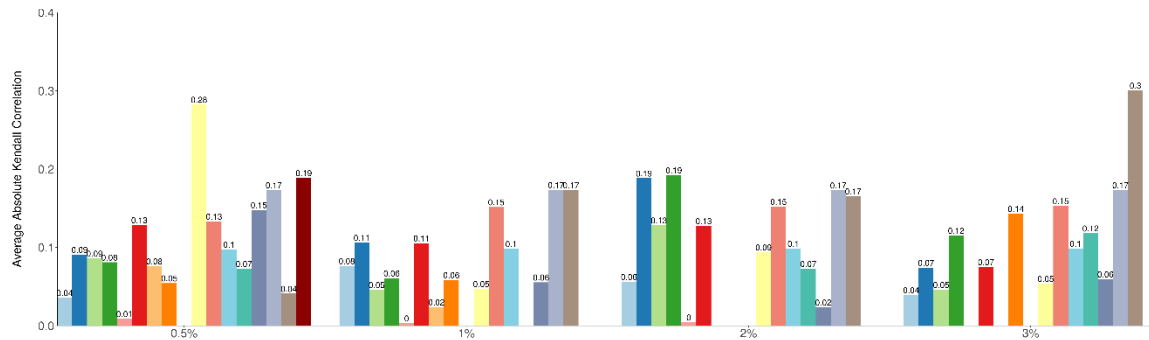


Table S1. List of 15 scRNAseq data sets used for benchmarking DR methods through cell clustering. The table contains data set ID (1st column), data set name (2nd column), species (3rd column), experimental platform (4th column), year of publication (5th column), how the true clusters were determined (6th column), number of genes/transcripts (7th column), number of cells (8th column), number of cell types (9th column) and unique molecular identifiers (UMI; 10th column). We colored different categories in each column by different colors.

ID	Data set	Species	Protocol	Year	Determination	# Genes/Transcripts	# Cells	#Cluster	UMI
GSE111108	FreytagGold	human	10xGenomics Chromium	2018	FACS	58,302	925	3	Yes
GSE115189	GSE115189Silver	human	10xGenomics Chromium	2018	clustering	58,302	2,590	11	Yes
SRP073767	Zhengmix4eq	human	10xGenomics GemCode	2017	FACS	15,568	3,994	4	Yes
	Zhengmix4uneq	human	10xGenomics GemCode	2017	FACS	16,443	6,498	4	Yes
	PBMC3k	human	10xGenomics GemCode	2017	FACS	58,302	3,205	11	Yes
	PBMC4k	human	10xGenomics Chromium	2017	FACS	58,302	4,292	11	Yes
GEO67835	Darmanis	human	Smart-Seq2	2017	clustering	22,085	420	4	No
GSE73727	Pancreatic	human	Smart-Seq2	2016	FACS	139,918	60	6	No
GSE84133	Baron	human	inDrop	2016	clustering	14,878	1,886	13	Yes
GSE75748	ChuBatch1	human	SMARTer	2016	FACS	19,097	350	5	No
	ChuBatch2	human	SMARTer	2016	FACS	19,097	425	6	No
GSE60361	Zeisel	mouse	Smart-Seq	2015	clustering	19,972	1,800	7	No
GSE60749	Kumar	mouse	Smart-Seq	2014	culture conditions	45,159	246	3	No
SRP073808	Koh	human	SMARTer	2016	FACS	48,981	531	9	No
GSE99254	Guo	human	Smart-Seq2	2018	FACS	18,178	12,346	25	No

Table S2. List of 15 scRNAseq data sets used for benchmarking DR methods through trajectory inference. The table contains data set ID (1st column), data set name (2nd column), species (3rd column), experimental platform (4th column), year of publication (5th column), how the true lineage were determined (6th column), number of genes (7th column), number of cells (8th column), unique molecular identifiers (UMI; 9th column) and lineage type (10th column). We colored different categories in each column by different colors.

ID	Data set	Species	Platform	Year	Determination	# Genes	# Cells	UMI	Lineage Type
GSE60783	Schlitzer	mouse	Fluidigm	2015	FACS	4480	238	No	Linear
E-MTAB-3929	Petropoulos	human	Smart-Seq2	2016	timeseries	8,772	1,289	No	Linear
GSE86146	LiM	human	Smart-Seq2	2017		4,777	649	No	Linear
	LiF	human	Smart-Seq2	2017	timeseries	5,319	666	No	Linear
GSE87375	ZhangBeta	mouse	Smart-Seq2	2017	timeseries	6,138	562	No	Linear
	ZhangAlpha	mouse	Smart-Seq2	2017		6,138	322	No	Linear
GSE63818	GuoF	human	Tang et. al.	2015	timeseries	8,772	100	No	Linear
	GuoM	human		2015	timeseries	8,772	166	No	Linear
GSE59114	KowalczykYoung	mouse	Smart-Seq	2015	FACS	2,227	493	No	Linear
	KowalczykOld	mouse		2015	FACS	2,815	873	No	Linear
GSE98664	Hayashi	mouse	RamDA-seq	2018	timeseries	23,658	414	No	Linear
GSE48968	ShalekLPS	mouse	Smart-seq	2014	timeseries	4,158	504	No	Linear
GSE52529	Trapnell	human	SMARTer	2014	timeseries	8,772	290	No	Linear
GSE70245	Olsson	mouse	SMARTer	2016	FACS	3,594	316	No	Linear
GSE119945	Cao	mouse	Sci-RNA-seq3	2019	timeseries	26,183	2,058,652	Yes	Linear

Download links for 15 data sets used in cell clustering:

FreytagGold: The data set consists of three human lung adenocarcinoma cell lines, HCC827, H1975, and H2228, which were cultured separately and mixed together for sequencing [1]. The dataset was sequenced by 10x Genomics Chromium Controller. Cell subpopulation information was established by applying demuxlet (version 0.0.1) on single nucleotide variants (SNVs) to explore the genetic difference and then identify near absolute truth labels of the cells. Raw counts were downloaded from <https://www.ncbi.nlm.nih.gov/geo/query/acc.cgi?acc=GSE111108>.

GSE115189Silver: The data set consists of five fresh human peripheral blood mononuclear cells (PBMCs) [1]. The dataset was sequenced by 10x Genomics Chromium Controller. Cell subpopulation information was established by applying cell labeling approach from 10x Genomics. The cell type labeling obtained through this approach has high consistency with literature. Raw counts were downloaded from <https://www.ncbi.nlm.nih.gov/geo/query/acc.cgi?acc=GSE115189>.

Zhengmix4eq: The data set consists of four pre-sorted cell types (B-cells, naive cytotoxic T-cells, CD14 monocytes, regulatory T-cells) that were combined with equal proportions, with 1,000 cells per cell type [2]. The data were sequenced by 10x Genomics, and the Cell Ranger Single-Cell Software Suite was used to perform sample demultiplexing, barcode processing and single-cell 3' gene counting. The cell type for each cell were known through the pre-sorting process and is considered as the underlying truth. Raw UMI counts were downloaded from <https://support.10xgenomics.com/single-cell-gene-expression/datasets>.

Zhengmix4uneq: The data set consists of four pre-sorted cell types (B-cells, naive cytotoxic T-cells, CD14 monocytes, regulatory T-cells) that were combined with unequal proportions, with 1,000, 500, 2,000, and 3,000 cells for the four cell types, respectively [2]. The data were sequenced by 10x Genomics, and the Cell Ranger single cell software suite was used to perform sample demultiplexing, barcode processing and single-cell 3' gene counting. The cell type for each cell were known through the pre-sorting process and is considered as the underlying truth. Raw UMI counts were downloaded from <https://support.10xgenomics.com/single-cell-gene-expression/datasets>.

PBMC4K: The data set consists of 11 cell types obtained by fluorescence-activated cell sorting (FACS). The data were generated with an earlier version of the microfluidics instrument, the 10x Genomics GemCode Controller. Raw counts were downloaded from <https://support.10xgenomics.com/single-cell-geneexpression/datasets/1.2.0/pbmc4k>.

PBMC3k: The data set consists of 11 cell types obtained by fluorescence-activated cell sorting (FACS). The data set consists of 11 cell types obtained by fluorescence-activated cell sorting (FACS). These 11 cell types include CD14+ Monocyte (446 cells),

CD19+ B (406 cells), CD34+ (17 cells), CD4+/CD25 T Reg (198 cells), CD4+/CD45RA+/CD25- Naive T (242 cells), CD4+/CD45RO+ Memory (465 cells), CD4+ T Helper2 (76 cells), CD56+ NK (428 cells), CD8+/CD45RA+ Naive Cytotoxic (510 cells), CD8+ Cytotoxic T(398 cells), Dendritic (19 cells). The data were generated with the latest instrument, the 10x Genomics Chromium Controller. Raw counts were downloaded from <https://support.10xgenomics.com/single-cell-gene-expression/datasets/2.1.0/pbmc4k>.

Darmanis: This data set originally contains 10 distinct cell groups. Clusters 1-8 consist of adult brain cells, whereas cluster 9 and 10 consist of fetal brain cells. We excluded two mixed groups of cells that is probably due to contamination of each cell with pieces of myelin debris or noisy gene expression profile [3], remaining 8 major brain cell types: astrocytes (62 cells), oligodendrocytes (38 cells), oligodendrocyte precursor cells (OPCs; 18 cells), neurons (131 cells), microglia (16 cells), fetal quiescent (110 cells), fetal replicating (25 cells) and endothelial (20 cells). First, we used an unbiased approach to sort all 466 individual cells into distinct groups defined by the entirety of their molecular signatures. Raw count data were downloaded from <https://www.ncbi.nlm.nih.gov/geo/query/acc.cgi?acc=GSE67835>.

Koh: This data set comprises of 9 different cell types that include H7 hESCs, H7-derived anterior primitive streak populations, H7-derived mid primitive streak populations, H7-derived lateral mesoderm, H7-derived FACS-purified GARP+ cardiac mesoderm, H7-derived FACS-purified DLL1+ paraxial mesoderm populations, H7-derived day 3 early somite progenitor populations, H7-derived dermomyotome populations, and H7-derived FACS-purified PDGFR α + sclerotome populations. RNA was extracted from either whole cell populations or alternatively, cell subsets purified by fluorescence activated cell sorting (FACS). Raw data can be downloaded from <https://www.ncbi.nlm.nih.gov/sra?term=SRP073808>. In our comparison, we directly downloaded the processed data from conquer [4].

Baron: This data set characterized pancreatic cells from human donors and was sequenced by the inDrop platform. Raw count data were downloaded from <https://www.ncbi.nlm.nih.gov/geo/query/acc.cgi?acc=GSE84133>.

ChuBatch1: This is the batch 1 part of Chu et al. data [5]. Chu et al contains four lineage-specific progenitor cells derived from human pluripotent stem cells (hPSCs) and were sequenced by Fluidigm C1 platform. Raw data was downloaded from <https://www.ncbi.nlm.nih.gov/geo/query/acc.cgi?acc=GSE75748>.

ChuBatch2: This is the batch 2 part of Chu et al. data [5]. Chu et al contains four lineage-specific progenitor cells derived from human pluripotent stem cells (hPSCs) and were sequenced by Fluidigm C1 platform. Raw data was downloaded from <https://www.ncbi.nlm.nih.gov/geo/query/acc.cgi?acc=GSE75748>.

Pancreatic: This data set contains human islet cells from one human donor [6]. This dataset was sequenced by Smart-seq2 and raw data were download from <https://www.ncbi.nlm.nih.gov/geo/query/acc.cgi?acc=GSE73727>. We excluded undefined cells in scRNAseq samples and focused on the remaining 60 cells in our evaluation.

Zeisel: This data set contains cells of the somatosensory cortex and hippocampal CA1 region from mouse brains and was sequenced by the Fluidigm C1 platform. Raw counts were downloaded from <http://linnarssonlab.org/cortex/>.

Kumar: This data set contains three populations of mouse embryonic stem cells (mESCs): (1) v6.5 mESCs cultured in serum+LIF media (183 individuals); (2) v6.5 mESCs cultured in 2i+LIF media (94 individuals); (3) Dgcr8-/-mESCs (constructed in a v6.5 background), which lack mature miRNAs due to knockout of a miRNA processing factor in the cells, are cultured in serum+LIF (84 individuals). Raw count data can be downloaded from <https://www.ncbi.nlm.nih.gov/geo/query/acc.cgi?acc=GSE60749>. In our experiments, we directly downloaded the processed data from the conquer website [4].

Guo: This data set contains 25 populations of 12346 T cells from the tumour, adjacent normal tissues and peripheral blood from 14 treatment-naïve NSCLC patients [7]. Following the original paper, we removed CD4 iNKT, CD4 MAIT, DN diverse, DN iNKT, DN MAIT, DP diverse, and other cell subpopulations, and retained 9055 cells with 16 cell subpopulations, including CD4_C1-CCR7 (531 cells), CD4_C2-ANXA1 (665 cells), CD4_C3-GNLY (433 cells), CD4_C4-CD69 (1084 cells), CD4_C5-EOMES (161 cells), CD4_C6-GZMA (668 cells), CD4_C7-CXCL13 (342 cells), CD4_C8-FOXP3 (427 cells), CD4_C9-CTLA4 (939 cells), CD8_C1-LEF1 (303 cells), CD8_C2-CD28 (206 cells), CD8_C3-CX3CR1 (1192 cells), CD8_C4-GZMK (674 cells), CD8_C5-ZNF683 (832 cells), CD8_C6-LAYN (493 cells), and CD8_C7-SLC4A10 (105 cells). Raw count data can be downloaded from <https://www.ncbi.nlm.nih.gov/geo/query/acc.cgi?acc=GSE99254>.

Download link for 15 data sets used in trajectory inference:

In our comparison, all scRNAseq data sets with trajectory information were downloaded from <https://zenodo.org/record/1443566#.XNV25Y5KhaR> [8]. The detailed information of each data sets is as follows:

Schlitzer: This data set contains three cell types at three different developmental stages: common dendritic cell progenitor (CDP; 89 cells); macrophage and DC precursor (MDP; 57 cells); and Pre-DC (92 cell), from the first ontogeny of dendritic cell (DC) development in the bone marrow. Raw data can be downloaded from <https://www.ncbi.nlm.nih.gov/geo/query/acc.cgi?acc=GSE60783>.

Petropoulos: This data set is from a human embryo development study. The data includes the sequenced transcriptomes of 1,529 individual cells from 88 human preimplantation embryos. The data includes five developmental stages: E3 (81 cells), E4 (190 cells), E5 (377 cells), E6 (415 cells), and E7 (466 cells). The read count expression matrices for all cells is available on ArrayExpress: <https://www.omicsdi.org/dataset/arrayexpress-repository/E-MTAB-3929>.

Trapnell: This data set contains human skeletal muscle myoblasts cells collected over a time-course of serum-induced differentiation. At four different time points, cells were captured and processed with the Fluidigm C1 platform followed by Illumina sequencing. The underlying lineage in the data is known and was determined based on the collection time for the cells. The raw data is available at <https://www.ncbi.nlm.nih.gov/geo/query/acc.cgi?acc=GSE52529>.

Olsson: This data set was performed on stem/multipotent progenitors (LSK; lin-Sca1+c-Kit+; 92 cells), common myeloid progenitors (CMP; 92 cells), and granulocyte monocyte progenitors (GMP; 57 cells) that included granulocytic precursors. To isolate LSK, CMP and GMP, lineage stained cells were stained with: Streptavidin APC-Cy7 (Becton, Dickinson and Company), CD16/32-PerCp-ef710 (clone 93, eBioscience), CD117-APC (clone 2B8, Becton, Dickinson and Company), Sca-1-Pe-Cy7 (clone D7, Becton, Dickinson and Company) and CD34-BV421 (clone RAM34, Becton, Dickinson and Company). GMP and CMP gates were set using CD34 FMO. The data set can be downloaded from <https://www.ncbi.nlm.nih.gov/geo/query/acc.cgi?acc=GSE70245>.

LiM: This data set was collected from male fetal gonads with intact morphology and reasonable cell viability from embryos spanning a time period of 4 weeks (4W) to 26W. The stages of human embryos in this study were calculated from the estimated fertilization time, rather than last menstruation bleeding time. The clinicians who obtained the samples made this determination. The number of replicates for each developmental stage was no more than three. In total, 12 male embryos were collected: 21W samples had three biological replicates; 10W, 19W samples each had two biological replicates; and 4W, 9W, 12W, 20W and 25W each had one biological replicate. Raw data can be downloaded from <https://www.ncbi.nlm.nih.gov/geo/query/acc.cgi?acc=GSE86146>.

LiF: This data set was collected from female fetal gonads with intact morphology and reasonable cell viability from embryos spanning 4W to 26W. The stages of human embryos in this study were calculated from the estimated fertilization time, rather than last menstruation bleeding time. The clinicians who obtained the samples made this determination. The number of replicates for each developmental stage was no more than three. In total, 17 female embryos were in this study: 5W, 18W, 20W, 23W and 24W samples had two biological replicates; and 7W, 8W, 10W, 11W, 12W 14W and

26W had one biological replicate. Raw data can be downloaded from <https://www.ncbi.nlm.nih.gov/geo/query/acc.cgi?acc=GSE86146>.

ZhangBeta: This data set contains mouse pancreatic beta cells collected from seven developmental stages. The overall goal of this study was to define the roadmaps for pancreatic β -cell development. Specifically, we performed single-cell RNAseq at various developmental stages of E17.5, P0, P3, P9, P15, P18 and P60 of β -cells. Cells are sorted through FACS and followed by single-cell RNAseq using SMART-seq2. The lineage was determined based on the cell collection time. The raw data is available at <https://www.ncbi.nlm.nih.gov/geo/query/acc.cgi?acc=GSE87375>.

ZhangAlpha: This data set contains mouse pancreatic alpha cells collected from six developmental stages. The overall goal of this study was to define the roadmaps for pancreatic α -cell development. Specifically, we performed single-cell RNAseq at various developmental stages of E17.5, P0, P9, P15, P18 and P60 of α -cells. Cells are sorted through FACS and followed by single-cell RNAseq using SMART-seq2. The lineage was determined based on the cell collection time. The raw data is available at <https://www.ncbi.nlm.nih.gov/geo/query/acc.cgi?acc=GSE87375>.

GuoF: This data set contains human female primordial germ cells collected at five different time points. Cells are sorted through magnetic-activated cell sorting (MACS) or FACS and followed by scRNAseq using a modified single-cell cDNA amplification method [9]. The lineage was determined based on the cell collection time. The raw data is available at <https://www.ncbi.nlm.nih.gov/geo/query/acc.cgi?acc=GSE63818>.

GuoM: This data set contains human male primordial germ cells collected at five different time points. Cells are sorted through magnetic-activated cell sorting (MACS) or FACS and followed by single-cell RNAseq using a modified single-cell cDNA amplification method [9]. The lineage was determined based on the cell collection time. The raw data is available at <https://www.ncbi.nlm.nih.gov/geo/query/acc.cgi?acc=GSE63818>

KowalczykYoung: This data set contains mouse long-term hematopoietic stem cells, short-term hematopoietic stem cells and multi-potent progenitors from young mice (2~3 months of age). Cells are sorted through FACS and followed by single-cell RNAseq using Smart-seq. The lineage was determined based on the FACS. The raw data is available at <https://www.ncbi.nlm.nih.gov/geo/query/acc.cgi?acc=GSE59114>.

KowalczykOld: This data set contains mouse long-term hematopoietic stem cells, short-term hematopoietic stem cells and multi-potent progenitors from old mice (>20 months). Cells are sorted through FACS and followed by scRNAseq using Smart-seq. The lineage was determined based on FACS. The raw data is available at <https://www.ncbi.nlm.nih.gov/geo/query/acc.cgi?acc=GSE59114>.

Hayashi: The data set is from a cell differentiation time series study with RamDA-seq samples. The data contains 414 RamDA-seq samples of mouse ES cells that were collected at 0 (89 cells), 12 (67 cells), 24 (89 cells), 48 (79 cells), and 72 (90 cells) hours after the induction of cell differentiation into PrE cells. The samples were sequenced by Smart-Seq technology. The counts data can be downloaded from <https://www.ncbi.nlm.nih.gov/geo/query/acc.cgi?acc=GSE98664>.

ShalekLPS: This data set contains mouse dendritic-cells along a time-course of LPS-stimulation. At five different time points, cells were captured and processed with the Fluidigm C1 platform followed by scRNASeq using Smart-seq. The lineage was determined based on the cell collection time. The raw data is available at <https://www.ncbi.nlm.nih.gov/geo/query/acc.cgi?acc=GSE48968>.

Cao: This data set contains over 2 million cells derived from 61 mouse embryos staged between 9.5 and 13.5 days of gestation, including 0.8 \times at E9.5 (200,000 cells per embryo; 152,000 profiled across all replicates), 0.3 \times at E10.5 (1.1 million cells per embryo; 378,000 profiled), 0.2 \times at E11.5 (2.6 million cells per embryo; 616,000 profiled), 0.08 \times at E12.5 (6 million cells per embryo; 475,000 profiled) and 0.03 \times at E13.5 (13 million cells per embryo; 437,000 profiled) [10]. In our experiments, we randomly selected 10,000 cells from each stage to perform the trajectory analysis. The raw data is available at <https://www.ncbi.nlm.nih.gov/geo/query/acc.cgi?acc=GSE119945>.

Reference

1. Freytag S, Tian L, Lonnstedt I, Ng M, Bahlo M: **Comparison of clustering tools in R for medium-sized 10x Genomics single-cell RNA-sequencing data.** *F1000Res* 2018, **7**:1297.
2. Duo A, Robinson MD, Soneson C: **A systematic performance evaluation of clustering methods for single-cell RNA-seq data.** *F1000Res* 2018, **7**:1141.
3. Darmanis S, Sloan SA, Zhang Y, Enge M, Caneda C, Shuer LM, Gephart MGH, Barres BA, Quake SR: **A survey of human brain transcriptome diversity at the single cell level.** *Proceedings Of the National Academy Of Sciences Of the United States Of America* 2015, **112**:7285-7290.
4. Soneson C, Robinson MD: **Bias, robustness and scalability in single-cell differential expression analysis.** *Nature Methods* 2018, **15**:255-261.
5. Chu LF, Leng N, Zhang J, Hou ZG, Mamott D, Vereide DT, Choi J, Kendziorski C, Stewart R, Thomson JA: **Single-cell RNA-seq reveals novel regulators of human embryonic stem cell differentiation to definitive endoderm.** *Genome Biology* 2016, **17**:173.
6. Li JC, Wang L, Guo H, Shi LS, Zhang K, Tang MN, Hu SS, Dong SS, Liu YL, Wang TY, et al: **Targeted sequencing and functional analysis reveal brain-size-related genes and their networks in autism spectrum disorders.** *Molecular Psychiatry* 2017, **22**:1282-1290.
7. Guo XY, Zhang YY, Zheng LT, Zheng CH, Song JT, Zhang QM, Kang BX, Liu ZZR, Jin L, Xing R, et al: **Global characterization of T cells in non-small-cell lung cancer by single-cell sequencing.** *Nature Medicine* 2018, **24**:978-985.
8. Saelens W, Cannoodt R, Todorov H, Saeys Y: **A comparison of single-cell trajectory inference methods.** *Nat Biotechnology* 2019, **20**:547-554.
9. Guo F, Yan LY, Guo HS, Li L, Hu BQ, Zhao YY, Yong J, Hu YQ, Wang XY, Wei Y, et al: **The Transcriptome and DNA Methylation Landscapes of Human Primordial Germ Cells.** *Cell* 2015, **161**:1437-1452.
10. Cao JY, Spielmann M, Qiu XJ, Huang XF, Ibrahim DM, Hill AJ, Zhang F, Mundlos S, Christiansen L, Steemers FJ, et al: **The single-cell transcriptional landscape of mammalian organogenesis.** *Nature* 2019, **566**:496-501.